The author(s) shown below used Federal funding provided by the U.S. Department of Justice to prepare the following resource:

Document Title:	**A Rapid, Microfluidic Transcriptomic Method for Body Fluid Identification from Forensic Samples**
Author(s):	**James P. Landers, Ph.D.**
Document Number:	**310050**
Date Received:	**January 2025**
Award Number:	**2020-DQ-BX-0027**

National Institute of Justice

2020-DQ-BX-0027

A Rapid, Microfluidic Transcriptomic Method for Body Fluid Identification from Forensic Samples

PI: Dr. James P. Landers, Commonwealth Professor of Chemistry
landers@virginia.edu, 434-243-8658

Submitting Official: Ms. Judy Mallory, Senior Grants and Contracts Administrator, Office of Sponsored Programs, ospnoa@virginia.edu, 434-924-4270

November 25, 2024

DUNS: [redacted], EIN: [redacted]

The Rector & Visitors of the University of Virginia
1001 North Emmet Street, PO Box 400195, Charlottesville, VA 229044195

Project Period: January 1- 2021-August 31, 2024

Reporting Period End Date: August 31, 2024

Final Report

Signature of Submitting Official:

NIJ Progress Report

"A Rapid, Microfluidic Transcriptomic Method for Body Fluid Identification from Forensic Samples"

November 2024

I. Introduction

Body fluid identification (BFID) is a critical component of crime scene analysis as it contextualizes a crime scene and informs downstream analysis.[1] Standard BFID methods involve a presumptive test followed by some form of confirmatory analysis. Presumptive tests include chemical, enzymatic, or immunological assays, and while rapid and simple, these have multiple drawbacks. Specifically, interpretation is subjective, often leading to false positives, and these tests are limited in specificity and sensitivity, particularly when applied to mixed samples.[2] Confirmatory testing usually involves microscopic analysis for visual confirmation such as presence of sperm. Further, samples collected from crime scenes are often limited in volumes, making serological analysis, which consumes the scarce sample, incompatible for downstream DNA identification- a critical consideration for investigators. This results in the need for a time efficient serological analysis method that is both sensitive and selective while retaining enough sample for downstream DNA profiling.

The standard serological methods use analysis such as alternative light sourcing, lateral flow immunochromatographic assay, or spectroscopic methods. These types of analysis usually probe for proteins or enzymes present within body fluids, such as prostate specific antigen (PSA) within seminal fluid, limiting specificity as these analytes can be seen in small quantities throughout other biological samples, leaving a demand for higher specificity approaches for BFID.[2] Alternative transcriptomics approaches for BFID have been investigated including messenger RNA (mRNA)[3,4], microRNA (miRNA)[5], differentially methylated DNA regions[6,7], and microbial DNA[8]. RNA analysis is a promising alternative to conventional BFID due to the low sample volume required and the ability to retain co extracted DNA for downstream DNA identification.[2]

Our collaborators at the Environmental Science and Research Institute (ESR) have developed tissue-specific mRNA markers that have been validated as robust identification markers for forensically relevant body fluids within three primer panels: the duplex panel contains two markers for saliva; the quadruplex panel contains four markers for venous and menstrual blood; the pentaplex primer contains five markers for semen and vaginal fluid.[3] ESR's validated transcriptomic-based BFID "CellTyper 2" workflow includes RNA extraction and purification followed by a two-step, reverse transcriptase polymerase chain reaction (RT-PCR) that amplifies the specific mRNA sequences for all forensically relevant body fluids. These amplicons are then separated by capillary electrophoresis (CE), a size-based separation method that detects the fluorescent signal corresponding to fluorescently-tagged sequences.[1] Unfortunately, there are numerous manual steps (e.g., tube transfers, pipetting, mixing, etc.) that make this workflow laborious, time-consuming, and prone to contamination. Additionally, this methodology requires multiple stand-alone instruments to perform individual assays – quantification via qPCR, RT-PCR amplification, and electrophoretic separation – in addition to the instrumentation required for

incubation and centrifugation steps during the co-extraction process. The instrumentation required for these assays is cumbersome and calls for expensive reagents and consumables to operate, limiting them to use only in a centralized laboratory. These exigencies ultimately increase the turnaround time of analysis to weeks as samples need to be collected at a crime scene and transported to a laboratory where each step of the workflow may consume as much as 1-2 days alone. Since the primary shortcomings of this workflow hinge within the instrumentation, a system that integrates these individual assays into a single, portable device for use at the point-of-need (PON) would facilitate faster analysis of body fluids while preserving DNA for genetic profiling.

Microfluidic technologies are attractive for laboratory and field-based applications as they address many of the shortcomings described above. Specifically, rapid analysis times due to a high surface area-to-volume ratio, reduced sample and reagent volumes, and the potential for automation make microdevices promising alternatives to traditional instrumentation.[9,10] Additionally, microfluidics offers a potential for integration of multiple analytical processes to create micro-total analysis systems (μTAS) with sample in-answer out capabilities.[11,12] These devices are often designed with a small footprint to be portable for PON applications. While advancements in μTAS are often seen in academic laboratories, commercialization and adoption of these microsystems is limited, especially in the forensic community, typically due to the significant cost.[13]

To address the cost barrier, prior work in our lab focused on developing a cost-effective method for rapid, iterative prototyping of centrifugal microfluidic discs, termed the 'Print, Cut, and Laminate' (PCL) method[14] that has been used to fabricate microdiscs with complex architectures for chemical and biochemical assays. The PCL fabrication method involves designing microfluidic architecture using AutoCAD software, laser ablating polymeric materials (e.g., polyethylene terephthalate (PET) and poly(methyl methacrylate) (PMMA)), and bonding individual layers together using heat sensitive- or pressure sensitive adhesive (HSA or PSA, respectively). In terms of polynucleic acid analysis, the PCL technique has been leveraged to create devices that perform DNA and RNA extraction and enrichment[15–17], multiplexed PCR-based amplification[18–21], and electrophoretic separation[19,22,23] for clinical and forensic applications. In 2016, the Landers Lab was funded by the Department of Defense to create a μTAS for the Rapid DNA initiative[24] that integrates DNA extraction, multiplexed PCR, microchip electrophoresis (ME), and laser-induced fluorescence (LIF) detection for forensic human identification. The designed system, termed 'faSTR', leveraged the PCL method to create a microdisc that integrated these analytical processes for STR typing from buccal swabs, and the corresponding instrument contained all the hardware and software necessary to perform all on-disc operations (e.g., spinning, valving, heating, voltage application, fluorescence detection, etc.).[25]

The proposed research leverages ESR's validated workflow (a 9-step, multi-day process) and the microfluidic expertise of the Landers Laboratory to create a μTAS for BFID. Analysis of body fluids will be conducted using ESR's three body fluid panels with the goal of completing microfluidic BFID, including RNA extraction, multiplexed amplification via RT-PCR, and ME with LIF detection, in under 90 minutes. At a high level, the objectives of this grant were to develop

(1) a microfluidic sample preparation disc by integrating extraction and amplification, (2) a microdisc for ME, and (3) an instrument capable of performing all on-disc operations.

The three specific aims that guided our research investigations were as follows:

1. Develop a DNA and RNA co-extraction method with an RNA purification and DNase treatment that will allow for PCR-ready DNA and RNA in less than 15 mins.
2. Optimize an RNA reverse transcription (RT) and polymerase chain reaction (PCR) assay to allow for successful amplification of multiple messenger RNA targets in less than 45 mins on a portable microfluidic device.
3. Develop hardware and software for instruments that perform on-disc NA co-extraction–RT-PCR in <1.5 hrs and disc-based electrophoresis.

II. Specific Objectives

1. Rapid Enzymatic Extraction

1.1 Universal Extraction Method for All Body Fluids

ESR's validated 'CellTyper 2' body fluid analysis workflow utilizes an extraction protocol that requires the use of magnetic beads and silica columns to extract and separate the RNA and DNA fractions from body fluid samples, with additional purification steps that result in an overall time-consuming and laborious process. We have made efforts to replace this extraction method with a 15-minute process that is entirely enzyme-based and requires simple thermocycling to lyse cells for RNA and DNA isolation. The proposed workflow for the process is shown in **Figure 1**. The *prep*GEM enzyme, in combination with different buffer types, facilitates cell lysis and consequent nucleic acid (NA) release. Buffer selection is dependent on the cell type to be lysed and per manufacturer protocols, extraction of NAs from saliva is to be done with "Blue buffer", seminal fluid and vaginal fluid require the use of "Orange buffer", and venous and menstrual blood NA extraction requires the use of "Red buffer".

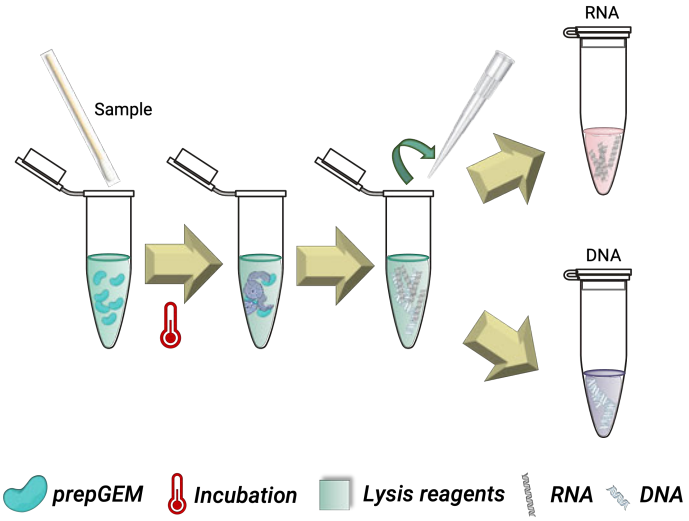

Figure 1. Proposed fully-enzymatic co-extraction process. The first step consists of lysing the body fluid-specific cells with *prep*GEM (MicroGEM) by incubating at 75°C to activate the enzyme, followed by a 95°C deactivation. The eluate is then split into two fractions: RNA for body fluid identification via transcriptomics and DNA for downstream profiling.

Since one of the main aims is to integrate this process into a microfluidic disc, we made efforts to use a single buffer type for the extraction of all body fluids. Figure 2 depicts a comparison between extraction of body fluids with their recommended, designated buffer (i.e., 'Blue' for Figure 2 depicts a comparison between extraction of body fluids with their recommended, designated buffer (i.e., 'Blue' for saliva, 'Orange' for seminal and vaginal fluids, and 'Red' for venous and menstrual bloods, vs. a 'universal' protocol, in which all body fluids were extracted by using the 'Blue' buffer.

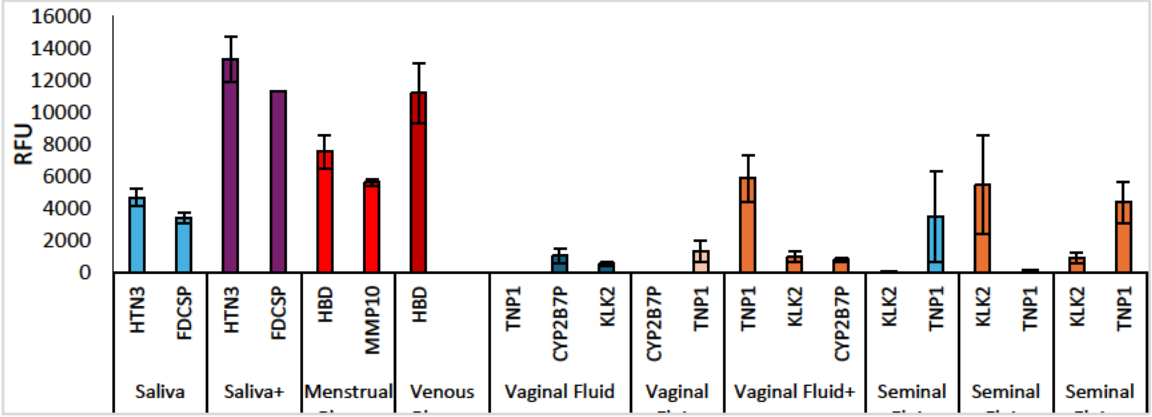

Figure 2. Buffer comparison of body fluids extracted with the enzymatic protocol. Body fluids denoted with '+' signs (i.e., Saliva+, Menstrual Blood+, Venous Blood+, Vaginal Fluid+, Seminal Fluid+) refer to body fluids extracted with ESR's magnetic/silica-based protocol, which we use as positive control(s)). Saliva extracted with 'Blue' buffer shows expression of both HTN3 and FDCSP markers. Only positive controls for menstrual and venous blood are shown since no markers were observed for blood extracted enzymatically, either with 'Red' or 'Blue' buffers. Vaginal and seminal fluids (shaded area) demonstrate the presence of specific markers with both the 'Orange' and 'Blue' buffers (n=3).

Extraction eluates are amplified via one-step RT-PCR, separated using capillary electrophoresis, and analyzed by GeneMarker software, where relative peak heights or relative fluorescence units (RFUs) per gene marker are averaged and plotted as a bar graph. It is important to note that the enzymatic extraction for venous and menstrual blood (both with the 'Red' and 'Blue' buffers) resulted in no apparent markers (not shown). Blood is known to be a convoluted matrix and to contain components that inhibit PCR, so we made efforts to address these shortcomings, which will be explored in the next sections. The shaded area in **Figure 2** depicts body fluids for which comparison between the manufacturer recommended buffer and the proposed 'universal' buffer was successful. The blue bar graphs refer to the 'universal', 'Blue' buffer, whereas the red/orange shaded bar graphs refer to the recommended 'Orange' buffer. Allelic marker expression are low and inconsistent across samples-possibly due to age of the samples. Because of these issues with low expression, an additional DNase purification step was tested to see if expression could be improved.

1.2 DNase Treatment of Enzymatically Extracted RNA

Expression intensities for allelic markers have been lower than desired for the transition of the extraction chemistries onto the microfluidic level. To ameliorate these low intensities, it was hypothesized that treatment of the RNA extracts would remove potential interferents from the eluates, and additional DNase purification step was tested. For this purpose, four buccal swabs were submitted to enzymatic extraction for detection of saliva markers. The eluate was split in two fractions: one was directly used for downstream analysis and the other was treated with DNase before amplification and electrophoresis. **Figure 3** depicts these results and indicates that this additional purification step did not have any significant effect on the expression of saliva targets.

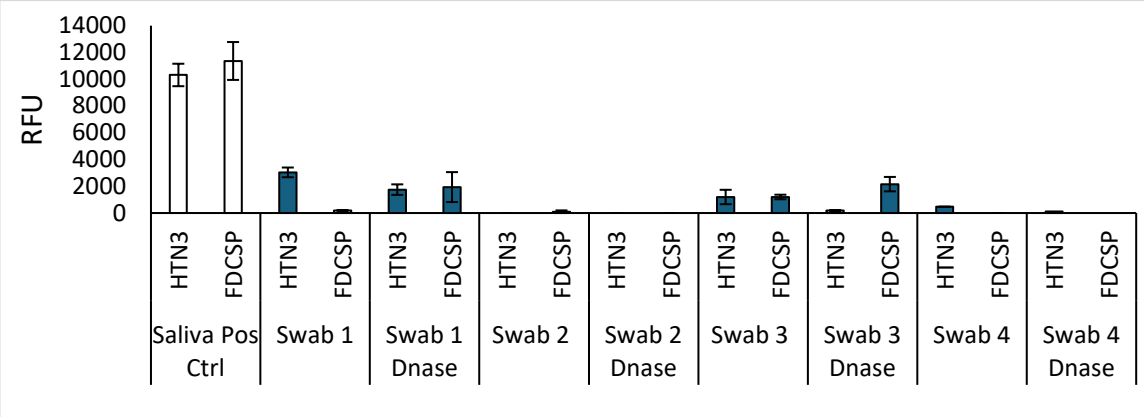

Figure 3. Enzymatic extraction of saliva with DNase treatment (n=4).

1.3 Inhibition Studies

Due to the low RFU values observed from the enzymatic extraction of all body fluids regardless of buffer or DNase treatment, we investigated whether a component of the enzymatic extraction chemistry was inhibiting downstream amplification and separation. To test this hypothesis, saliva samples were extracted following ESR's conventional extraction protocol

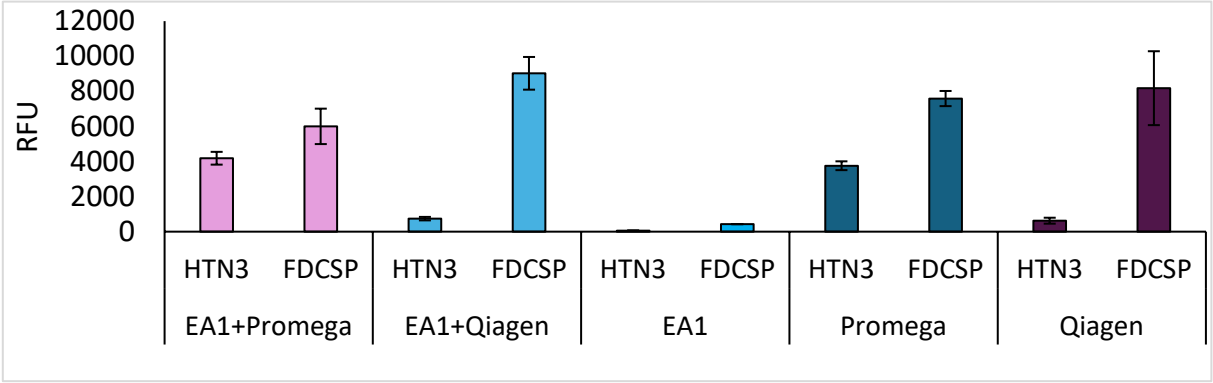

Figure 4. Inhibition verification of enzymatic extraction chemistry. Saliva extracted with the gold-standard protocols (Promega and Qiagen) were spiked with enzymatically-extracted saliva. There is no deleterious effect on the expression of saliva markers for Promega and Qiagen when eluate from enzymatically-extracted saliva is added to the extract (n=3).

This resource was prepared by the author(s) using Federal funds provided by the U.S. Department of Justice. Opinions or points of view expressed are those of the author(s) and do not necessarily reflect the official position or policies of the U.S. Department of Justice.

(Promega) and a second, 'gold-standard' RNA extraction protocol (Qiagen), then amplified via RT-PCR and separated; results were compared to those obtained using enzymatic extraction. Further, the extracts originating from the enzymatic extraction were mixed with both the Promega and Qiagen extracts to verify whether any inhibition would be observed. Results shown in **Figure 4** indicate no significant difference between the expression of saliva markers for samples extracted with Promega and Qiagen protocols alone vs. mixed extracts (all p-values <0.05), confirming that the enzymatic chemistry is not inhibitory of downstream assays.

1.4 Incubation Evaluation

Once we had determined that the enzymatic extraction chemistry was not inhibitory to downstream analysis, it was proposed that the insufficiency of allelic markers could be attributed to instability of the RNA present within the sample. The incubation protocol for the *prep*GEM extraction kit recommends an incubation of 75°C for 5 minutes to activate the enzyme and 95°C for 5 minutes for deactivation. Literature has seen issues with RNA stability at temperatures higher than 60°C for long periods of time; based on this, the incubation times were tested at varied conditions (**Figure 5**) to determine if this heating step was destabilizing the RNA present in the extracts. **Table 1** depicts the conditions tested. From these, saliva markers were only seen for condition 1 (i.e., 75°C for 5 min and 95°C for 5 min), or the protocol incubation. This confirmed that the RNA was not being degraded due to the temperature conditions, and other variables are impacting the extraction efficiency.

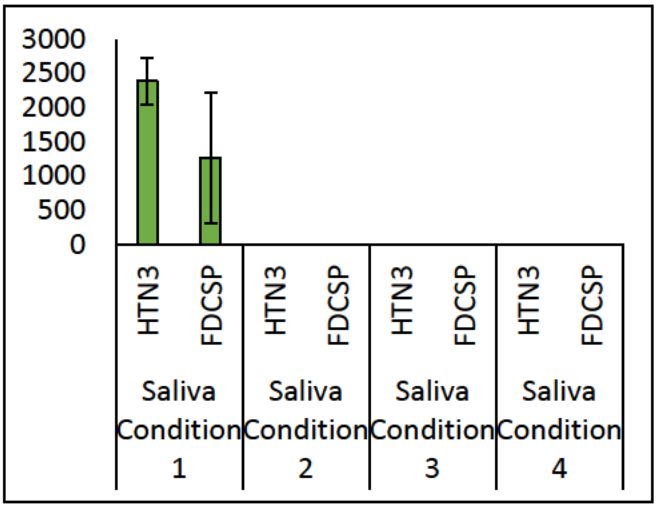

Figure 5. Incubation evaluation. Average RFU values for saliva markers from enzymatically extracted buccal swabs under four different conditions (Table 1) (n=4).

Table 1. Incubation conditions for enzymatic extraction.

Condition	Incubation
1	75 C/5 min and 95 C/5 min
2	75 C/5 min and 95 C/1 min
3	75 C/5 min
4	95 C/1 min

This resource was prepared by the author(s) using Federal funds provided by the U.S. Department of Justice. Opinions or points of view expressed are those of the author(s) and do not necessarily reflect the official position or policies of the U.S. Department of Justice.

Furthermore, two different thermocyclers (that take tubes of different sizes) were compared. The Prime thermocycler is able to house a larger 0.5 mL tube in comparison to the 0.2 mL tube used in the Veriti thermocycler. This larger tube allowed more efficient application of the extraction reagent as well as ensured that the swab head was completely submerged in the extraction buffer. Three swabs per condition were extracted and eluates combined to account for genetic variances. It was seen that there was on average for the three Prime replicates, higher expression of the HTN3 saliva marker (**Figure 6**). We hypothesize that the larger tube allowed for more efficient heating and enzyme saturation.

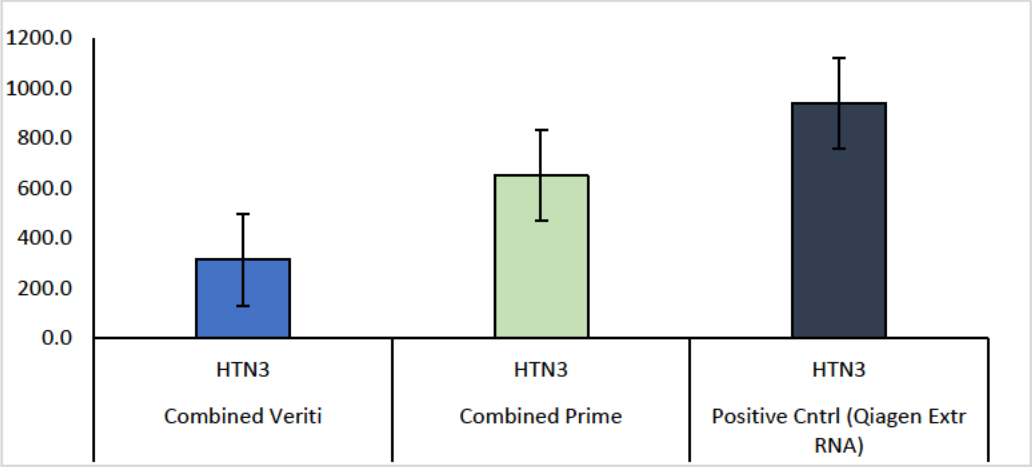

Figure 6. Thermocycler comparison. Average RFU values for saliva markers from enzymatically-extracted buccal swabs with two different thermocyclers.

Previous work with this extraction method showed lower fluorescence units than desired. Because of this re-optimization of the lysis incubation and enzyme volume was conducted. After reviewing protocols, it was seen that an incubation of 75°C for 10 min was conducted in contrast to the protocol incubation of 75°C for 5 min for enzyme activation and 95°C for 5 min for deactivation. This incubation protocol was tested using saliva with varying amounts of enzyme to

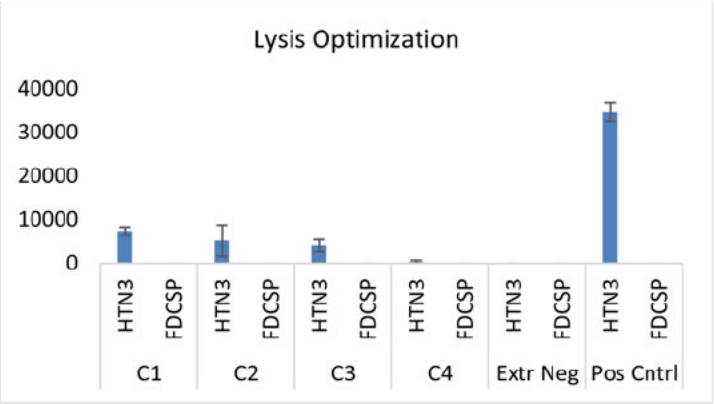

Condition	Enzyme Vol
C1	5 µL
C2	10 µL
C3	15 µL
C4	20 µL

Figure 7. Enzyme Lysis Optimization Testing. Incubation testing was tested at 75 C for 10 minutes for enzyme activation with the removal of the 95 enzyme kill step. Varying amounts of enzyme was titrated from 5 to 20 µL as seen by the table. Average RFU values for saliva markers from enzymatically extracted saliva swabs (n=3).

This resource was prepared by the author(s) using Federal funds provided by the U.S. Department of Justice. Opinions or points of view expressed are those of the author(s) and do not necessarily reflect the official position or policies of the U.S. Department of Justice.

asses lysis achievement. Four conditions were tested as seen within the table of **Figure 7.** From this testing it was seen that the first condition of 5 µL of enzyme with the new incubation parameters showed successful cell lysis. Ultimately, after these various purification methods were attempted but mostly unsuccessful for venous blood, vaginal fluid, and menstrual blood it was then decided to attempt the gold-standard Qiagen column based extraction for these fluids with the use of prepGEM enzyme instead of the commercial Pro K used. From this testing all parameters were kept the same with all buffers and washes used within the commercial step used, the only change made was instead of the initial cell lysis using Proteinase K, the prepGEM enzyme was used and that lysate was run through the Qiagen RNeasy columns, the lysate was purified, amplified with the usual quadraplex primers and electrophoretically separated by benchtop CE. These testings also did not result in the amplification of any blood markers although the co-extract DNA was run using QuantTrio for the amplification of TPOX and DNA was observed. From this testing it is unsure where the RNA is being lost, and the prepGEM enzyme is not inhibiting the PCR chemistry but at some point within the extraction, RNA is being lost. This could be hypothesized to be due to these fragments to already be degraded within these difficult sample matrixes or the enzyme is lysing fragments to such a short size that the RNA is being lost to the purification column or unable to be amplified. Moving forward subsequent testing was completed using saliva and seminal fluid as those biological samples were compatable with the prepGEM enzyme. Future testings assessing other chemistries would need to be completed in order to assess a one-step enzymatic extraction for all forensically relevant body fluids.

1.5 Co-Extraction Microfluidic Disc Dye Study

The microfluidic co-extraction disc described consists of five layers comprised of a top and bottom layer of clear PET, a middle optically dense black PET (bPET)-the valving component, and layers bonded by a proprietary HSA. Accessory architecture of PMMA can be added onto the top of the disc by PSA to increase the available volume. The microfluidic architecture of the co-

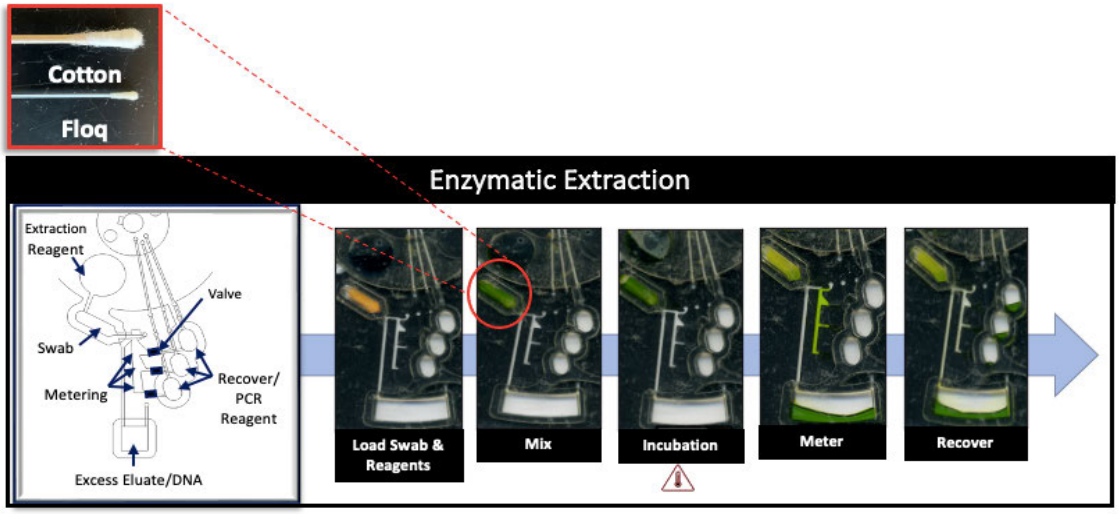

Figure 8. Enzymatic Extraction Microfluidic Dye Study. Schematic of dye study mimicking the enzymatic extraction workflow to ensure fluid movement throughout architecture.

extraction disc was validated by performing dye studies to ensure successful unit operations on disc (**Fig. 8**). In this study a FLOQswab was dried in yellow dye and placed in the swab chamber with 50 µL of green dye pipetted into the extraction reagent chamber to imitate the prepGEM extraction buffer. The disc was mounted on the Power, Time, and Z-height Actuated laser (PrTZAL)5 system used within the Landers lab to perform operations of spinning, mixing, and laser valve opening7. The green dye was spun down into the swab chamber and then heated on the stand-alone Peltier system at 75°C for 5 minutes and 95°C for 5 minutes. The valve below the swab chamber was optically opened via laser ablation, and the "extraction eluate" was spun down to fill metering chambers, with remaining eluate overflowing into the Excess Eluate/DNA Chamber. Valves are laser opened once more and "eluate" is spun into Recovery/PCR Chambers. This dye study was able to show successful unit operations necessary for the co-extraction assay on disc.

1.6 UVA Co-extraction via Microfluidic Disc with FLOQ Swab Testing

To mimic the lysis optimization on-disc, this chemistry was tested on the co-extraction microfluidic disc using wet saliva FLOQ swabs to determine if this chemistry would be compatable with the microfluidic device. Extraction on disc was testing using the above Condition 1 and 2 of 5 and 10 µL of enzyme, respectively. Extraction eluates were pulled off the microfluidic disc and amplified via RT-PCR in-tube and electrohoretically separated via a Promega Compact Spectrum Genetic Analyzer. The results of this testing can be seen by **Figure 9** comparing the relative fluorescence units (RFUs) of the on-disc extraction in comparison to the in-tube testing. This testing resulting in extremely low relative fluorescence for both the on-disc and in-tube replicates, and it was concluded that the nylon material of the FLOQ swabs retain fewer cells within the nylon fibers as opposed to the cellulose material of the cotton swabs.

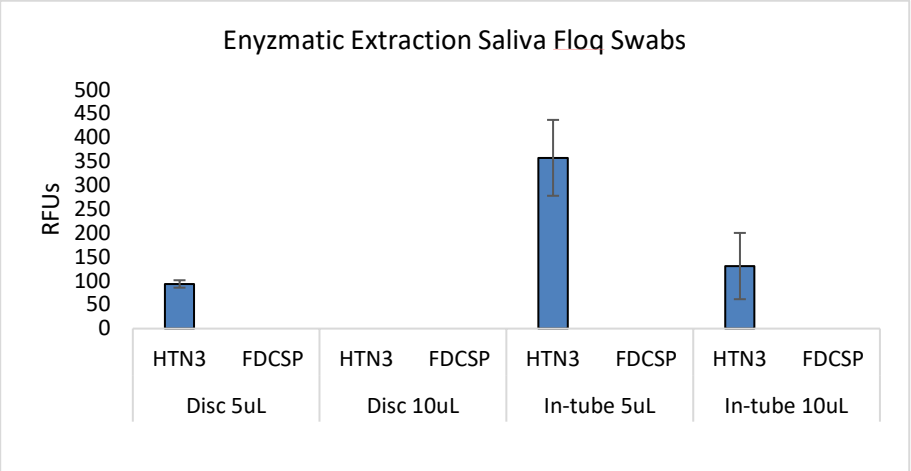

Figure 9. Enzymatic Extraction of Saliva on Microfluidic Device. Average RFU values for saliva markers from enzymatically extracted saliva FLOQ swabs(n=3).

1.7 UVA Co-extraction via Microfluidic Disc with Cotton Swab Cutting

This resource was prepared by the author(s) using Federal funds provided by the U.S. Department of Justice. Opinions or points of view expressed are those of the author(s) and do not necessarily reflect the official position or policies of the U.S. Department of Justice.

After determining that the FLOQ swabs would not be compatible for the on-disc extraction, this testing was repeated using cotton swab cuttings. As the previous testing showed no expression of saliva markers using the 10 µL of enzyme, the first condition of 5 µL was concluded as the optimal parameter and was used for all future testing. Swab heads containing saliva were cut and placed within the swab chamber and on-disc lysis was completed with in-tube replicates mimicking on-disc processes for comparison. **Figure 10** shows the average RFUs for the saliva extracted RNA with higher expression observed from the on-disc condition showing successful extraction of saliva mRNA markers via the microfluidic disc.

With this validation completed, and successful extraction of saliva RNA seen in-tube, as well as, on-disc for the enzymatic extraction this optimized extraction protocol was then applied to seminal fluid for on-disc testing with results also shown in **Fig. 10**.

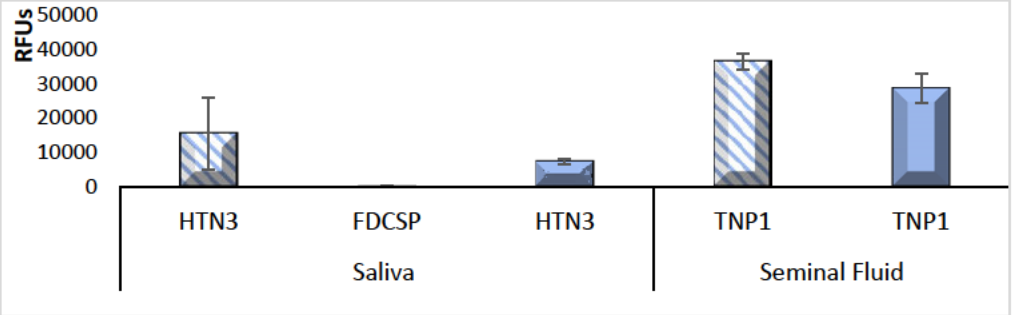

Figure 10. Enzymatic Extraction of Saliva and Seminal Fluid on Microfluidic Device. Average RFU values for saliva markers from enzymatically extracted saliva cotton swab cuttings (n=3).

2. Reverse-Transcription Polymerase Chain Reaction (RT-PCR)

2.1. Optimization of sample volume and on-disc heating for RT

In order to achieve amplification on disc the next phase of this project worked to integrate the on-disc RT and PCR that came prior to separation, on a microfluidic device called the μAmpDisc. The architecture of the μAmpDisc permits the RT reaction to flow into the PCR chamber as the sample input (**Fig. 11).**

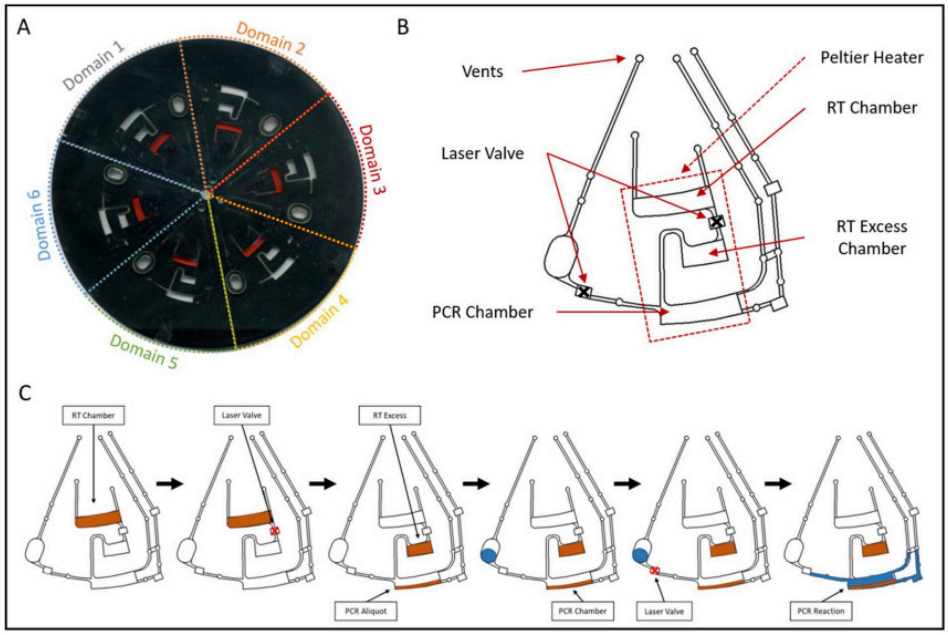

Figure 11: μAmpDisc with six identical RT & PCR domains. (**A**) The disc consists of five layers of polyethylene terephthalate (PeT), heat sensitive adhesive (HSA), and black PeT. (**B**) Each domain has individual chambers for RT, excess cDNA, and PCR. (**C**) Fluidic movement within the layers of the disc.

The size of the chambers was approximated in AutoCAD and the experimental volume moving into the PCR chamber was tested to verify the correct sample volume for the PCR reaction. The architecture of the μAmpDisc included a laser valve and RT Excess chamber upstream of the PCR chamber to aliquot the necessary sample volume in the PCR reaction. Additionally, extra cDNA in the RT Excess chamber can be pipetted off disc and amplified in-tube, if necessary. Previous studies by ESR scientists used either 2 or 10 µL of sample in the in-tube PCR reactions, thus the architecture for the μAmpDisc was fabricated to produce a sample input that averaged the two volumes. The size of the RT Excess chamber was designed to hold the remaining 4 µL of cDNA after spinning the sample (6 µL) into the PCR chamber. To determine fluid volumes, known volumes of red dye (0.5 to 10 µL), were pipetted into the PCR chamber and imaged for pixel count. The number of red pixels were counted using FIJI and a standard curve was constructed to approximate the volume flowing into the PCR chamber (**Fig. 12A; R2=0.9945**). Multiple μAmpDiscs were fabricated with different RT Excess chamber heights (y-axis) to vary the volume of sample input to the PCR chamber. To simulate the correct volumes, 10 µL of red dye was pipetted into the RT chamber, the laser valve was opened, and the μAmpDisc was centrifugally spun into the RT excess and subsequently the PCR chamber. The number of red pixels were measured, and the volumes were determined based on the standard curve (Fig. **12B**). It was

determined that the optimal height for the RT Excess chamber chosen was ~1.43 mm (y-axis), permitting a sample input of ~6 µL for the PCR reaction.

Using the μAmpDisc, the Peltier heaters were optimized to produce the desired in chamber temperatures for the RT protocol. The temperature was tested by inserting a thermocouple into the

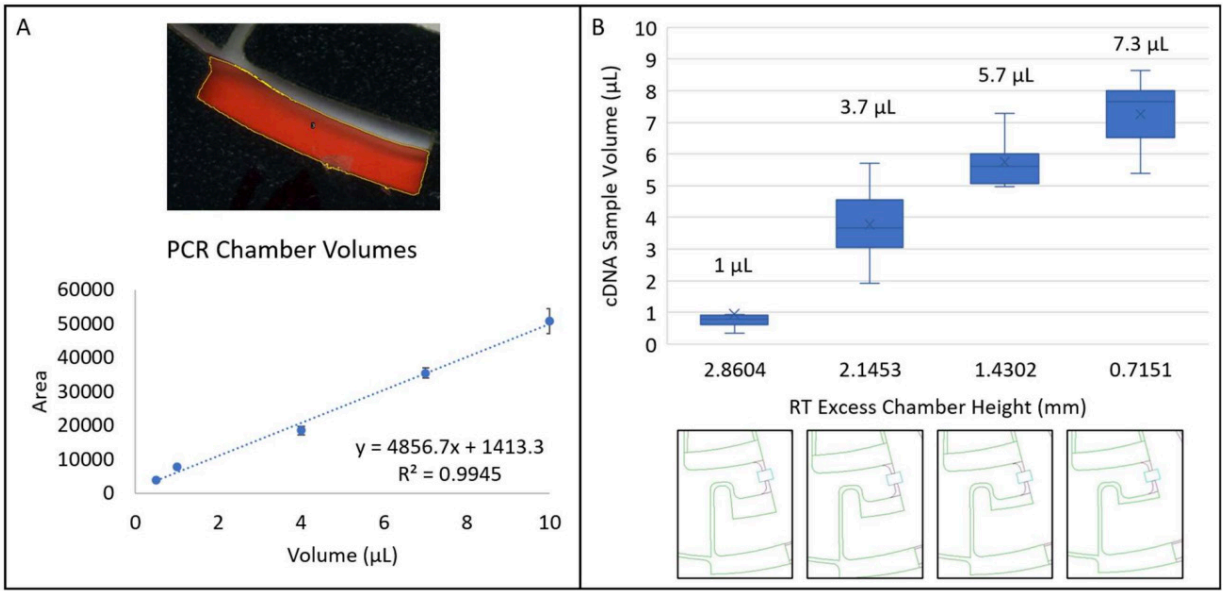

Figure 12: Analyzing the volume of cDNA in the PCR reaction after RT assay. (**A**) Using FIJI software, the pixels colored red were located and counted for each volume of liquid inside the PCR chamber. A standard curve was generated to determine the volume of cDNA overflowing into the PCR chamber. (**B**) The RT Excess chamber was changed in size to change the volume flowing into the PCR reaction. The liquid flowed into the PCR chamber was averaged to determine the sample volume in the PCR reaction.

RT chamber with or without 10 µL of water and recording the measured temperature with a Versalog. Both Peltier heaters sandwiched the μAmpDisc, while the software inputs were toggled. **Fig. 13A** shows minimal difference between the temperature when testing air or water and demonstrates a very stable temperature across replicates. The 25 °C step was the most difficult to optimize due to the proximity to room temperature (22-23 °C). Initially, it was thought the reaction could sit in-chamber for the 25 °C step time without the use of Peltier heaters, but the temperature did not average at 25 °C (**Fig. 13B**). In testing of the Peltier heaters, it was determined that a software input of 26 – 28 would illicit an average response temperature of 25 °C in the requisite chamber and the software inputs for 25, 37, 85 °C were 26, 41, 97, respectively. Once the software input temperatures were determined, the RT protocol was tested multiple times (n=5) to show stability of the temperature from run to run (Fig. **13C**).

This resource was prepared by the author(s) using Federal funds provided by the U.S. Department of Justice. Opinions or points of view expressed are those of the author(s) and do not necessarily reflect the official position or policies of the U.S. Department of Justice.

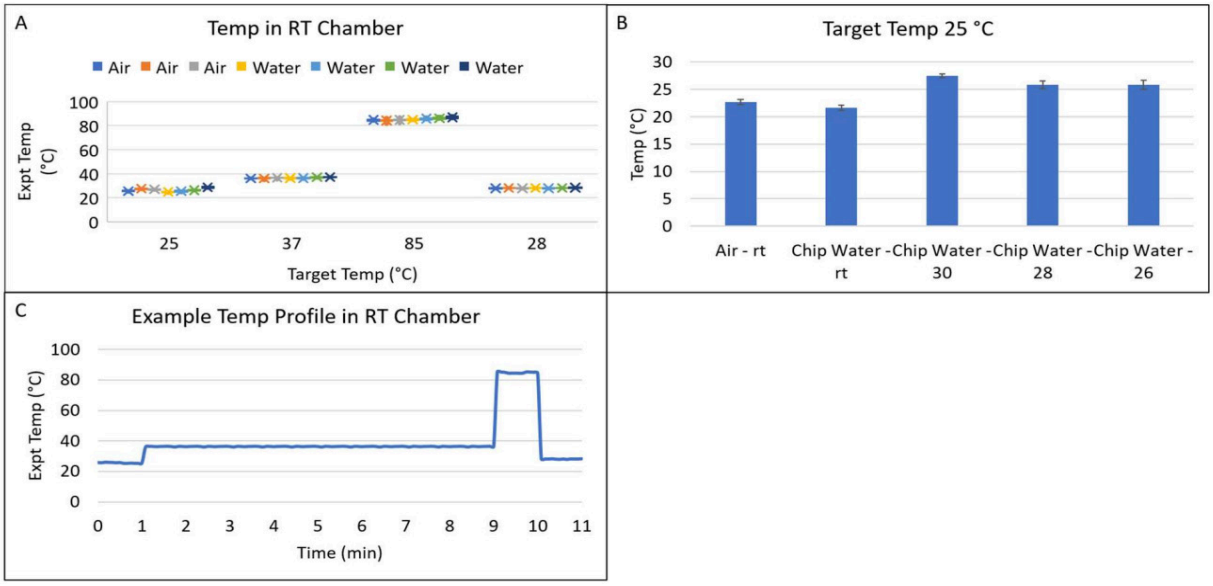

Figure 13: Temperature optimization inside RT and PCR chambers. (**A**) Air and water temperature measurements averaged over 60 sec inside the RT chamber. (**B**) Exemplary temperature profile with the optimized RT protocol. (**C**) Optimization for the 25 °C temperature.

2.2 Decreasing overall time of RT reaction on-disc relative to in-tube

After the in-chamber temperature was optimized, each step of the RT protocol was decreased and assessed for cDNA quantity via qPCR. Initially, the RNA from a blood sample was converted to cDNA in-tube with and without the RT enzyme (**Fig. 14A**). The conversion without the RT enzyme was performed to determine if any residual DNA in the RNA lysate would amplify the 18S target, while the conversion with the RT enzyme served as a 'baseline' for total RNA in the blood sample. The results indicate that the neat sample with RT enzyme converted RNA to cDNA

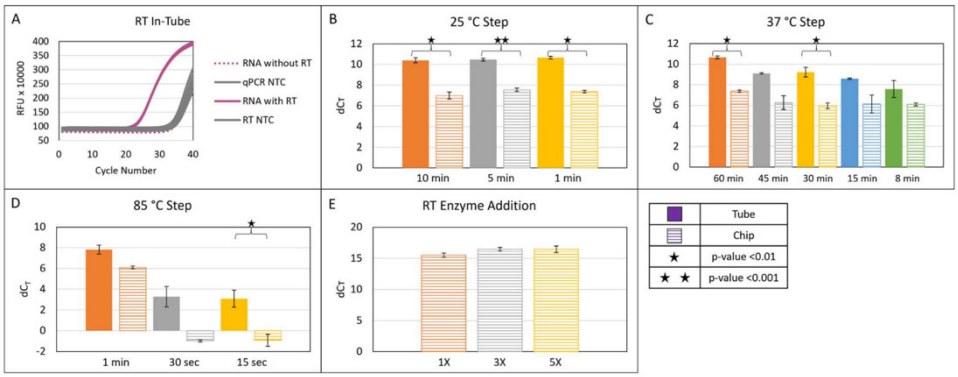

Figure 14: Optimization of each RT step for sufficient cDNA production using a neat venous blood or saliva Total RNA sample. (**A**) RT performed in-tube (solid) using previously optimized protocol. (**B-D**) Decreasing time of each step in the RT protocol to compare tube (solid) vs chip (striped) cDNA production. (**E**) Additional enzyme was added to optimized protocol. The dCT was calculated the negative control minus sample for in-tube and on-disc.

This resource was prepared by the author(s) using Federal funds provided by the U.S. Department of Justice. Opinions or points of view expressed are those of the author(s) and do not necessarily reflect the official position or policies of the U.S. Department of Justice.

and amplified around cycle 25. **Fig. 14B-D** shows how each step of the RT protocol can be reduced significantly to decrease the overall assay time.

The 25 °C primer annealing step was reduced from 10 min to 1 min. However, there was a statistical difference between the in-tube and on-disc cDNA production at all three intervals. The 37 °C step was the most reduced from 120 min to 8 min with a slight difference in cDNA production, as was evidenced by the shifting Ct value. While this step is critical step to this assay, this data shows it can be drastically reduced with similar results as in-tube reactions. Comparing in-tube vs. on-disc cDNA production, a statistical difference from a t-test was found at 60, 45, 30 min, but not at 15 and 8 min. When the 85 °C step was reduced from 5 min to 1 min, the production of cDNA changed based on dCT value for both in-tube and on-disc but decrease the time any further and the quantity of cDNA diminishes. There was a significant difference in cDNA production between the in-tube and ondisc with 30 and 15 sec, but not at 1 min. However, **Fig. 14D** does show we can reduce this step by 4 minutes and still produce cDNA. Finally, the concentration of the RT enzyme was increased to determine if more cDNA could be produced. Fig. 15E shows that an increase in enzyme can slightly increase cDNA production, however, there was no significant difference. Additionally, if more RT enzyme were added to the reaction, the price per reaction would increase by $2 – 4 (USD). To be time-reducing, the final RT protocol was optimized at ~11 minutes with 1X RT enzyme, which saves roughly 110 min from the RT protocol. This RT protocol was used to amplify known single source body fluids obtained from ESR. The fluids were lysed and purified for RNA by the scientists at ESR and sent to the Landers lab at UVA. Donors from all five body fluids were reverse transcribed using the optimized protocol (**Fig. 15**). All of the samples amplified at or before cycle 25 using the 18S rRNA targets and were determined to be statistically different from the NTC (p-value <0.01:Tube Buccal D2, Tube V Fluid D1, Disc Buccal D2, Disc M Blood D1; p-value <0.001: remaining samples). Comparing the in-tube vs on-disc RT reactions, there was ~ 2-5 cycle difference with more cDNA being produced in the in-tube reactions, but no statistical difference between the in-tube and on-disc RT reactions. The on-disc reactions produced sufficient cDNA that can be amplified in downstream PCR reactions and electrophoresed for body fluid profiling. Overall, this data sets up the next phase of this project: optimization of the ESR's PCR protocol on-disc.

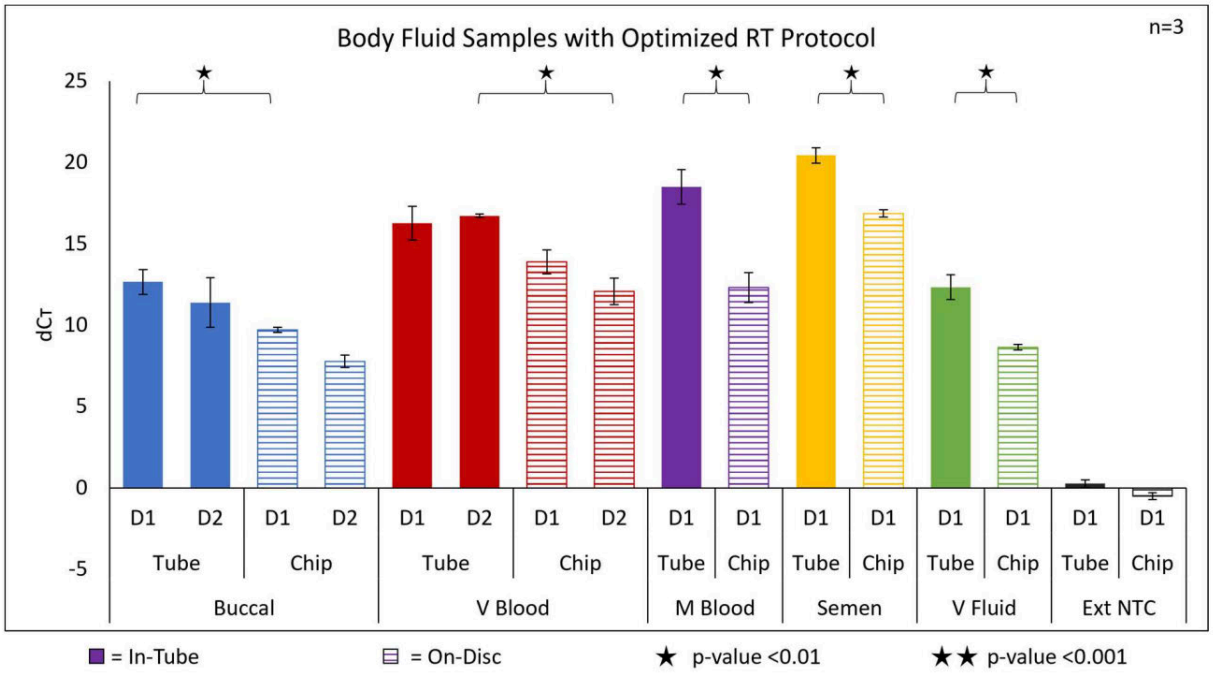

Figure 15: Bar graph showing optimized RT protocol with various body fluids. The 18S rRNA gene was quantified to determine cDNA productions via Total RNA concentration in triplicate of two donors.

2.3 In-Tube PCR Optimization

2.3.1 Evaluation of ESR's Two-Step Amplification Chemistry

Initial work focused on evaluating the amplification portion of ESR's CellTyper 2 workflow and modifying the assay to be compatible with a microfluidic disc. This workflow includes a two-step reverse transcription polymerase chain reaction (RT-PCR) method for amplification of tissue-specific mRNA targets using three primer panels that were previously validated. The primer panels include a Duplex panel, containing two targets for saliva, a Quadruplex panel, which has two targets for both venous blood and menstrual blood, and a Pentaplex panel that probes spermatozoa (two targets), seminal fluid (two targets), and vaginal fluid (one target), or body fluids relevant to sexual assault kit testing. Amplification using this panel combines a RT reaction to make cDNA followed by PCR; however, the RT step is 2 hour 15 minutes, and the PCR portion requires 3 hours 30 minutes, consuming over 6 hours in total without counting preparation. It was immediately understood that these assays would not be compatible with our microfluidic discs as long incubations at high temperatures cause our devices to deform, delaminate, and lose fluid.

Accordingly, efforts were centered on reducing the total amplification time associated with the CellTyper 2 chemistry, beginning with the RT assay.

Previous work, described above, optimized the RT assay by reducing incubation intervals in a step-wise manner using RNA extracted from buccal swabs containing saliva. Briefly, the dwell time associated with Step 1 was reduced from 10 minutes to 5 minutes and 1 minute, and the resultant cDNA was relatively quantified using qPCR. Results indicated Step 1 of the RT assay could be decreased from 10 minutes to 1 minute without a significant change in the resultant cycle

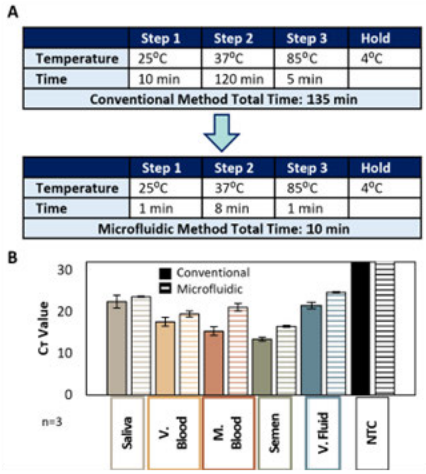

Figure 16. Reduction of RT assay incubation intervals. (**A**) Time comparison between the conventional and optimized microfluidic disc. (**B**) Relative quantification of cDNA produced with all body fluids from the conventional and microfluidic assay.

threshold (C_T) values. As such, this step was held at 1 minute and the dwell time for Step 2 was reduced in an analogous, stepwise manner. This methodology was applied to the entire assay, and once a new RT protocol was determined, the optimized dwell times were tested with all body fluids both in-tube and on the microfluidic disc. **Figure 16** shows a comparison of the resultant C_T values from the conventional 135 minute assay conducted in-tube with all body fluids versus the optimized 10 minute assay performed on-disc. While there was a slight increase in C_T values when looking at the microfluidic method, these differences are <5 C_T values apart, which is an equitable tradeoff considering the overall assay time was reduced by 92.6%.

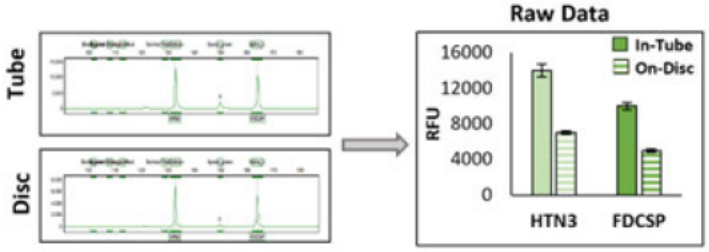

Figure 17. Data analysis workflow for interpretation of electropherograms to bar graphs. Peak heights from raw electropherograms in terms of relative fluorescence units (RFUs) are plotted as a bar.

A similar methodology was applied to optimization of the PCR assay using extracted saliva, but capillary electrophoresis was used as the downstream detection method, and resulting peak heights for alleles were graphed based on relative fluorescence units (RFU) (**Figure 17**). Beginning with the initial enzyme activation step, the dwell times for each phase of the amplification workflow were systematically reduced, with shortened dwell times selected based on which condition maintained relatively high RFU values for the alleles. The goal is to retain peak heights well above 5000 RFUs knowing that a further reduction in peak height will be observed when the assay is transferred to a microfluidic platform. While the enzyme activation and cycling denaturation steps were able to be reduced from 15 minutes and 30 seconds to 4 minutes and 15 seconds, respectively, the remaining annealing and extension steps could not be shortened without a near total loss in RFU (**Figure 18**). Even with the reduction of the enzyme activation and cycling denaturation steps, the total amplification time still consumed two hours and 45 minutes (**Figure 18**), which would likely cause fluid evaporation and delamination when applied to a microfluidic disc.

In an effort to increase RFUs enough to subsequently enable a further reduction in thermal cycling time, various components of the PCR reaction were titrated, including input cDNA volumes (**Figure 18C**) as well as salt ($MgCl_2$) and enzyme (DNA polymerase) concentrations (**Figure 18D**). Decreasing the input cDNA volume from 2 µL to 1 µL caused a slight increase in resultant peak height. Similarly, a slight improvement in RFUs was seen when the polymerase concentration was increased by 1.5X and the salt concentration remained the same. However, even with these titration results, RFUs were still too low (i.e., not >5000 RFU) to further reduce the dwell times, and the incubation times were too long to be compatible with our microfluidic discs, so alternative chemistries conducive to rapid RT-PCR were sought.

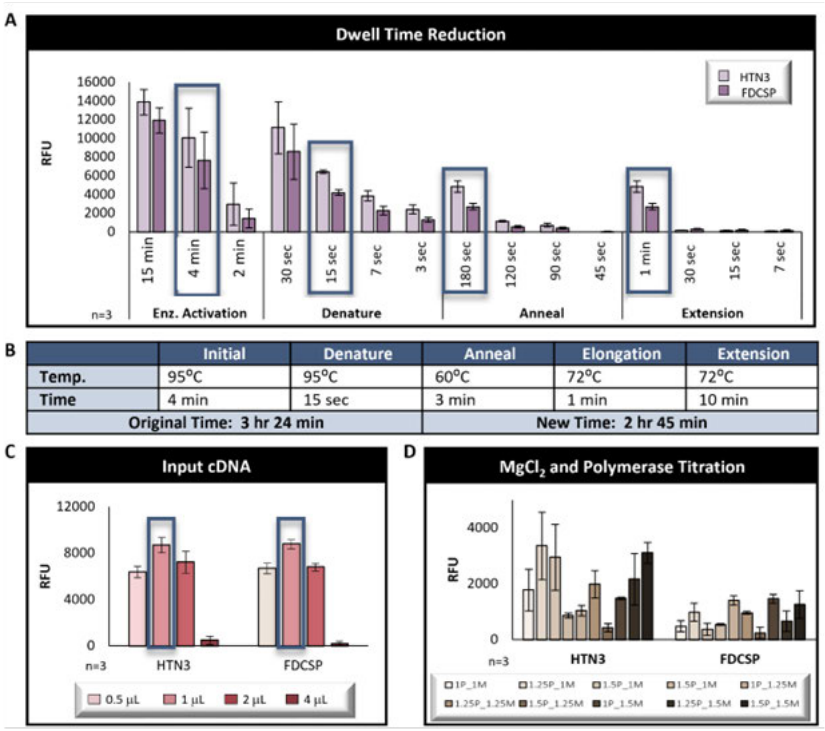

Figure 18. Optimization of the ESR's PCR assay. (**A**) Dwell time reduction for each step of the RT-PCR workflow with purple boxes indicating selected dwell times. (**B**) Optimization of cDNA volume input into each 20 µL reaction. (**C**) Resultant RFUs from the titration of salt and enzymes in the PCR reaction.

2.3.2 New Amplification Chemistry Evaluation and Selection

An extensive literature search was undertaken to select possible alternative RT-PCR chemistries that were suitable for multiplexed amplification and shown to be conducive to rapid thermal cycling. A preferred, but not required, criteria was that the chemistry be a one-step reaction to minimize the manual labor associated with reaction setup and simplify the microfluidic architecture required to run the assay. In total, seven different amplification kits were selected for evaluation, including (1) ESR's two-step RT-PCR chemistry that uses Qiagen's Multiplex PCR Master Mix, (2) ESR's RT chemistry with Qiagen's Fast Cycling PCR kit, (3) TaqMan Fast Universal qPCR kit, (4) Invitrogen's Platinum II Taq Hot-Start kit, (5) Monte Biotech's TikTaq Hot Start Kit, (6) Takara's PrimeSTAR kit, and (7) Qiagen's TaqPath 1-Step Multiplex Master Mix kit (**Figure 19**). To examine each kit, extracted saliva was amplified since this body fluid was the most easily collected and it was used for the previous optimization experiments with ESR's validated protocol, enabling comparisons. Additionally, each master mix was tested using two different concentrations of primers: 'ESR' used ESR's recommended primer concentrations of 0.03 µM and 0.05 µM for FDCSP and HTN3, respectively, while the 'Protocol' condition used primer concentrations in the manufacturer's recommended range (e.g., 0.1-1 µM). For all 'Protocol' conditions, 10 times ESR's recommended primer concentration was used, or a final primer concentration of 0.3 µM and 0.5 µM for FDCSP and HTN3, respectively. **Figure 19** shows

peak heights obtained from 5 of the 7 examined chemistries; two of the amplification kits did not produce electrophoresis results obtained using each master mix. Generally, ESR's primer concentration did not produce peaks on the electropherograms, likely due to too insufficient concentration of primers for amplification. The TaqPath 1-Step Multiplex Master Mix and 'Protocol' primer concentrations clearly produced the highest peak heights, while all other chemistries barely produced peaks of equal height to ESR's validated Qiagen Multiplex chemistry. Furthermore, this TaqPath chemistry consumed approximately 1.5 hours, which is a significant improvement over ESR's validated assay that required over 6 hours not counting manual setup.

Qiagen extracted RNA from buccal swabs was used for all preliminary experiments with

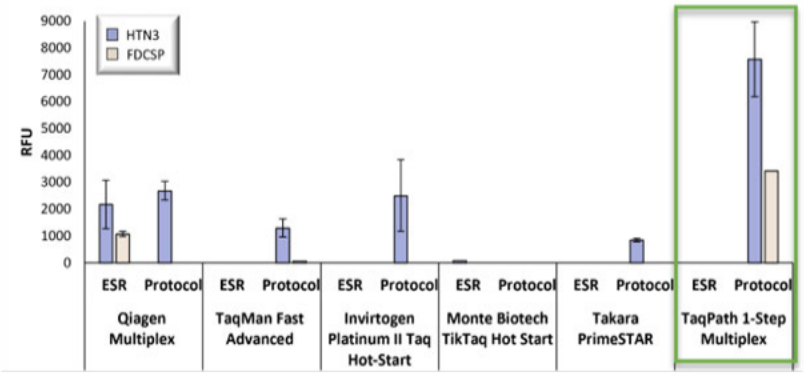

Figure 19. Results from testing alternative RT-PCR chemistries. Electropherogram peak heights are shown in terms of RFUs and the green box indicates the chemistry selected for further experimentation (n=3).

various RT-PCR chemistries. Amplification kits examined included ESR's two-step RT-PCR chemistry, Qiagen Fast Cycling PCR Kit (Qiagen, MD, USA) following ESR's validated RT chemistry, TaqMan Fast Universal qPCR Master Mix (ThermoFisher Scientific, MA, USA), Invitrogen's Platinum II Taq Hot-Start Master Mix (2X) (ThermoFisher Scientific, MA, USA), Monte Biotech's TikTaq Hot-Start RT-qPCR Master Mix (company absorbed by ThermoFisher Scientific, MA, USA), Takara's PrimeSTAR Max Premix (Takara Bio USA, Inc., CA, USA), and TaqPath 1-Step Multiplex Master Mix (ThermoFisher Scientific, MA, USA).

All RT-PCR protocols were conducted per the manufacturer's protocol (**Table 2**), but two different concentrations of primers were used for each protocol, including either ESR's recommended primer concentration or 10X ESR's recommended primer concentration for the two saliva mRNA targets ('Protocol'). For example, ESR's recommended primer concentration for HTN3 in a PCR reaction is 0.05 µM, so the 'Protocol' primer concentration in the amplification

reaction was made to be 0.5 µM. The 'Protocol' concentration was selected as it fell within the range of the manufacturer's recommended primer concentration.

Table 2. Amplification mastermix recipes and associated thermal cycling protocols for various kit chemistries examined. For each condition, ESR's validated primer concentration and 10x ESR's primer concentrations were evaluated. Stock primers were diluted to a 10x concertation so the final concentration in each reaction was 1x.

Qiagen's Multiplex Protocol

Component	Volume (µL)
2X Qiagen MultiPlex PCR Mix	12.5
Primers	2.5
Nuclease-Free Water	5
Sample (cDNA)	5
Total	25

Thermal Cycler Conditions					
Initial	35 Cycles			Extension	Total Time
95°C	95°C	60°C	72°C	72°C	
4 min	15 sec	90 sec	1 min	10 min	2.5 hrs

Qiagen Fast Cycling PCR Kit

Component	Volume (µL)
Qiagen Fast Cycling PCR Master Mix	10
Primers	2
Nuclease-Free Water	6
Sample (cDNA)	2
Total	20

Thermal Cycler Conditions					
Initial	40 Cycles			Extension	Hold
95°C	96°C	60°C	68°C	72°C	4°C
5 min	5 sec	5 sec	6 sec	1 min	hold

TaqMan Fast Universal qPCR Master Mix

Component	Volume (µL)
TaqMan Fast Universal PCR Master Mix	10
Primers	3.6
Nuclease-Free Water	4.4
Sample (cDNA)	2
Total	20

Thermal Cycler Conditions					
UNG	Synthesis	40 Cycles		Extension	Total Time
50°C	95°C	95°C	60°C	4°C	
2 min	2 min	1 sec	20 sec	7 min	40 min

Invitrogen Platinum II Taq Hot-Start (1X)

Component	Volume (µL)
Platinum II Hot-Start PCR Master Mix (2X)	10
Primers	0.8
Nuclease-Free Water	7.2
Sample (cDNA)	2
Total	20

Thermal Cycler Conditions					
Initial	25-35 Cycles			Hold	Total Time
94°C	94°C	60°C	68°C	4°C	
2 min	15 sec	15 sec	15 sec	hold	22 mins

Monte Biotech TikTaq Hot-Start RT-qPCR

Component	Volume (µL)
TikTaq Hot Start PCR 2X Master Mix	10
Primers	2
Nuclease-Free Water	10
Sample (cDNA)	3
Total	25

Thermal Cycler Conditions					
Initial	40 Cycles			Hold	Total Time
94°C	94°C	55-60°C	72°C	4°C	
2 min	30 sec	30 sec	1 min/kbp	hold	42 min

Takara's PrimeSTAR Max Premix

Component	Volume (µL)
PrimeSTAR Max Premix (2X)	25
Primers	2
Nuclease-Free Water	3
Sample (cDNA)	2
Total	32

Thermal Cycler Conditions				
	30-35 Cycles		Hold	Total Time
98°C	60°C	72°C	4°C	
10 sec	15 sec	60 sec	hold	1 hr

TaqPath 1-Step RT-qPCR Master Mix (4X)

Component	Volume (µL)
4X TaqPath 1-step RT-qPCR Master Mix	5
Primers	1
Nuclease-Free Water	9
Sample (cDNA)	5
Total	20

Thermal Cycler Conditions					
UNG	RT	40 Cycles			Total Time
25°C	50°C- RT	95°C	95°C	60°C	
2 min	15 min	2 min	15 sec	1 min	1 hr 9 min

It is worth noting that this set of data was obtained by conducting preliminary experiments as opposed to complete optimization of multiple chemistries (e.g., full primer dilutions, testing various annealing temperatures, titrating salts and enzymes, etc.) due to time and financial constraints of the grant. Had none of the chemistries produced better results compared to ESR's chemistry, a more thorough evaluation of amplification kits would have been conducted. Fortunately, this was not necessary as the TaqPath 1-Step Multiple Master Mix produced significantly higher peak heights when using the 'Protocol' recommended primer concentrations,

and the assay was approximately 75% faster than ESR's validated amplification. Based on these results, this chemistry was selected for further evaluation and optimization.

2.3.3 New RT-PCR Assay Optimization for Microfluidic Adaptation

Upon selection of a new RT-PCR kit, the chemistry needed to be further optimized to ensure compatibility with our microfluidic platform. This included increasing ramp rates and reducing incubation times. All initial experiments were conducted in-tube using saliva targets, and amplicons were separated via CE for comparison of peak heights. Optimization began by titrating primers at 0.2, 0.4, 0.5, 0.6, and 0.8 µM to see which condition resulted in the highest RFUs and ideal peak balance based on ESR's validation work.[1] Reduction of total amplification time was carried out by increasing the ramp rate on the QuantStudio-5 Real-Time PCR instrument from the standard 2.66 °C/s (standard cycling) to 4.00 °C/s (fast cycling). For optimization of the protocol incubation lengths, the dwell time of one step (e.g., RT) was reduced while all other steps retained the manufacturer suggested protocol. Evaluation of the TaqPath chemistry with all body fluids used either 0.5 µM primers for body fluids or 10 times the concentration of ESR's validated primers. The final evaluation experiment compared the 'Manufacturer Protocol' to the 'Optimized Protocol', both using 10X ESR's validated primer concentrations. The Manufacturer Protocol is described above, while the Optimized Protocol used the following thermal cycling program: 25 °C for 0 min, 53 °C for 5 min, 95 °C for 10 sec followed by 40 cycles of 95 °C for 1 sec and 60 °C for 30 sec. Of the examined concentrations, 0.5 µM was selected for both targets as the resulting RFUs were high (~12000 and ~7000 for HTN3 and FDCSP, respectively) and the FDCSP peak height was approximately half the HTN3 peak height (**Figure 20**).

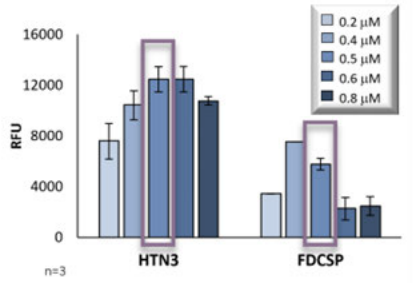

Figure 20. Primer dilution using saliva mRNA targets and newly selected TaqPath 1-Step Multiplex RT-PCR chemistry. Boxed bars indicate the selected primer concentrations on 0.5 µM.

Using the optimized 0.5 µM primer concentration, reduction of the overall amplification time was conducted to achieve our goal of a 45 minute amplification and to minimize the chance of deforming/delaminating the microfluidic disc. We began by increasing ramp rates during thermal cycling, which dictates how quickly temperature changes. By increasing the ramp rate on the instrument from 2.66 °C/s (standard cycling) to 4.00 °C/s (fast cycling) the RT-PCR reaction time decreased from 1 hour 33 minutes to 40 minutes, which was within our target amplification time of 45 minutes (**Figure 21A**). Even so, reduction of dwell times was examined since reducing the length of incubations will increase the chance of successful amplification on disc. As previously described, each incubation time of the RT-PCR assay was systematically reduced, and incubation lengths were selected based on which time resulted in little to no reduction in RFUs. **Figure 21B** shows the selected dwell times of 0 minutes, 5 minutes, 10 seconds, and 1 second for the UNG incubation, RT, enzyme activation, and cycling denature steps, respectively. When the annealing step was reduced beyond 30 seconds,

no amplification occurred, which was unsurprising given the complex multiplexing needs of the assay. These reductions led to a total assay time of 30 minutes, a 67.7% reduction in time from the starting 1 hour 33 minutes, without a significant loss in sensitivity. Further, the total assay time for this optimized 1-step RT-PCR kit represents a 91.3% decrease in time compared to ESR's

A

Standard Cycling	UNG Incubation	Reverse Transcription	Polymerase Activation	Cycling Denature	Cycling Anneal
Temp.	25°C	53°C	95°C	95°C	60°C
Time	2 min	10 min	2 min	15 sec	30 sec
Total Time: 1 hr 33 min					

Fast Cycling	UNG Incubation	Reverse Transcription	Polymerase Activation	Cycling Denature	Cycling Anneal
Temp.	25°C	53°C	95°C	95°C	60°C
Time	0 min	5 min	10 sec	1 sec	30 sec
Total Time: 30 min					

B

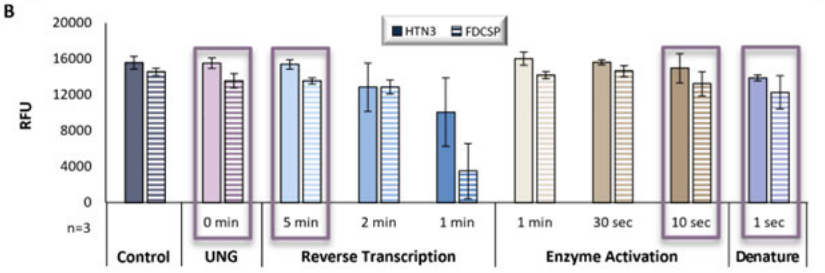

Figure 21. Reduction of total amplification time in-tube. (A) Increasing ramp rates by changing thermal cycling speed from Standard to Fast Cycling. (B) Decreasing dwell times for each step of RT-PCR assay; purple boxes indicate selected dwell times.

validated 2-step RT-PCR assay.

Since the initial optimization of the TaqPath chemistry was completed with saliva, we needed to examine compatibility with all other body fluids. Using the optimized 0.5 µM primer concentration, selected based on results in **Figure 20**, all body fluid targets were amplified using the manufacturer's recommended protocol. It was clear that primer concentrations would need to be individually optimized for each body fluid, but the purpose of this experiment was to simply evaluate if this new chemistry was compatible with all mRNA targets. The solid bars **Figure 22** show resultant peak heights from all body fluids amplified with 0.5 µM primers. Generally, amplification of all body fluids was present, but peak imbalances were present (e.g, HTN3 should have a higher peak height relative to FDCSP) across alleles for the same body fluid and large standard deviations were seen for certain targets (e.g., HBD and TNP1), both of which can be attributed to a lack of optimization for primer concentrations. The vaginal fluid sample showed expression of TNP1, implying either the presence of sperm due to the sample being post-coital, which cannot be addressed with chemistry adjustments, or cross-reactivity of the Pentaplex primer panel, which could be adjusted by changing primer concentrations. Additionally, expression of the venous blood and semen targets were particularly low. We believed these samples to be degraded since the collection date on the body fluid collection containers was over 1 year old. Therefore, fresh samples were collected, extracted, amplified, and electrophoresed: results show better expression and peak balance of all targets except for PRM1, which did not express with the new

or old samples (**Figure 22 striped bars**). We hypothesize the lack of PRM1 expression to be due to the primer concentration. Overall, this experiment demonstrated that all body fluids could be amplified with this new TaqPath chemistry, but additional optimization of primer concentrations needed to be explored.

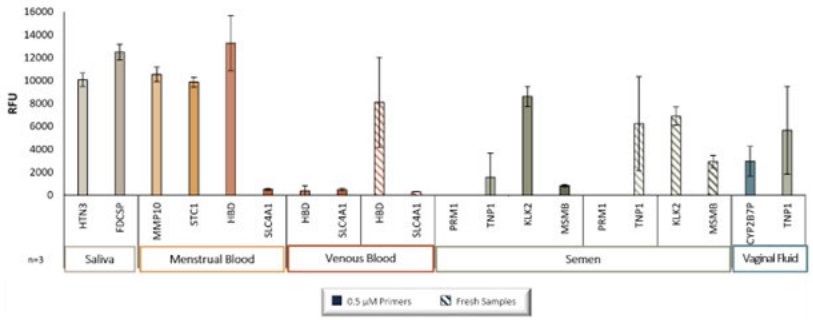

Figure 22. Electrophoresis results from amplification of all body fluids using 0.5 µM primers. Striped bars indicate results from samples that needed to be re-collected and analyzed due to degradation of the original samples (solid bars).

As mentioned, we were aware that primer concentrations would need to be optimized for each individual body fluid, but at the time, resources (both in time and reagents) were too limited to conduct multiple primer titrations for each target. Instead, the goal here was to see if more efficient amplification of targets could be obtained in-tube prior to adapting this chemistry to a microfluidic disc. As a starting point, the same RNA eluates were amplified using 10 times ESR's recommended primer concentrations, as was done in **Figure 19**, since this allowed for primer ratios to be more balanced across targets and within the recommended primer concentration range for the amplification chemistry (0.1 - 1.0 µM). Additionally, by using the same RNA eluates, variability of conditions due to sample collection and extraction was avoided. **Figure 23** compares resultant peak heights from the two different primer conditions. Using 10X ESR's recommended primer concentrations created better peak balance across alleles (e.g., HTN3 peak height was higher than FDCSP), reduced the size of error bars, and even improved expression of some targets. Looking at individual body fluids, peak balance for saliva and menstrual blood targets improved while the RFUs remained relatively high across conditions. While venous blood targets (HBD and SLC4A1) were detected in the menstrual blood, this lack of specificity is very common with body fluid analysis. Looking at venous blood, there was no statistically significant difference in peak heights, but the error bar on the HBD target was much smaller with the new primer concentration. For all semen targets, there was improved peak heights, a reduction in error bar size for TNP1, and observed expression of PRM1 when the new primer concentrations were employed. Similarly, there was a slight increase in expression of vaginal fluid targets using 10 times ESR's primer concentration. A full primer optimization for each body fluid will be conducted by our collaborators at ESR since they developed and validated the original primer panels, and they have more sensitive CE instrumentation to obtain more accurate results. Since these results were sufficient enough (generally >5000 RFU) to apply this chemistry to a microfluidic platform, the

new 10X concentration of ESR's validated primers was implemented in additional experiments based on the results demonstrated here.

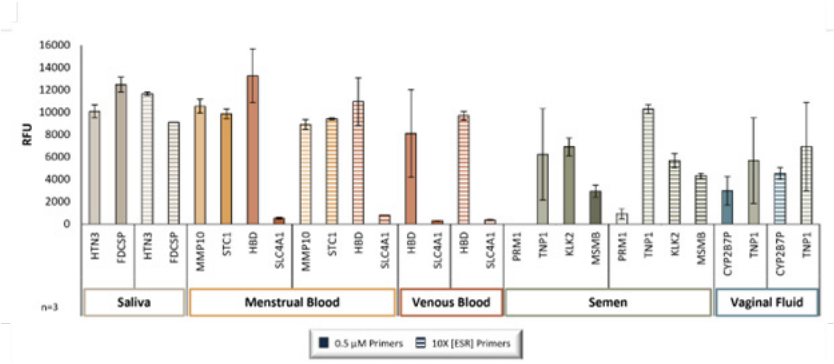

Figure 23. Amplification of all body fluids using two different primer concentrations. Specifically, 0.5 µM primers (solid bars) and a new dilution that is 10x ESR's validated primer concentration (striped bars) were evaluated.

With a preliminary optimization of the new TaqPath chemistry completed, including reduced dwell times, increased ramp rates, and 10X primer concentrations, a comparison of the standard manufacturer amplification protocol to our newly optimized protocol was necessary prior to implementing this assay on a microdisc. Specifically, the 'Manufacturer Protocol' for the TaqPath chemistry used the recommended ramp rates and incubation times that resulted in a total amplification time of 1 hour and 33 minutes with the 10X primer concentrations. Conversely, the 'Optimized Protocol' employed the 10X primer concentrations with the shortened dwell times and faster ramp rates, resulting in a 30-minute amplification (**Figure 24)**. Generally, the optimized protocol resulted in RFUs statistically equal to or slightly less than those amplified with the longer protocol, which was expected as longer incubation times generally result in more efficient amplifications. However, there was no allele dropout for any target and RFUs across all body fluids were over 5000 RFUs, except for the venous blood, which can be attributed to the sample storage conditions causing some amount of degradation prior to extraction. Thus, we believe a 64% reduction in amplification time is worth a slight reduction in RFUs as the faster RT-PCR will be more conducive to the microfluidic platform.

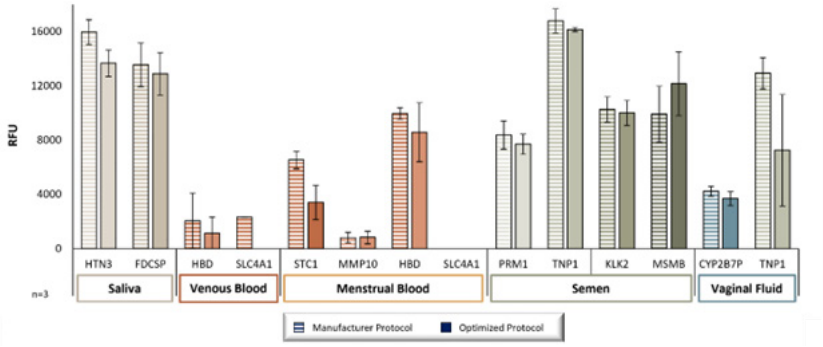

Figure 24. Peak heights resulting from amplification of all body fluids via the manufacturer's recommended RT-PCR protocol and the optimized protocol. While both protocols implemented 10x ESR's validated primer concentration, the optimized protocol included reduced incubation times and increased ramp rates.

2.4 Microfluidic Architecture Development

In addition to optimizing the amplification assay in-tube, simultaneous development of microfluidic architecture for an amplification disc was undertaken with the overall objective of designing a microdisc that integrates co-extraction and RT-PCR amplification. Towards this end, separate discs for each assay were designed to individually validate the architectures prior to integration. The devices are fabricated using the PCL technique[14] that is cost-effective and amenable to rapid prototyping. Both microfluidic discs are comprised of five total layers, including polyethylene terephthalate (PET), heat-sensitive adhesive (HSA), optically dense black PET (bPeT), and poly(methyl methacrylate) (PMMA) that is adhered to the disc using a pressure-sensitive adhesive (PSA). The microfluidic architecture for each layer is designed using AutoCAD software that is transferred to a CO_2 laser cutter where the design is engraved into each layer of the device. Standard office laminators are used to activate the heat-sensitive adhesive that bonds the layers together. Discs are further incubated under weights (~15 pounds) to ensure the complete bonding of all layers.

Once fabricated, the microdevices can be mounted on instrumentation built in-house to perform all on-disc operations, including valving, spinning, and heating. Since the integrated faSTR system was being engineered for BFID simultaneously with the development of fluidic architecture, all on-disc operations were performed on two individual instruments: the Power, Time, and Z-Height Adjustable Laser (PrTZAL) system[26] performed laser-actuated valving and spinning of the disc to generate centrifugal force both of which control fluidic movement, while the Stand-Alone Peltier system[17,27] performed active heating and cooling via dual-clamping Peltiers. Separating unit operations (e.g., heating from spinning and valving) enabled us to control for complex engineering-related variables inherent to an integrated instrument (i.e., faSTR) while focusing on identifying failure modes associated with microfluidic architecture. If one of the systems needed to have hardware or software adjusted, pinpointing and addressing the issue is a simpler task on an individual system compared to an integrated system.

2.4.1 Two-Step RT-PCR Microfluidic Disc

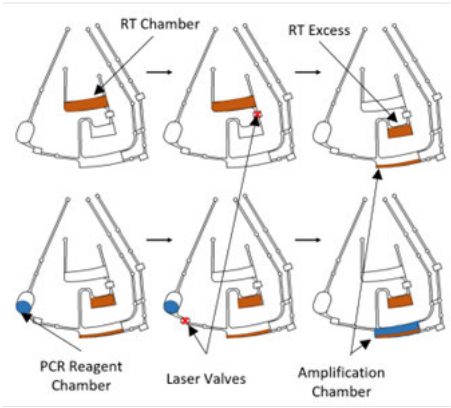

Figure 25. AutoCAD rendering of microfluidic architecture conducive to a two-step RT-PCR amplification. Orange indicates RT reagents while blue represents PCR reagents. A red X on a laser vlave indicates an open valve.

Development of microfluidic architectures for an amplification disc began concurrently with in-tube optimization of ESR's amplification assay thus, initial architecture was designed to be conducive to a two-step RT-PCR amplification. **Figure 25** shows the initial design of the RT-PCR architecture, which was modified from the PCR domain of the faSTR disc[25]. Here, RT reagents and RNA are pipetted into the RT Chamber and reverse transcribed. A laser-actuated valve is then opened, and cDNA is metered into an RT Excess Chamber where a syphon valve enables overflow (2 µL) to be delivered to the PCR Chamber; the volume delivered to the PCR Chamber can be tuned by adjusting the dimensions of the RT Excess Chamber. PCR reagents, which are pipetted or stored in the PCR Reagent Chamber, are added to the cDNA in the PCR Amplification Chamber by opening a second laser valve. Once reagents are mixed in the Amplification Chamber, the disc is positioned under thermoelectric heaters (Peltiers) for thermal cycling.

Previous described the metering associated with the RT portion of this architecture was optimized to ensure 2 µL cDNA was delivered to the PCR chamber,[28] but the PCR architecture needed to be examined. To evaluate functionality of the PCR architecture, a dye study was performed (**Figure 26**). In this experiment, blue dye, representing cDNA, and yellow dye, representing PCR reagents, were pipetted into the appropriate chambers, and the blue dye was metered into the RT Excess Chamber and subsequent PCR Chamber. **Figure 26A** shows the disc before and after only 10 cycles of PCR; since this was a preliminary dye study, performing 40 cycles of PCR was excessive. It was clear that there was fluid movement from the PCR Chamber back to the RT Excess Chamber. We believed this to be due to excess air in the PCR chamber prior to thermal cycling, enabling

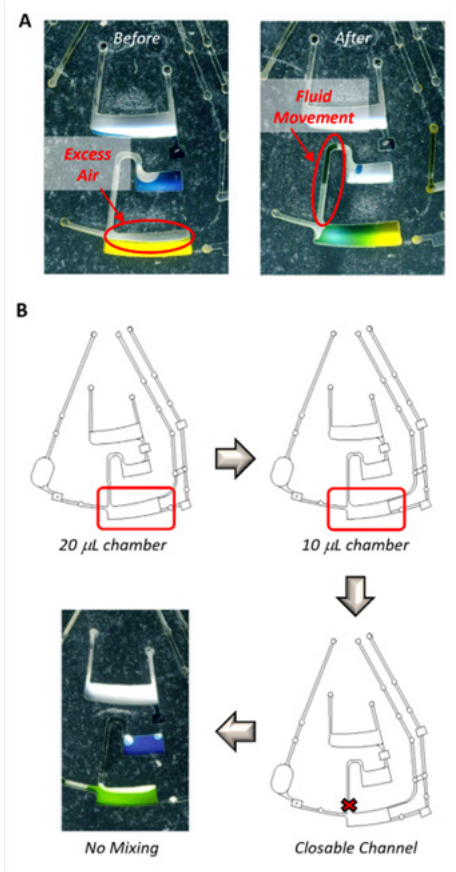

Figure 26. Dye study evalutating microfluidic architecture for a two-step RT-PCR assay. (A) Scanned images showing thermal pumping in one domain of a disc after 10 cycles of PCR. (B) Architecture modifications made to prevent fluidic mixing during 10 cycles of PCR.

the air to expand and contract during temperature cycles and causing thermal pumping of fluid throughout the architecture. To address this, two changes were made to the architecture, including reducing the PCR chamber size so it holds a theoretical 10 µL instead of 20 µL (measurements made in AutoCAD) and adding a closable channel between the Amplification and RT Excess chambers (**Figure 26B**). These modifications prevent mixing during 10 cycles of PCR once cDNA (blue dye) was added to the PCR reagents (yellow dye) in the PCR Chamber.

As a final test of the fluidic architecture, we performed PCR thermal cycling on-disc according to our optimized protocol for ESR's validated two-step amplification. Again, dye was used in place of reagents for this preliminary study in the interest of saving costs. **Figure 27** shows an image of the disc scanned post-heating where it is apparent no fluid was retained during thermal cycling. Not only did fluid evaporate through vents, but the long incubation times at high temperatures enabled fluid to leach into the HSA and caused architecture to deform, as is particularly evident around a valve that was under the Peltier. This study verifies that the optimized protocol for ESR's chemistry, which was modified to have reduced incubation times, was still too long of an amplification assay to be compatible with our microfluidic discs. Based on these results, and the in-tube assay optimization data, architecture needed to be adjusted to accommodate a new amplification chemistry.

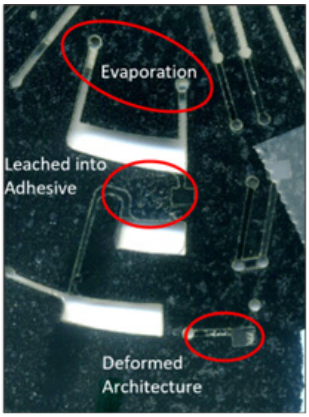

Figure 27. Scanned images of a disc domain after 40 cycels of PCR following the optimized protocols for ESR's validated amplification assay. Red circles indicate failure modes caused by extended heating steps during thermal cycling

2.4.2 One-Step RT-PCR Microfluidic Disc

Upon selection of the TaqPath 1-Step Multiplex Master Mix amplification chemistry a new disc was designed with architecture to accommodate a one-step RT-PCR reaction. **Figure 28A** shows the fluidic architecture for simultaneous amplification of the three individual body fluid panels (Duplex, Quadruplex, and Pentaplex). This disc design leveraged closable valves and hydrophobic membranes in anticipation of needing to address the issues observed with the two-step RT-PCR disc described above. Each domain consists of three Reagent Chambers where amplification reagents are pipetted into the inlet/vent or for on-disc storage of lyophilized reagents. Upon opening laser-actuated valves, fluid is driven from Reagent Chambers to the RT-PCR Chambers. Prior to thermal cycling, the opened valves are closed via laser-actuation, then all three RT-PCR chambers undergo simultaneous thermal cycling. Hydrophobic membranes made of polytetrafluoroethylene (PTFE) were added to the RT-PCR chamber vents to enable expansion and contraction of air during thermal cycling while keeping fluid retained in the amplification chambers; it was hypothesized that by adding these membranes, fluid evaporation and leaching into the HSA would be mitigated. After thermal cycling, valves downstream of the amplification

chambers are opened to drive fluid into the Recovery Chambers where amplicons can be recovered and electrophoresed off-disc via conventional benchtop instrumentation.

Figure 28B depicts an exemplary dye study validating functionality of the architecture, including fluidic chamber sizes (designed to accommodate 20 µL reactions), channel widths for closable valving, vent placements, and alignment of all 3 amplification chambers under a single Peltier for simultaneous thermal cycling. Iterative dye studies enabled optimization of laser height for opening and closing valves as well as radial and angular measurements for valve positioning to ensure accurate, semi-automated laser firing, streamlining the on-disc workflow. Results confirmed the hypothesis that the hydrophobic membranes allowed for thermal pumping while retaining fluid throughout 40 cycles of PCR. It is worth noting that the manufacturer's recommended RT-PCR thermal cycling protocol was used for these studies, and based on the results, we are confident that the optimized protocol comprised of shortened incubation lengths will be successful on-disc. Furthermore, no visible deformation of the disc or leaching of fluid into the HSA was observed, confirming that the selected TaqPath chemistry is compatible with these microdevices. To date, studies are underway to integrate real samples onto the disc and perform amplification on the modified faSTR system whereby further validation studies will be underway.

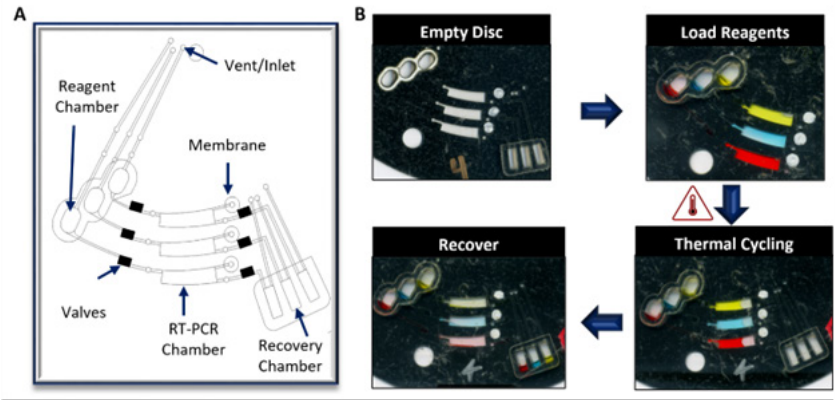

Figure 28. Microfluidic disc for RT-PCR. (**A**) Labeled AutoCAD schematic of architecture in one domain of the microfluidic disc; this architecture is arrayed around the disc 4 total times. (**B**) Scanned images of a dye study in one domain to validate device functionality.

The RT-PCR microfluidic disc architecture design functionality was confirmed via dye studies as seen by **Figure 28**. Initially these studies were completed previously with the use of a heat sensitive adhesive (HSA) material , and on-disc amplification testing were begun. With these studies consistent inhibition was seen on the disc for the amplification of RNA markers. With the transition from in-tube to on-disc it is known that there will be a decrease in sensitivity due to the loss of nucleic acids to the channel walls but severe inhibition on disc had yet to be seen with the use of the HSA. Due to this abnormality the manufacturer of the material was contacted, and it was revealed that the proprietary coating on the material had been changed and this was likely causing the inhibition. Due to this material change, the HSA was exchanged for a pressure sensitive adhesive (PSA) that did not contain this coating. This material change resulted in having to

redesign and optimize the disc architectures for both PCR and extraction microfluidic devices as fluidics would differ from the structural change resulting in a large amount of time lost. For the PSA re-optimization issues presented consisted of fluid bursting through disc layers during thermal cycling, consistent valve opening and channel closure, and ensuring "amplicon" recovery fluid is metered into the three separate recovery chambers. These issues were mitigated by the incorporation of hydrophobic polytetrafluoroethylene (PTFE) membranes to allow for the escapement of air during thermal cycling, optimizing the valve opening and closing laser settings by calculating radial and angular measurements, and increasing radial lengths of channels leading to recovery chambers. After iterative prototyping and multiple dye studies, the fluid flow of version fourteen was validated and used for the system (**Fig. 29A-D**). These dye studies illustrate successful fluid retention during heating, efficient valve opening and closure, and individual fluid recovery throughout the disc without mixing into other channels or spinning out. Once this dye study was complete, the preliminary testing of Qiagen-extracted saliva was amplified on-disc and in parallel in-tube. Through this testing, amplification was not observed in the on-disc replicates (data not shown), and it was hypothesized the inhibition was due to the proprietary HSA materials within the PCR chemistry. From this study, discs were then fabricated using the PSA as the bonding material, and dye studies were completed again. To further evaluate the PSA disc, the recovery of fluid post-thermal cycling was assessed by measuring the volume of dye moved to the Recovery Chamber in order to quantify the recovered fluid volume is greater than the 1 µL that is needed for downstream ME.

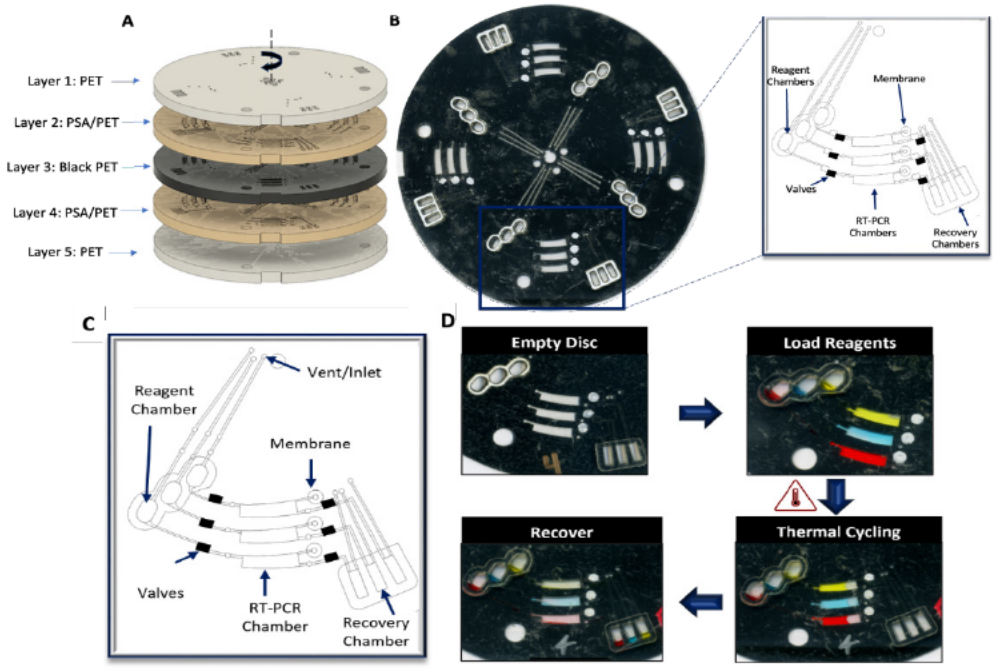

Figure 29. Microfluidic disc for RT-PCR with PSA material. (**A**) Exploded view of the RT-PCR microfluidic disc with the addition of PSA layers. (**B**) Image of fabricated disc with inset to the microfluidic architecture. (**C**) Labeled AutoCAD schematic of architecture in one domain of the microfluidic disc; this architecture is arrayed around the disc 4 total times. (**D**) Scanned images of a dye study in one domain to validate device functionality.

A calibration study disc was designed consisting of repeating Recovery Chamber units (**Fig. 30a**), where varied amounts of blue dye (1 µL, 3 µL, 5 µL, 7 µL, 9 µL, 11 µL, 13 µL, 15 µL, and 17 µL) were pipetted into the Recovery Chambers and imaged by a desktop scanner. The images were analyzed in ImageJ software to measure the pixel numbers, as previously described8 in order to create a calibration curve correlating the measured pixel count to the pipetted volume (**Fig. 30B, R^2=0.9908**). Triplicate dye studies were performed on the amplification discs, the discs were imaged (**Fig. 30C**), and the volumes driven to the Recovery Chambers were quantified (**Table 3**). This study verified that sufficient amplicon volume was maintained (>1 µL) for downstream ME. The recovery volumes showed a decrease from the initial reaction volume of 20 µL to around 5-9 µL. The fluid loss can be attributed to vaporization during thermal cycling and loss of fluid to adhesion within the microfluidic architecture. Once it was confident sufficient volume was recovered, saliva extracts were amplified on-disc.

	Chamber	Pixel Count	Volume (µL)
Domain 1	a	8600	8.947
	b	8400	8.739
	c	8676	9.03
Domain 2	a	5220	5.428
	b	7020	7.302
	c	5220	5.428
Domain 3	a	6808	7.081
	b	7400	7.698
	c	6000	6.24

Figure 30. Calibration Disc and Volume Quantification (A) Schematic of calibration disc architecture. (**B**) Graph of volume calibration values for volume vs average pixel counts. (**C**) Retesting of RT-PCR dye study for Recovery Chamber quantification. **Table 3.** Pixel counts and corresponding volumes calculated for individual Recovery Chambers per 3 domains

2.5 UVA Amplification of Body Fluids on the RT-PCR Microfluidic Disc

Once this work to was completed to ensured microfluidic unit operations within the RT-PCR disc were functional via dye studies, and image analysis was completed to ensure sufficient volume was recovered, sample was then moved onto the microfluidic disc for amplification. The amplification chemistry of 2µL extraction eluate and 18µL of the previously selected One-Step Taq mastermix were pipetted into the Reagent Chambers and rotationally-driven into PCR Chambers that underwent thermal cycling of the previously reduced dwell times for the optimized

protocol, previous studies tested the One-Step Taq mastermix manufacturer protocol on disc, but from the long incubations required all fluid was lost to thermal pumping with delamination of the disc observed (data not shown). The recovered amplicons from the on-disc amplification were separated by benchtop CE and analysed via GeneMarker software. Forensically relevant body fluids of saliva, seminal fluid, venous blood, vaginal fluid, and menstrual blood have been tested with current successful amplification seen for all body fluids as seen by **Figure 31,** with each body fluid tested on one disc per 3 domains with the final domain reserved for a PCR negative. Qiagen extracted RNA was used for the amplification testing, and future work will include the integration of this PCR amplification in combination with the RNA extracted from the one-step rapid enzymatic extraction chemistry as described above.

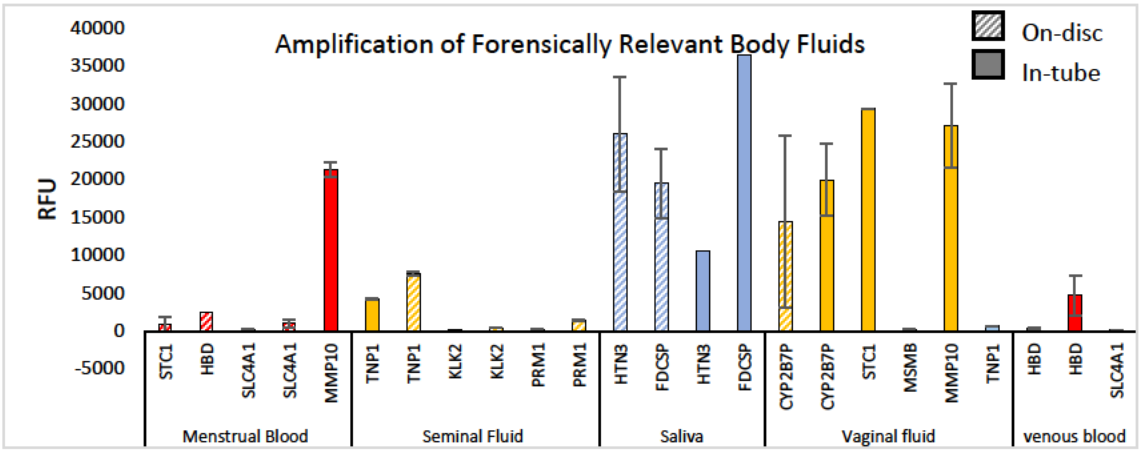

Figure 31. Amplification Body Fluids On-Disc. Amplification of industry standard menstrual blood, seminal fluid, vaginal fluid, and venous blood on the RT-PCR microfluidic disc with in-tube comparisons (n=3).

2.6 RT-PCR Reproducibility Studies

With the validation that all forensically relevant body fluids could be amplified on the microfluidic RT-PCR disc, it was then considered what the margin of error between disc domains would be for amplification. A total of three microfluidic discs were examined with the amplification of saliva for a total of nine domains tested. From this experiment it was seen that across nine domains there was variation present for the success of amplification seen. For a total of nine domains little to no amplification was seen across four domains for the desired 5000 RFU values (**Figure 32**). As three domains were tested per disc, this showed that across three discs, nonsufficient amplification was seen for at least one-domain per disc. This issue raised questions with the efficiency of the heaters being used for the on-disc amplification that will be further discussed in **Section 4 System Engineering**. These errors could be summarized to be caused by issues seen within heating as the insufficient amplification per domain could be due to fluid loss within these domains. This showed us that while amplification has previously been noted as successful there is a reproducibility issue within the hardware that must be addressed for more consistent heating on the microfluidic device that cannot be resovled from commercial peltier systems.

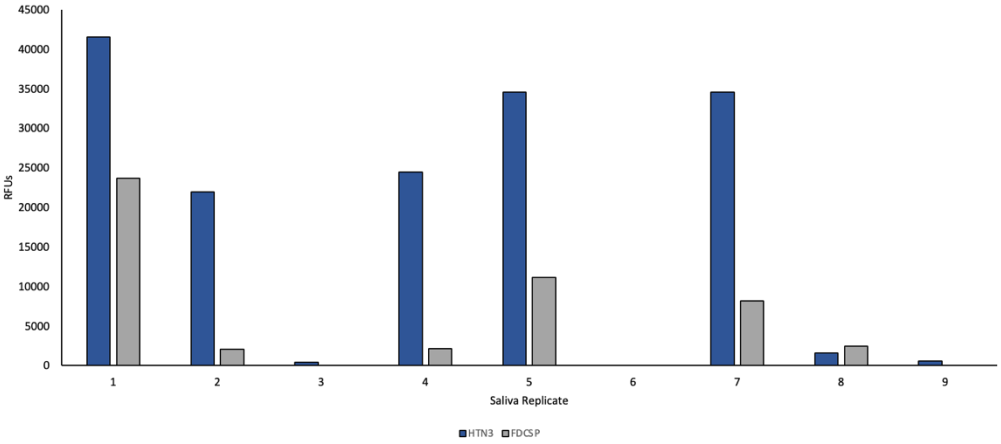

Figure 32. Saliva reproducibility studies. A total of nine domains across three discs were tested for amplification of saliva showing that there is an error within disc-to-disc heating on the peliter system.

2.7 ESR TaqPath Primer Optimization

The findings of the TaqPath™ Primer Optimisation in the 2023 annual report were replicated in triplicate in 2024. The TaqPath™ 1-Step Multiplex Master Mix was used for this research (henceforth referred to as TaqPath™) For these tests, three swabs representing each of five body fluids were amplified in triplicate, using unpooled RNA for the target multiplex and pooled RNA for cross-reactivity testing. For example, the duplex targets buccal samples. Therefore, buccal samples were amplified as single samples (not pooled) and each sample was amplified in triplicate, while RNA from the other body fluids (circulatory blood, menstrual fluid, semen, and vaginal fluid) were pooled for amplification with the duplex. **Table 4** shows the primer concentrations used.

A

Primer panel name	Marker	Primer concentration (µM) in reaction (each fwd and rev)
Duplex	FDCSP	0.04
	HTN3	0.03
Quadruplex	HBD	0.03
	SLC4A1	0.04
	MMP10	0.03
	STC1	0.02
Pentaplex	PRM1	0.05
	TNP1	0.015
	KLK2	0.17
	MSMB	0.015
	CYP2B7P	0.02

B

Thermocycling Conditions						
Temp	25°C	53°C	95°C	95°C	60°C	4°C
Time	2 min	10 min	2 min	15 sec	60 sec	∞
Cycles	1x			40x		

Table 4: Final primer concentrations for the TaqPath™ amplifications. The forward and reverse primers each had a final concentration in the reaction as shown. Adjust formatting/sizing her to match other captions (Panel A). Thermocycling conditions for amplification reaction (Panel B).

This resource was prepared by the author(s) using Federal funds provided by the U.S. Department of Justice. Opinions or points of view expressed are those of the author(s) and do not necessarily reflect the official position or policies of the U.S. Department of Justice.

Duplex

Figure 33 shows good peak balance across FDCSP and HTN3 in samples Bu12 and Bu22 at two input RNA dilutions (5X and 20X). In Bu6, HTN3 failed to amplify. Testing with CellTyper 2, HTN3 was detected in Bu6. As previously reported, the TaqPath™ amplification method was less sensitive than CellTyper 2, which may explain the drop out of HTN3 in Bu6. No cross reactivity was observed with any other body fluids.

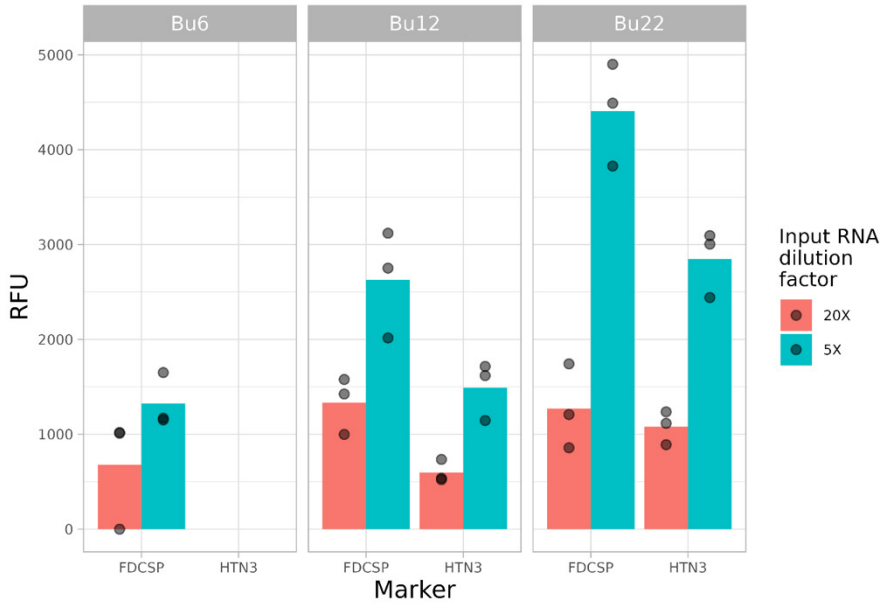

Figure 33: **Results of the triplicate testing of the TaqPath™ optimised primer concentrations, (HTN3: 0.03µM, FDCSP: 0.04µM) for the duplex.** Input RNA was diluted 5X and 20X, both are shown. Bu6 = donor ID 10599, Bu12 = donor ID 052718, and Bu22 = donor ID 3825. Swabs were extracted, purified and DNase treated according to the CellTyper 2 workflow, but amplified with the TaqPath™ polymerase.

Quadruplex

Figure 34 shows the results of the quadruplex TaqPath™ optimisation for the circulatory blood samples. There is good replication across the three replicates and good peak balance, although SLC4A1 is amplified slightly better than HBD as shown by the peak heights.

This resource was prepared by the author(s) using Federal funds provided by the U.S. Department of Justice. Opinions or points of view expressed are those of the author(s) and do not necessarily reflect the official position or policies of the U.S. Department of Justice.

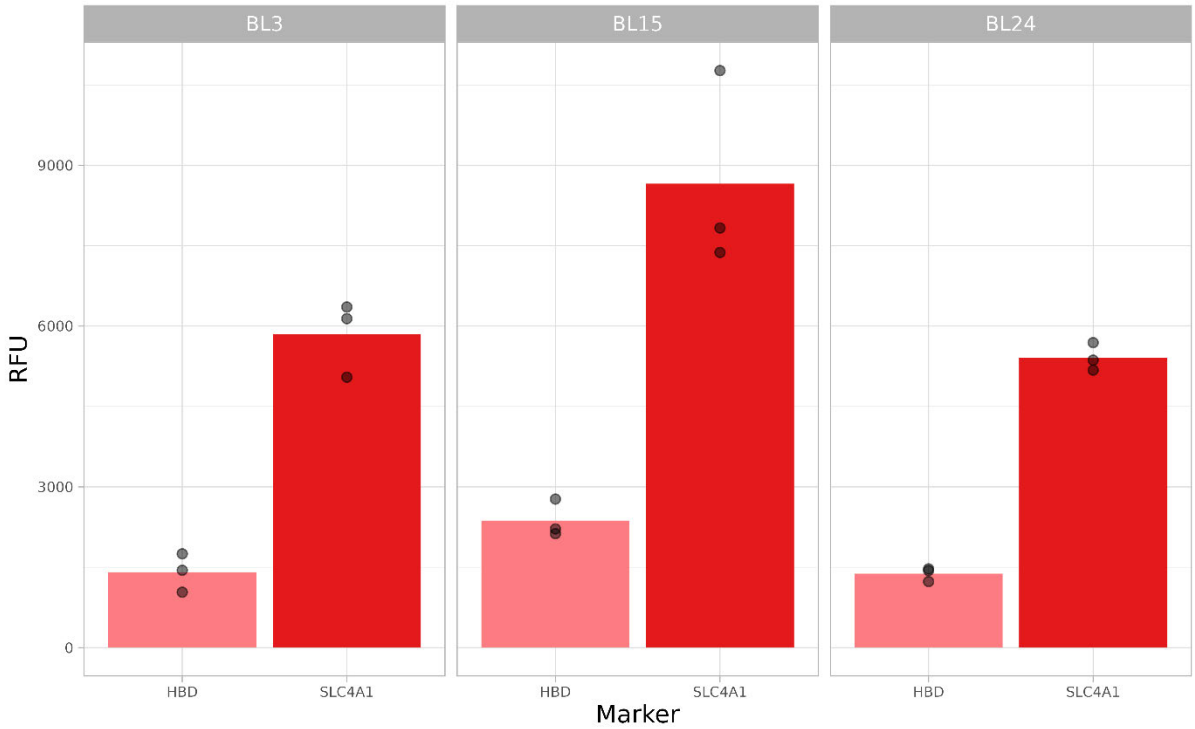

Figure 34: Results of the triplicate testing of the TaqPath™ optimised primer concentrations for the quadruplex, circulatory blood samples only. The final primer concentrations were: HBD: 0.03µM, SLC4A1: 0.04µM, MMP10: 0.03µM, STC1: 0.02µM. Input RNA was diluted 5X and 20X, 20X was omitted as many markers were not detected. BL3 was sourced from patient 1, BL15 was sourced from patient 3, and BL24 was sourced from patient 4. Swabs were extracted, purified and DNase treated according to the CellTyper 2 workflow, but amplified with the TaqPath™ polymerase.

Figure 35 shows the results of the quadruplex TaqPath™ optimisation for the menstrual blood samples. Again there is good replication across the three replicates and good peak balance, although MMP10 is amplified slightly more than the other markers. The MB30 sample has not been successfully amplified. This was also observed in MB30 with the standard CellTyper 2 workflow, which strongly suggests that there is an inherent issue with this sample.

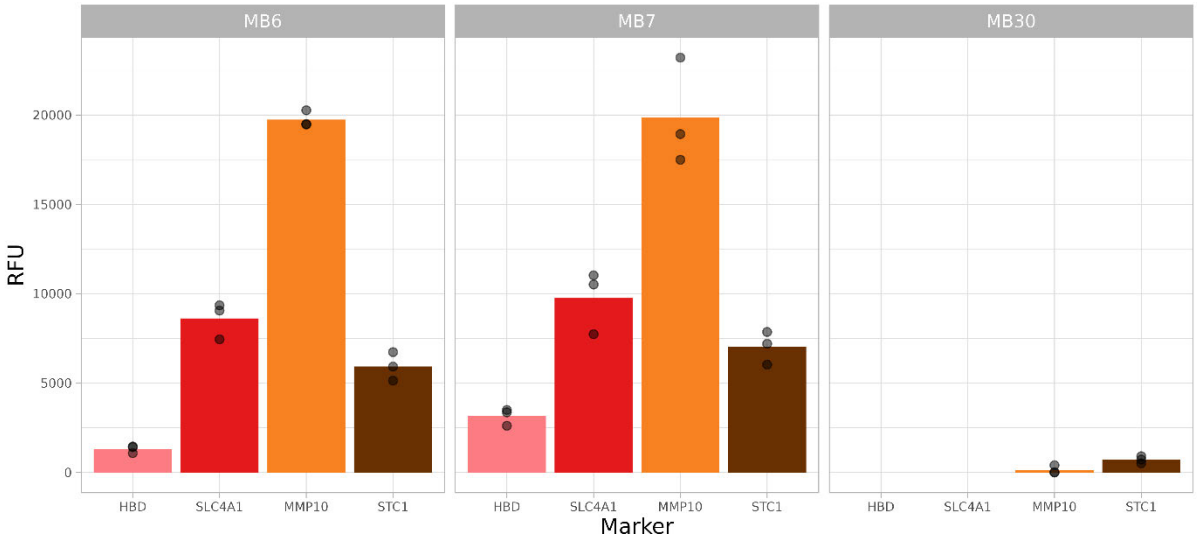

Figure 35: **Results of the triplicate testing of the TaqPath™ optimised primer concentrations for the quadruplex, menstrual blood samples only.** The final primer concentrations were: HBD: 0.03µM, SLC4A1: 0.04µM, MMP10: 0.03µM, STC1: 0.02µM. Input RNA was undiluted and diluted 5X. The 5X dilution is not shown as many markers dropped out. MB6 and MB7 = donor ID 033521 and MB30 = donor ID 3825. Swabs were extracted, purified and DNase treated according to the CellTyper 2 workflow, but amplified with the TaqPath™ polymerase.

In the cross reactivity test with buccal samples, the analysis software called some peaks as STC1 and MMP10. However, manual review of these peaks showed they were low RFU values, not of the expected length, not present in all replicates and are most likely artefacts induced by the TaqPath™ polymerase. Therefore, there was no significant cross reactivity observed.

Pentaplex

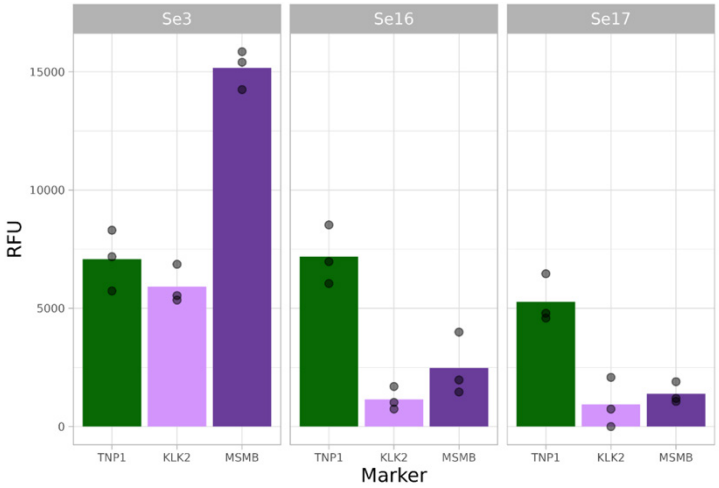

Figure 36: Results of the triplicate testing of the TaqPath™ optimised primer concentrations for the pentaplex, semen samples only. The final primer concentrations were: PRM1: 0.05µM, TNP1: 0.015µM, KLK2: 0.17µM, MSMB: 0.015µM, CYP2B7P: 0.02µM. Input RNA was diluted 100X. Se3 = donor ID "waterbird", Se16 = donor ID 0358 and Se17 = donor ID 0358. Swabs were extracted, purified and DNase treated according to the CellTyper 2 workflow, but amplified with the TaqPath™ polymerase.

Figure 36 shows the results of the pentaplex TaqPath™ optimisation for the semen samples. There is good replication in the three replicates, and good peak balance. As previously observed,

This resource was prepared by the author(s) using Federal funds provided by the U.S. Department of Justice. Opinions or points of view expressed are those of the author(s) and do not necessarily reflect the official position or policies of the U.S. Department of Justice.

PRM1 failed to amplify with the TaqPath™ polymerase. **Figure 37** shows the results of the pentaplex TaqPath™ optimisation for the vaginal fluid samples. CYP2B7P is detected as expected, with greater expression in the VF20 sample. The analysis software has called two TNP1 peaks in replicate 1 of VF3 and replicate 3 of VF20. These are not of the expected size, not present in all replicates and have low RFU values. Therefore, they are likely to be artefacts rather than true off-target amplification.

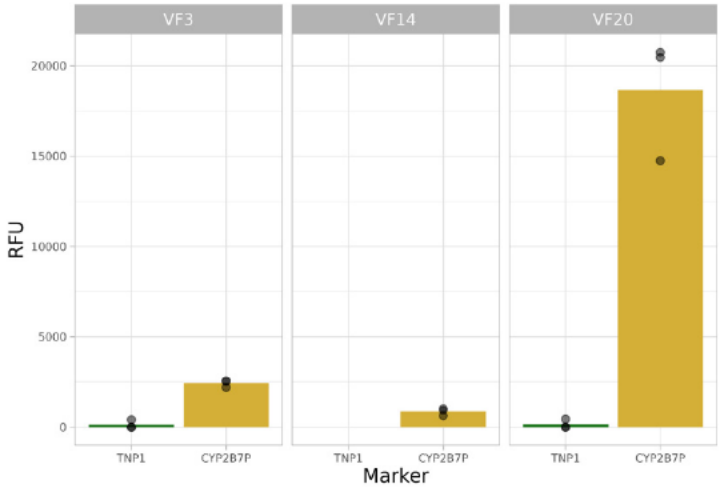

KLK2: 0.17µM, MSMB: 0.015µM, CYP2B7P: 0.02µM. Input RNA was diluted 100X. VF3 = donor ID 10599, VF14 = donor ID 1509 and VF20 = donor ID 052718. Swabs were extracted, purified and DNase treated according to the CellTyper 2 workflow, but amplified with the TaqPath™ polymerase.

CYP2B7P was also detected in all three replicates of the menstrual blood samples. This is expected in menstrual blood samples.The analysis software also called some TNP1 and PRM1 peaks in the buccal and menstrual blood cross reactivity test samples. However, manual review of these peaks showed they were not of the expected length, not present in all replicates and are most likely artefacts induced by the TaqPath™ polymerase. Therefore, there was no significant cross reactivity observed.

2.8 ESR Redesign of Primer Combination to a Single Multiplex

STv5 amplification results

The STv5 single multiplex results were replicated in triplicate. **Table 5** shows the markers and primer concentrations selected.

Table 5: STv5 marker selection and primer concentrations compared to the markers when amplified in three separate multiplexes and compared to STv1.

	Optimised TaqPath™ concentration in reaction (µM)	STv1 concentration in reaction (µM)	STv5 concentration in reaction (µM)
HTN3	0.03	0.03	0.03
SLC4A1	0.04	0.04	-
STC1	0.02	0.02	-
PRM1	0.03	0.03	-
KLK2	0.17	0.17	0.13

CYP2B7P	0.02	0.02	0.02
TNP1	0.015	-	0.02
HBD	0.03	-	0.03
MMP10	0.03	-	0.03

Figure 38 shows that the expected markers were observed in all body fluids. There were some low-level peaks called in off target markers and the no template control (NTC), but these were not present in all three replicates and are likely to come from the higher background noise observed in some TaqPath™ amplifications compared to the standard CellTyper 2 polymerase.

Novel PRM1 primers

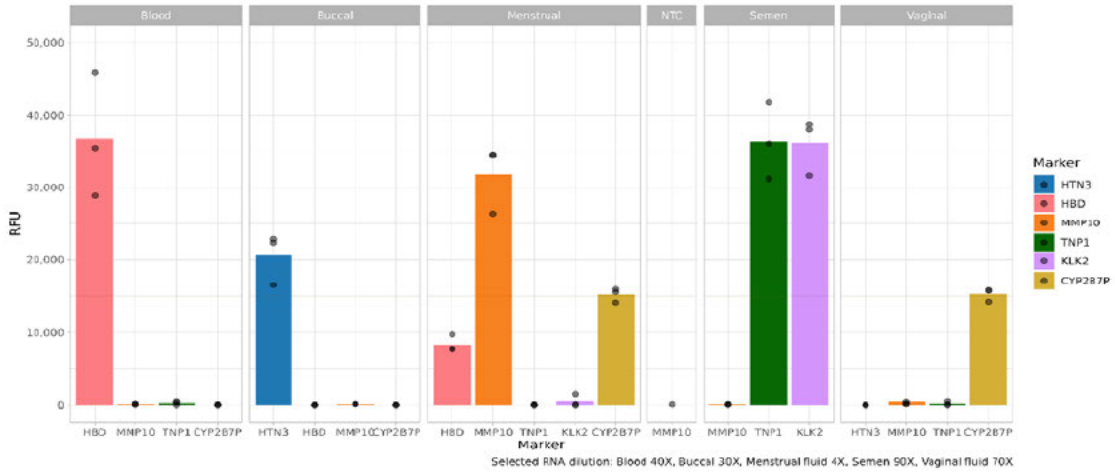

Figure 38: Results of the STv5 triplicate analysis. The same RNA input was used as in the TaqPath™ primer optimization, but aliquots of RNA from the three different donors for each body fluid were pooled.

As previously described, the traditional PRM1 primers consistently failed to amplify with the TaqPath™ polymerase. To address this issue, alternative novel PRM1 primers were designed and tested in 2024. These were designed to amplify in the same cycling conditions as the original PRM1 primers. **Figure 39** shows the position of these primers across two adjacent exons in the PRM1 gene. The new primers are positioned differently, do not have mismatches to the template (as seen in the original reverse primer), and have closer melting temperatures within each primer pair than the original PRM1 primers (as calculated by the PrimerExpress software).

Initial testing and optimisation of these three primer pairs suggested that the 184FC-279RC combination (designated PRM1-S) performed the best when amplified with both the standard CellTyper 2 polymerase and the TaqPath™ polymerase. The new primer pairs were also substituted into the pentaplex and tested with both the standard CellTyper 2 and TaqPath™ polymerases, to check there were no adverse interactions with other primers. Again, the PRM1-S primers performed the best. These primers amplified very highly compared to the other semen and

spermatozoa markers, even when the primer concentration in the reaction was decreased from 0.03µM to 0.01µM.When tested with the CellTyper 2 workflow, there was no evidence that the PRM1-S amplicon was produced in the non-target body fluids available (buccal, circulatory blood, menstrual blood, and vaginal fluid). Overall, the PRM1-S primer pair is a promising candidate for future work, if the TaqPath™ polymerase is used.

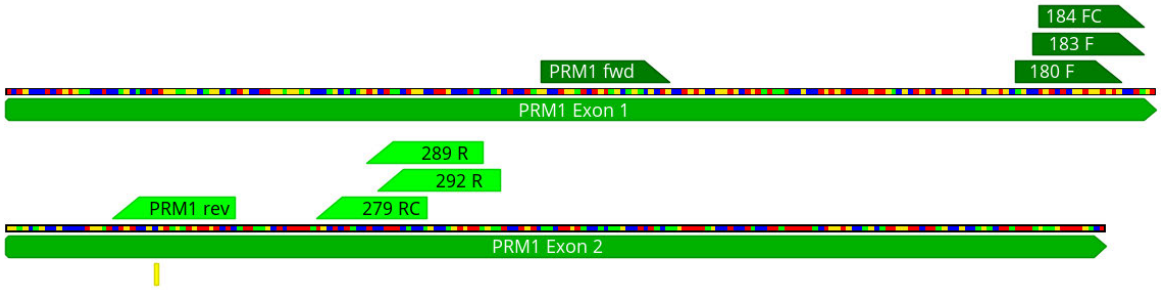

Figure 39: **Positions of the three newly designed primer pairs (180F-289R, 183F-292R and 184FC-279RC) compared to the original CellTyper 2 PRM1 primers across two adjacent exons in the human PRM1 gene.** Mismatches are indicated by a yellow box under the primer and exon sequences. Figure created using Geneious version 2022.1 created by Biomatters. Available from https://www.geneious.com.

2.9 ESR Mixture Typing for On-disc Integration

Swabs containing mixtures of body fluids were analysed with the ESR's CellTyper 2 workflow to provided data for future comparisons with the on-disc system. **Figure 40** shows the results of the saliva/circulatory blood mixed swabs. All expected markers were observed in all three swabs processed and no unexpected markers were observed.

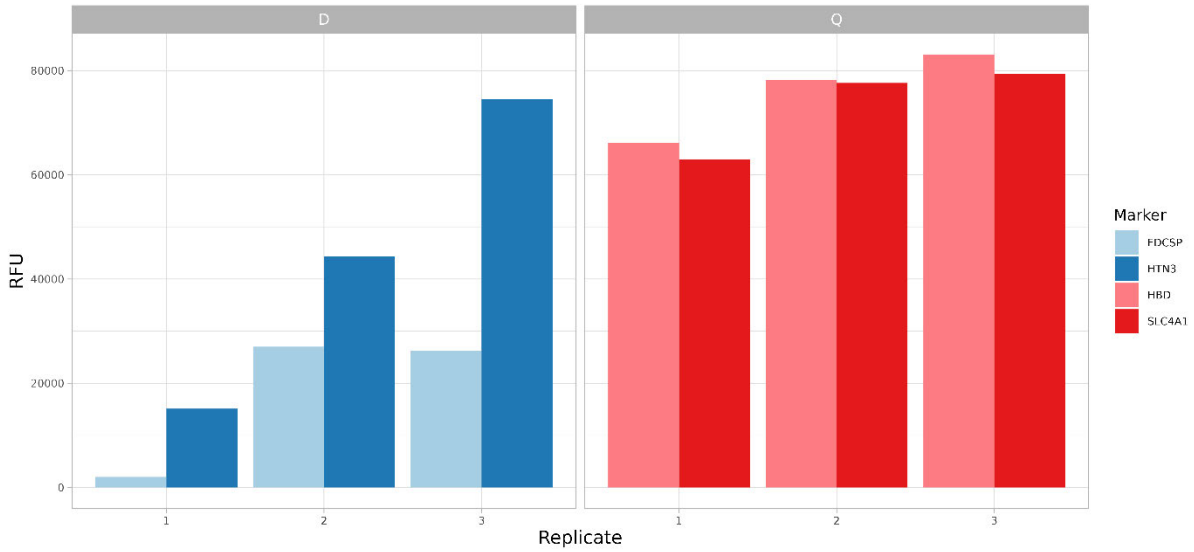

Figure 40: Results of the CellTyper 2 typing of the saliva/circulatory blood mixed swabs. Buccal swabs were collected and dried, then 20 µL of blood was pipetted directly to the buccal swab. An STC1 overamplification peak was removed manually from replicate 3. Sample input RNA was diluted 100X, controls were undiluted.

This resource was prepared by the author(s) using Federal funds provided by the U.S. Department of Justice. Opinions or points of view expressed are those of the author(s) and do not necessarily reflect the official position or policies of the U.S. Department of Justice.

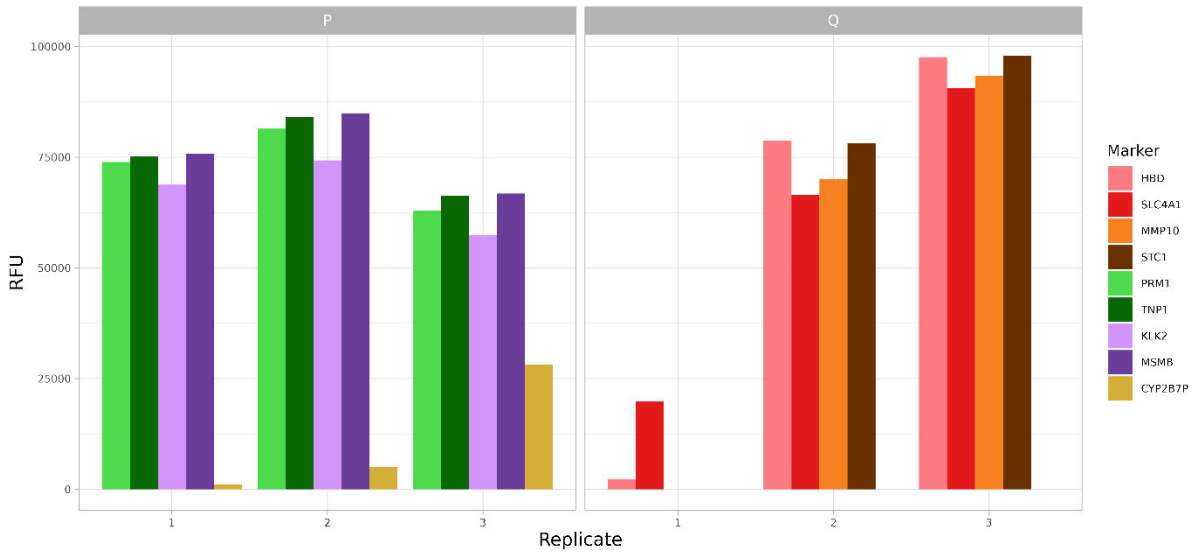

Figure 41. Results of the CellTyper 2 typing of the menstrual blood/semen mixed swabs. Menstrual blood was collected in swabs by the donor and dried, then 20 µL of neat sperm was pipetted directly to the MB swab. Sample input RNA was diluted 100X, controls were undiluted

Figure 41 shows the results of the menstrual blood/semen mixed swabs. All expected markers were observed in all three swabs processed, except for the menstrual blood markers from swab 1, which were missing. As these swabs were from different menstrual blood donors, it is possible that MMP10 and STC1 were not expressed by that donor at the time of collection. **Figure 42** shows the results of the vaginal fluid/semen mixed swabs from the pentaplex. All expected markers are present. The third and ninth replicates have lower CYP2B7P peaks than the other replicates. There are some comparatively low peaks in the reverse transcriptase negative controls for replicates 2, 3 and 4. These replicates needed a second DNase treatment before having a clear DNA quantification value. Possibly there is a very low level of DNA still present which causes these peaks. The high RFU values in the samples despite a 100X input RNA dilution suggests these swabs were a very

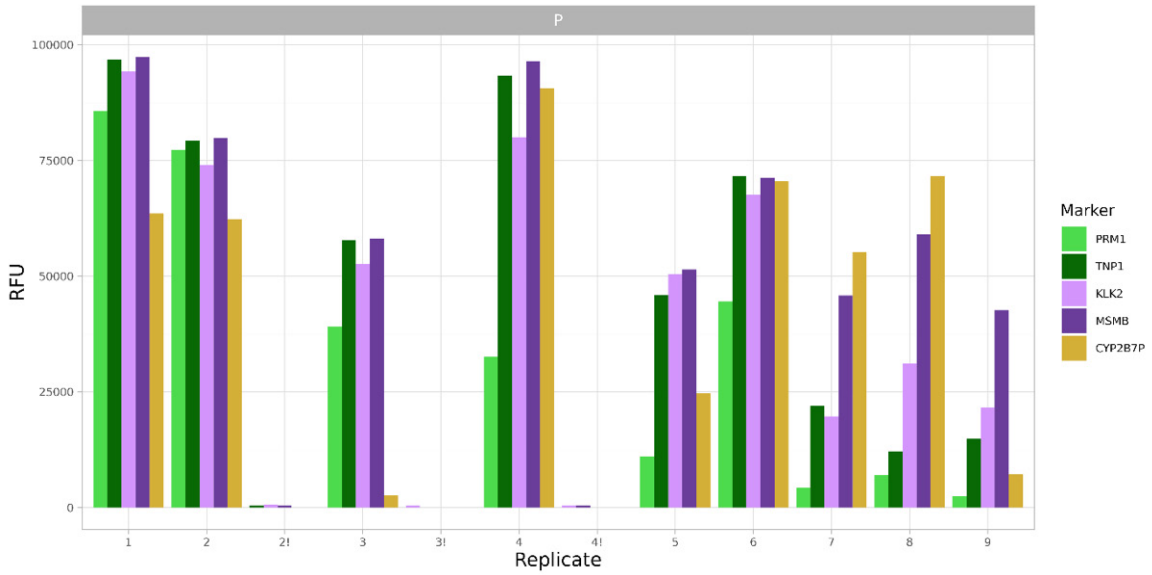

Figure 42: **Results of the CellTyper 2 typing of the vaginal fluid/semen mixed swabs (pentaplex only).** Vaginal fluid was collected in swabs by the donor and dried, then 20 µL of neat or diluted sperm was pipetted directly to the VF swab. Replicates 1-3 had neat semen added, 4-6 had 10X diluted semen added and 7-9 had 100X diluted semen added. Sample input RNA was diluted 100X, controls were undiluted. Replicates with an "!" indicate the reverse transcriptase negative control, which does not have reverse transcriptase enzyme added in the cDNA synthesis step.

rich source of nucleic acids. **Figure 43** shows the results of the vaginal fluid/semen mixed swabs from the quadruplex. Although these results would not necessarily be expected from a vaginal fluid/semen sample, depending on the vaginal fluid donor's menstrual cycle on the day of collection, there may still be some residual expression of the menstrual blood markers. All swabs in this mixture were collected from the same donor on the same day, which would explain why MMP10 has appeared in multiple replicates in this possible scenario. This analysis completed by ESR was then replicated by UVA for concurrence evaluations.

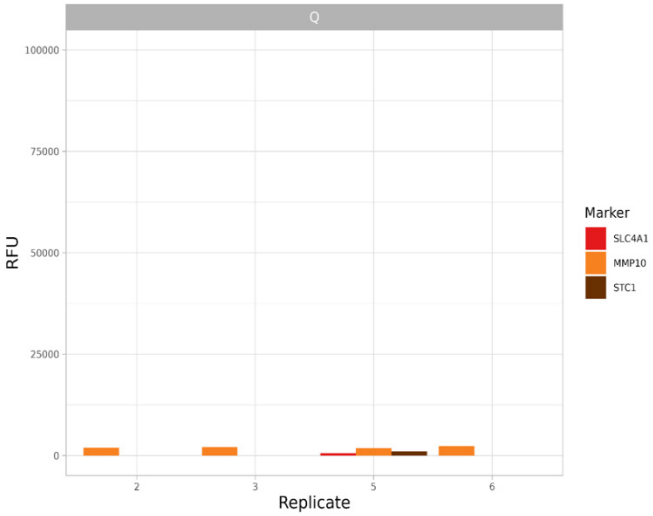

Figure 43: Results of the CellTyper 2 typing of the vaginal fluid/semen mixed swabs (quadruplex only). Vaginal fluid was collected in swabs by the donor and dried, then 20 µL of neat or diluted sperm was pipetted directly to the VF swab. Replicates 1-3 had neat semen added, 4-6 had 10X diluted semen added and 7-9 had 100X diluted semen added. Sample input RNA was diluted 100X, controls were undiluted. The same axis limits are retained from the pentaplex results from these swabs to maintain perspective.

This resource was prepared by the author(s) using Federal funds provided by the U.S. Department of Justice. Opinions or points of view expressed are those of the author(s) and do not necessarily reflect the official position or policies of the U.S. Department of Justice.

2.10 UVA Multiplex Primer Panel Concordance Testing

Additional testing of the STv5 single multiplex was also completed by UVA. This testing included the original primer recipes tested by ESR with testing beginning at an initial 10x increased concentration tested as previous work with ESR showed that sensitivity between the commercial CE instruments and implementation on disc required a 10x concentration increase (**Table 6**). These concentrations showed amplification of the originally required markers but once mixtures were tested, it was realized that the saliva and venous blood markers were not observed to the threshold that was desired for each markers, as well as, low expression of markers such as vaginal fluid (CYP2B7P) and menstrual blood (MMP10) not seen to the threshold that was desired (**Figure 44**). This was an issue, especially as the translation of this primer panel onto the microfluidic disc would result in a sensitivity hit.

Table 6. Original 10x ESR's STv5 primer panel

Panel	Primer	Volume 100uM stock (fwd and rev) for 10uM Dilution (uL)	Dilute each for 10uM stock	ESR Target Concentration in reaction	Volume of 10 uM stock for target (uL)	Dilute to 300 uL
Multiplex	HTN3	10	80	0.3	9	222
	KLK2	10	80	1.3	39	
	CYP2B7P	10	80	0.2	6	
	TNP1	10	80	0.2	6	
	HBD	10	80	0.3	9	
	MMP10	10	80	0.3	9	

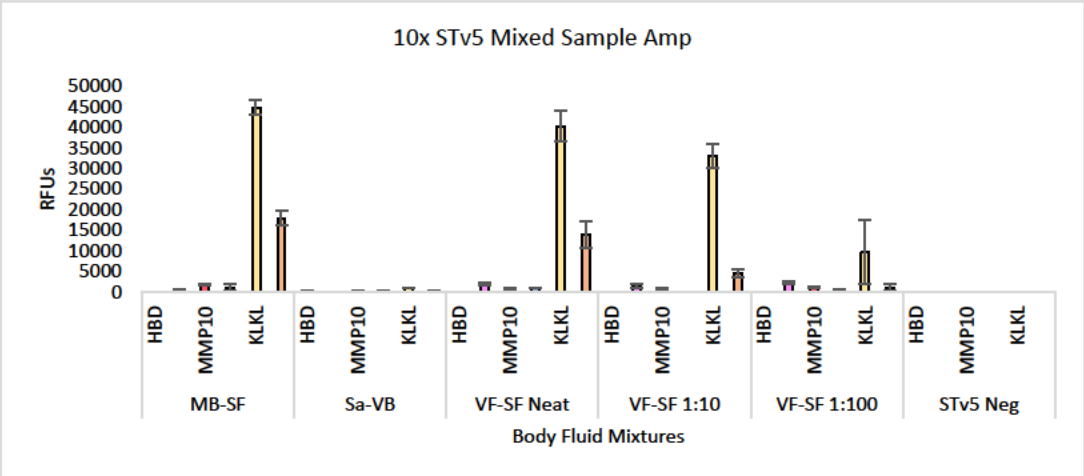

Figure 44. Amplification of mixed body fluids using 10x ESR's STv5 primer panel. Mixtures tested include menstrual blood and seminal fluid, saliva and venous blood, and vaginal fluid and seminal fluid (neat, 1:10, and 1:100 ratios to TE Buffer (n=3).

This resource was prepared by the author(s) using Federal funds provided by the U.S. Department of Justice. Opinions or points of view expressed are those of the author(s) and do not necessarily reflect the official position or policies of the U.S. Department of Justice.

This led to the re-optimization of the primer panel that included doubling the concentration of the HTN3 and HBD markers (**Table 7**). This testing resulted in more consistent amplification of the expected markers per body fluids, with some variability seen within the expression of TNP1 (**Figure 45**). Mixtures were then tested and both HBD and HTN3 markers were able to be seen within the venous blood and saliva mixture although fluorescence markers were still not observed to the extend that was desired, leading to an additional 10x concentration of all primers except KLK2 as expression of this marker was sufficient (**Figure 46**).

Table 7. 2x ESR's STv5 primer panel for HBD and HTN3

Panel	Primer	Volume 100uM stock (fwd and rev) for 10uM Dilution (uL)	Dilute each for 10uM stock	ESR Target Concentration in reaction	Volume of 10 uM stock for target (uL)	Dilute to 300 uL
Multiplex	HTN3	10	80	0.3	18	222
	KLK2	10	80	1.3	39	
	CYP2B7P	10	80	0.2	6	
	TNP1	10	80	0.2	6	
	HBD	10	80	0.3	18	
	MMP10	10	80	0.3	9	

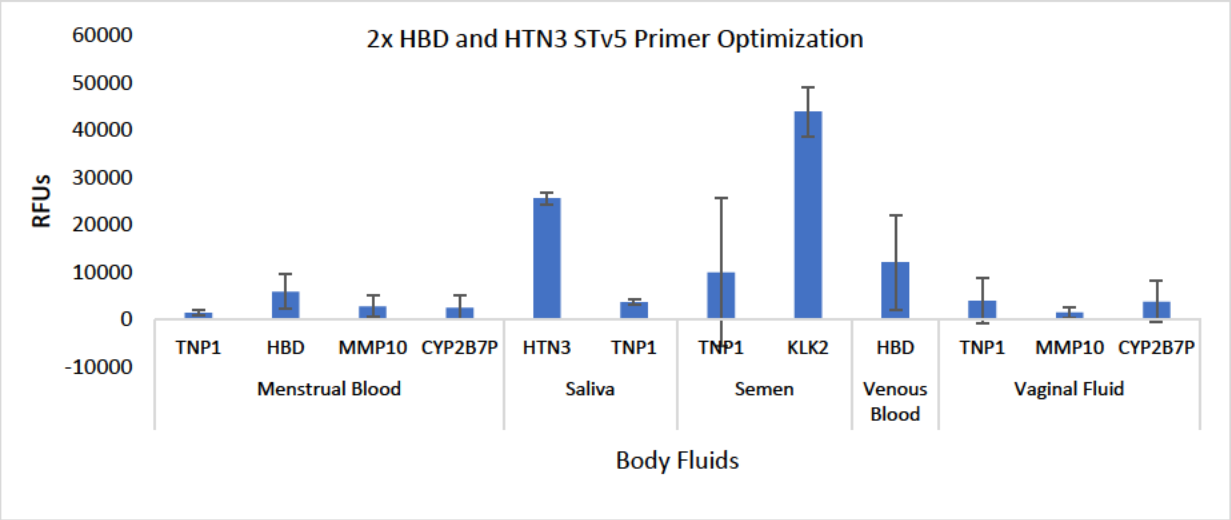

Figure 45. Amplification of body fluids with 2x HBD and HTN3 primers. Amplification of all body fluids in-tube (n=3).

This resource was prepared by the author(s) using Federal funds provided by the U.S. Department of Justice. Opinions or points of view expressed are those of the author(s) and do not necessarily reflect the official position or policies of the U.S. Department of Justice.

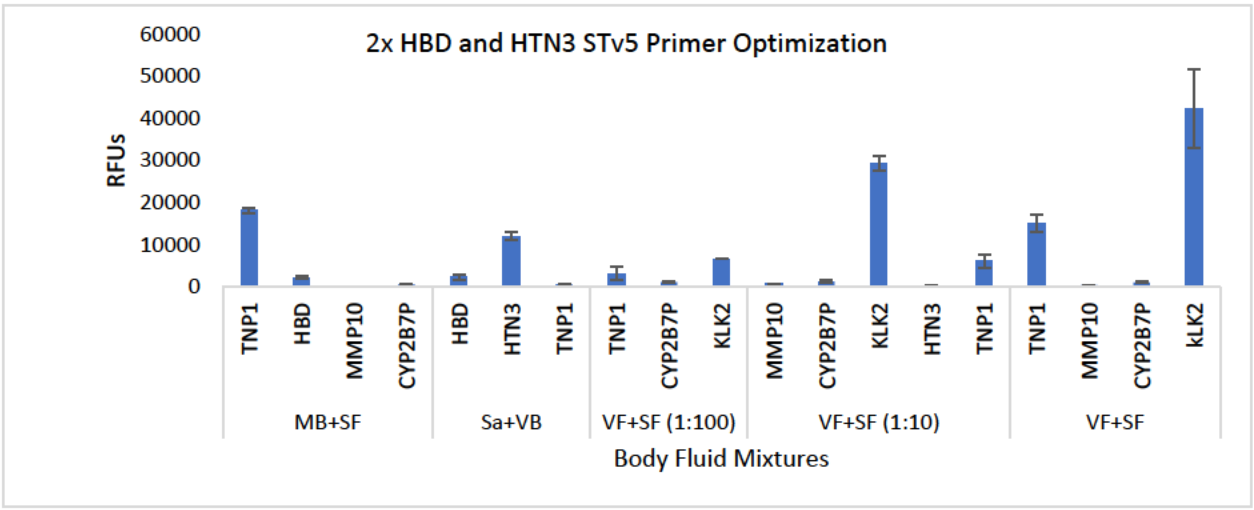

Figure 46. Amplification of body fluid mixtures with 2x HBD and HTN3 primers. Mixtures tested include menstrual blood and seminal fluid, saliva and venous blood, and vaginal fluid and seminal fluid (neat, 1:10, and 1:100 ratios to TE Buffer (n=3).

Once the primer panel was validated in tube it was then tested on disc but testing was unsuccessful. From this study, no markers were able to be seen for any body fluids besides trace amplification seen within seminal fluid. As previously stated, from previous work with ESR, it has been seen that primer sensitivities have differed between genetic analysers. Because of this difference, UVA typically uses a 10x concentration for all primer panels especially as the transition from in-tube to on-disc will impact sensitivity and from the primer concentrations provided by ESR these concentrations were incredibly low in contrast to the starting concentrations of the previous duplex, quadraplex, and pentaplex primers, thus, a full 20x concentration increase was not an unreasonable requirement. Again, all primers were subsequently increased an additional 10x. All body fluids were amplified individually with the 20x STv5 primer concentrations following **Table 8**. From this modification, successful amplification of all body fluids was able to be seen individually, as well as, in mixtures as shown by **Figure 47 and 48**.

Table 8: 10x STv5 marker selection and primer concentrations

Panel	Primer	ESR Target Concentration in reaction	Volume 100uM stock
Multiplex	HTN3	3	9
	KLK2*	13	39
	CYP2B7P	2	6
	TNP1	2	6
	HBD	3	9
	MMP10	3	9

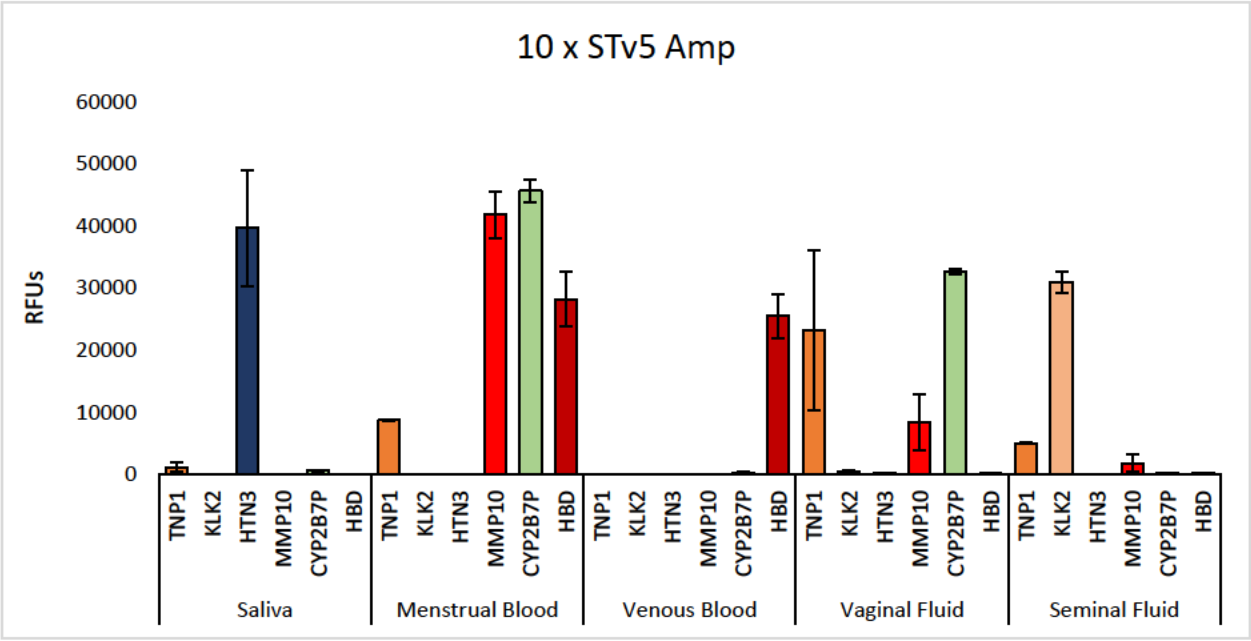

Figure 47: 10x STv5 primer panel amplification of all body fluids. n=3

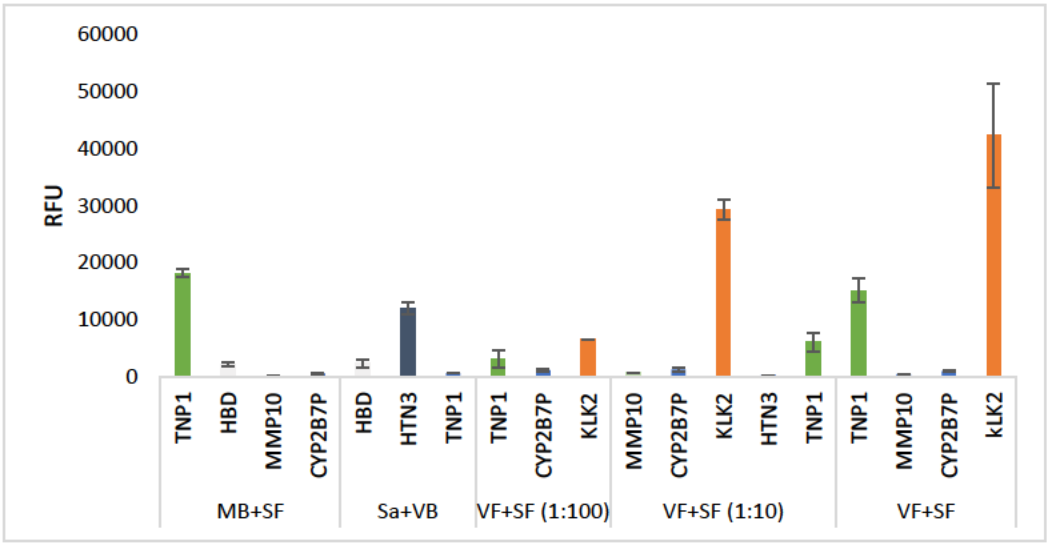

Figure 48: Results of UVA's amplification of mixed body fluids with the STv5 primer panel. Samples tested include menstrual blood and seminal fluid in mixture, saliva and venous blood in mixture, and vaginal fluid and seminal fluid (neat, 1:10, and 1:100 ratios) (n=3).

2.11 UVA 'Sample Preparation "Microfluidic Disc Dye Study"

The microfluidic sample preparation disc described consists of five layers comprised of a top and bottom layer of clear PET, a middle optically dense black PET (bPET)-the valving component, and layers bonded by a proprietary pressure sensitive adhesive (PSA). Accessory

architecture of polymethylmethacrylate (PMMA) can be added onto the top of the disc by PSA to increase the available reagent volume. This disc encompasses the microfluidic architecture of the previously described co-extraction and RT-PCR devices. These individual discs were combined in order to integrate the assay components into one process for both mRNA extraction and amplification. With the integration of these two individual architecture components many issues were observed before the final version 13 was able to be validated. These issues included severe back pressure that was observed between the valving components of the PCR Sample Chambers and the thermal cycling chambers. It was observed that once the extraction eluate was metered into the Sample Chambers the fluid would burst through the top two chambers into the bottom PCR Sample Chamber. This problem was attempted to be addressed by the addition of another vent going through the Sample Chamber where the air could be displaced for the fluid. Ultimately this resulted in the fluid bursting through the vent during thermocycling and did not fully address the problem. Additional edits included increasing and moving the Sample Chambers in order to allow for more fluid to be metered into the chambers without creating more pressure, as well as, snaking the vent through the top two layers of the microfluidic device and the bottom three and four layers. The vent snaking helped reduce the fluid loss during thermal cycling but did not help to reduce back pressure. Finally an alternative valving strategy was attempted of opening the valve after extraction metering and the valve leading into the thermal cycling chamber and spinning the extraction eluate and the PCR chemistry directly into the thermal cycling chambers. This method helped reduce the back pressure as the intermediate of the extraction eluate metered into the sample chambers along with the PCR reagents was not created which had resulted in the fluid bursting down through the disc layers.

The microfluidic architecture of the sample preparation disc was validated by performing dye studies to ensure successful unit operations on disc (**Fig. 45**). In this study a 100 µL of blue dye

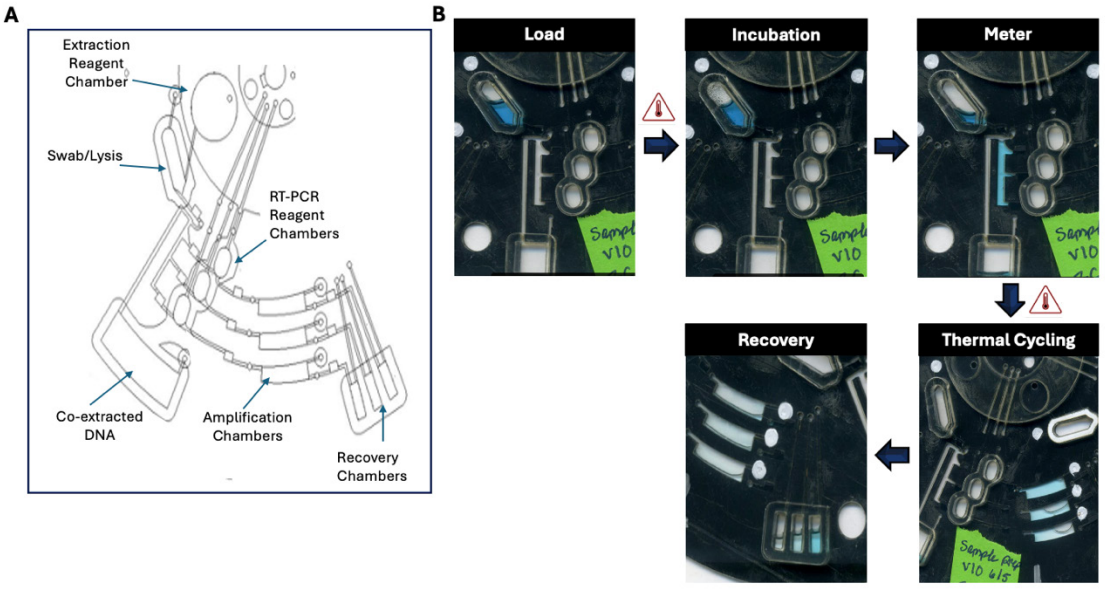

Figure 49. Sample Preparation v13 microfluidic device. (**A**) Schematic of the on-disc microfluidic architecture and (**B**) on-disc assay visually portrayed via dye study.

was pipetted into the extraction reagent chamber to imitate the extraction buffer. For initial validation studies, the disc was mounted on the Power, Time, and Z-Height Actuated Laser (PrTZAL) system used within the Landers Lab to perform operations of spinning, mixing, and laser valve opening. The blue dye was spun down into the swab chamber and then heated on the stand-alone Peltier system for cell lysis. The valve below the Swab chamber was optically opened via laser ablation, and the extracted eluate was spun down to fill metering chambers, with remaining eluate overflowing into the Co-Extracted DNA chamber. Valves are laser opened once more and "eluate" is spun into PCR thermocycling chambers where 18 µL of water, mimicking PCR master mix, is added and heated. Valves downstream of the thermocycling chambers are then opened and the fluid is spun into the "amplicon" recovery chambers, where they can be pulled off disc for electrophoresis. This dye study was able to show successful unit operations necessary for the co-extraction and RT-PCR assays on disc. This disc workflow includes a 10 minute lysis incubation for the enzymatic extraction and a 45 minute PCR amplification, with the additional 10 minutes it would take to perform microchip electrophoresis leaving an additional 25 minutes for any on-disc operations within the 90 minute time frame.

While these issues were addressed on the dye study of the microfluidic device and demonstrated successful fluidic operation, once biological sample was introduced tp the microdevice other issues were observed. As saliva and seminal fluid were successfully extracted within the enzymatic extraction microfluidic device both of these fluids were tested on the sample preparation disc with unsuccessful amplification observed. It was seen that as the biological samples were tested with the on-disc chemistries, the incredibly viscous reagents cause the fluids to backtrack throughout the disc as opposed to staying within the thermocycling chambers. This was not seen within the dye studies as the fluids used are much less viscous. While fluid on the microfluidic device will take the path of least resistance, the viscosity difference between the dye studies to the implementation of reagents on-disc did not create such a trail of reagents with the dye as the biological sample did, resulting in a path of fluid to easily wick back out of the thermal cycling chambers.

As previously addressed, the exchange of the HSA material to the PSA material caused issues that had not been previously observed within the Landers laboratory, as the HSA material is able to address channel closure in a way the PSA is not able to. With the laser valving mechanism used within the laboratory, the z-height of the laser can be raised in order to create a dispersed fan of the laser that can be absorbed by the HSA and melt the channels so that fluid cannot flow back into downstream architecture. After the material change, this method could not be used for channel closure as the PSA will not absorb the heat in this way and only create holes within the channels. Due to this issue an extensive literature search was commenced in order to asses an alternative valve closure strategy that could address this issue while still being compatible to the disc architecture already validated and would fit along the presented integrated system. After the literature search was completed it was determined that the optimal valving strategy would include a pinch valve as this method could be implemented along the top of the disc without altering the microfluidic architecture already presented. Testing began to address alternative pinch valves that

could be implemented along the sample preparation device, finally settling on a magnetically actuated pinch valve along the channels before the thermal cycling chambers to block fluid that would be pushed out of the thermal cycling chambers back up to the PCR Sample Chambers. These magnetically actuated valves are currently being assessed as magnets of varied strength have been purchased with preliminary studies being completed using valves that are able to situate along the opened valves without touching the Peltier components. Due to the malleability of the PSA material these magnets appear to be able to pinch off the fluid flow blocking the movement of sample from the thermal cycling chambers back up into upstream architecture along the microfluidic disc. Preliminary studies are still being completed to analytically determine the strength required of the magnetically actuated valves with a schematic of the magnets along the disc shown by **Figure 50**.

3. Microchip Electrophoresis

3.1 Microchip Electrophoresis and Data Analysis

For microchip electrophoresis, the automated mechatronic system, was connected to a PC laptop containing software to control all the necessary movements of the μEDisc as well as data collection and adaptation for analysis in GeneMarker HID software[22,25]. Sample input volumes, heating during separation, and injection times were varied to optimize electrophoresis conditions. The appropriate sample volume was determined by adding either 1, 2, or 3 µL of sample to 3 µL ILS and nuclease-free water to bring the total reaction volume to 13 µL. For heating studies, a metal stage in contact with the underside of the COC chip was either heated to 37 °C throughout

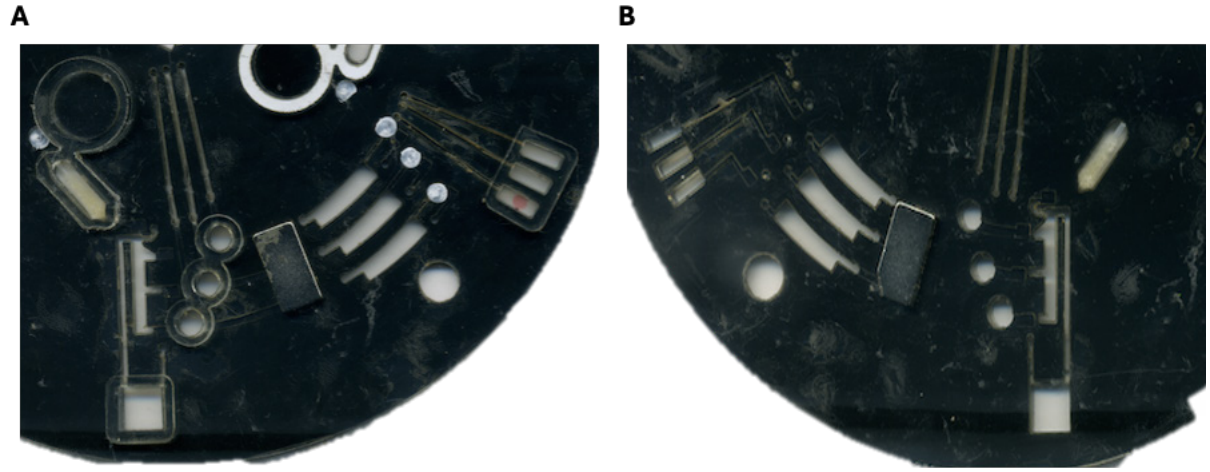

Figure 50. Magnetically actuated pinch valve along sample preparation device. (**A**) Image of the front of the Sample Preparation device with the magnet placed along the channels before the PCR Thermal cycling chambers and (**B**) an image of the back of the Sample Preparation microfluidc device with the underside of the magnetically actuated pinch valve.

separation via a Peltier heater or the stage was not heated during separation, and injection times were varied using 60, 90, 120, and 180 seconds. Prior to separation, a novel hydrophobically-modified polyacrylamide polymer [29] was centrifugally loaded via device rotation at 3000 RPM for 5 min, followed by the actuation of two laser valves[26] (described in Woolf *et al.*) to establish

electrical connectivity with the polymer in the sample waste (SW) and buffer (B) electrodes. A third laser valve was actuated and the μEDisc was spun at 3000 RPM for 10 sec to allow the sample to interface with the sample (S) electrode. Off chip, the sample was heated at 95 °C for 3 min then snap cooled on ice for 3 min then 3 µL of the cDNA was added to 3 µL WEN ILS 500 (Promega, Madison, WI, USA) and 6.5 µL nuclease-free water (Molecular Biologicals International, Inc., Irvine, CA, USA) prior to loading into the μEDisc. Once fluidic movement was complete, the μEDisc separation channel was located rotationally via the photo-interrupter and clamped by the clamping motor to establish contact between the gold pogo pins with the gold electrode pads on the μEDisc. Electrokinetic injection was performed at 600 V for 120 sec from S to SW electrodes, and separation at 1500 V from B to BW with a 200 V pullback voltage applied at S and SW for 500 sec. The effective length of separation (cross-t to detector) is 6 cm. At completion of the separation, integrated data analysis was performed in the software through a data analysis pipeline, which involves trimming of primer peaks, baseline subtraction, pullup correction, and 10X signal amplification using a digital filter. The processed data was then re-formatted and saved as a ".txt" file for compatibility with Microsoft Excel, as well as a ".fsa" file for forensic analysis in GeneMarker HID software (V2.8.2)[23]. The μEDisc and automated system were used to separate all of the single- and multiple-body fluid samples amplified with one of the three body fluid panels.

3.2 Microfluidic Disc and System Integration for Electrophoresis

In previous work, Albani et al. optimized three bfID panels consisting of eleven mRNA genes for identifying five forensically-relevant body fluids[2]. The Duplex Panel consists of FDCSP (170 bp; HEX) and HTN3 (138 bp; HEX) to identify buccal mucosa or saliva. The Quadruplex Panel consists of HBD (176 bp; FAM) and SLC4A1 (102 bp; HEX) to identify venous blood, and MMP10 (108 bp; HEX) and STC1 (105 bp; FAM) to identify menstrual blood. The Pentaplex Panel consists of PRM1 (150 bp; HEX) and TNP1 (102 bp; FAM) to identify spermatozoa, KLK2 (135 bp; HEX) and MSMB (142 bp; FAM) to identify seminal fluid, and CYP2B7P (113 bp; HEX) to identify vaginal fluid. For each panel, resultant amplicons can be electrophoretically-separated and detected using fluorescently labeled primers (FAM and HEX). All PCR amplicons were less than 200 base pairs (bp) in length, and widely published in the forensic literature whereby analysis was typically performed using conventional capillary electrophoresis (CE) instrumentation[30,31]. Conversely, we describe the adaption of such assays onto a microfluidic electrophoresis disc (μEDisc) capable of electrokinetic separation and LIF detection of these forensically relevant mRNA targets.

The microfluidic disc was fabricated using the cost-effective Print, Cut, and Laminate method, previously described[14]. The μEDisc consisted of three identical domains for electrophoresis, each containing chambers for separation polymer and sample, enclosed reservoirs for sample (S), buffer (B), sample waste (SW), and buffer waste (BW), as well as an injection molded COC chip containing the separation cross-T and channel (**Figure 51A**). The electrophoresis microchip has an effective separation length of 5 cm with ~1 cm arms connecting the cross-T to the the S, B, and SW reservoirs. Each domain has gold electrodes capping the S, B,

SW, and BW reservoirs to interface a voltage power supply with hermetically sealed fluid. To perform electrophoresis with this microdevice, sample/reagents and separation polymer are pipetted into the Sample Chamber and Polymer Chamber, respectively (**Figure 51B**). Polymer is then rotationally-driven into two metering chambers and through the COC chip containing the separation cross-T (**Figure 51C**). Valves are opened via laser actuation to allow the metered polymer to be centrifugally driven to the B and SW reservoirs (**Figure 51D**). Finally, the last laser valve is opened to enable the sample/reagents to flow to the S reservoir before electrophoresis can begin (**Figure 51E**).

An instrument capable of electrophoresis in a polyethylene disc with the corresponding software was developed to allow for automated microfluidic steps on a centrifugal microfluidic disc[25]. The same instrument and software were repurposed to permit flow and produce results with the mRNA targets in the body fluid panels on the μEDisc. Briefly, the disc is mounted onto a rotational platform, much like a CD-ROM, and an optical sensor placed near the outer perimeter of the disc allows for accurate positioning of the μEDisc (**Figure 52**). The motor driving the rotational platform is controlled by software (Atmel Studio v7.0) where the spin speed is defined by user input. The system associates architectural features with coordinates that are defined by: 1) the distance from the center of the disc, and 2) the number of degrees from 'home' (which is 0°); these are input to the software to align the red laser diode with valves that are opened by ablation. Similarly, defined by coordinates relative to 'home', the system can rotate the disc to the accurate position needed to align the gold POGO pins for contact with the gold electrodes for application of voltage to the separation microchannel. Specific voltage/times are used to define consistent

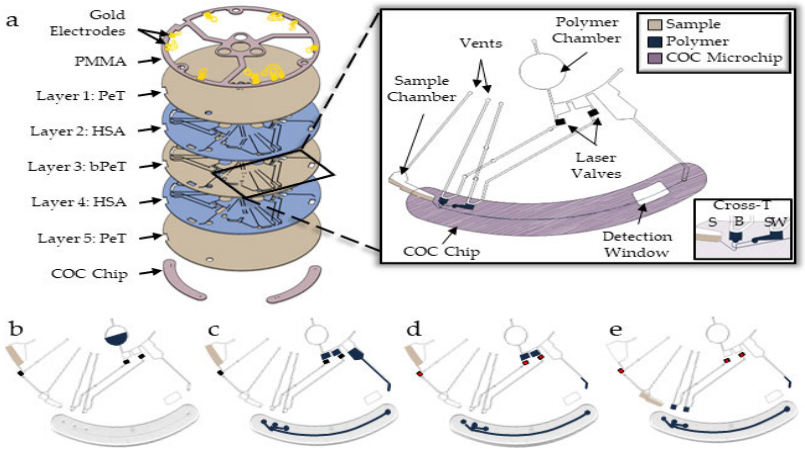

Figure 51. Design and architecture of μEDisc for electrokinetic separation of amplified forensically relevant fragments. (a) An exploded view of the 5 layer microfluidic disc, comprised of polyethylene terephthalate (PeT), heat sensitive adhesive (HSA), and black PeT with accessory pieces on the top and bottom of the disc, including poly(methyl methacrylate) (PMMA), gold electrodes, and an injection molded cyclic olefin copolymer (COC) separation chip. The inset shows a labeled schematic of an individual domain in the disc with a close-up of the separation cross-T and the sample (S), buffer (B), and sample waste (SW) reservoirs. Fluid was rotationally-driven through the architecture in four simple steps: (b) sample and polymer were pipetted into the respective chambers and (c) polymer was centrifugally metered. (d) Laser valves were then opened (as indicated by a red 'X'), and (e) the disc was spun to rotationally-drive fluid into the S, B, and SW reservoirs.

injection at the cross-t followed by size-based separation of the fragments. The detection system is equipped with a blue laser (488 nm) for excitation, with emitted light funneled by the optics to a four-color optical detector (photomultiplier tube) as fragments pass through the detection window.

3.3 Optimizing Separation Parameters for ME

Unlike commercial capillary electrophoresis (CE), the development of CE on novel systems such as the one described herein inherently requires that a number of parameters be optimized for effective functioning of the system[1]. Previous work has shown sufficient separation of 10 STR loci ranging from 80 to 500 bp using this on-chip platform[22,25], thus, in this study we focused on optimizing sample input, heating of the separation channel, and sample injection time to adequately separate the amplicons in three body fluid panels.

When compared to gold standard instrumentation, where the electrokinetically-injected sample contains amplified fragments, internal lane standard (ILS), and hi-di formamide, the sample injected on the μEDisc system contains amplified fragments, ILS, and water. While this difference (water versus formamide) may cause concern, previous work has shown this has no adverse effects on the size-dependent separation on-disc[23]. The ratio of sample volume to injection total volume is doubled on this system; in other words, 1 µL of amplified sample goes into 9 µL of Hi-Di formamide and ILS on a conventional CE system, whereas 3 µL amplified sample goes into 10 µL of water and ILS on this system. Due to differences between conventional CE and this system, the parameters for electrophoresis (i.e., sample volume, heating during separation, and injection time) should be optimized to show sufficient size separation of the amplified fragments.

To assure optimal conditions for separation of the fragments, we assessed the height, size, and shape of the fluorescent signal, or peaks, for three different fluorescent channels: the blue and green channels detected the alleles, and the red channel detected the ILS.

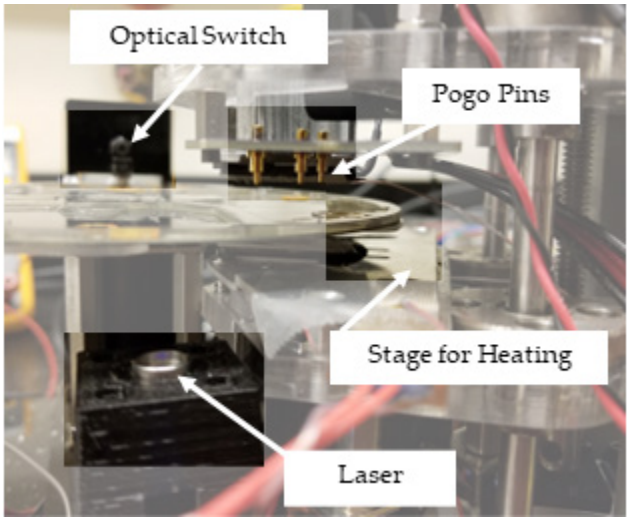

Figure 52. The automated system for microchip electrophoresis has a laser for opening valves, a stage that sits along the separation channel for heating, an optical switch for alignment, and pogo pins to apply voltages to electrodes on the disc during electrophoresis.

While 3 µL of amplicons added to 10 µL of water and 3 µL ILS for a total volume of 13 µL was previously demonstrated to be sufficient for separation of amplified STR fragments[23], here we analyzed a smaller input of amplified sample in the same total volume to determine if a similar input volume as the conventional CE system could be used on-chip (**Figure 53A**). However, a 3 µL volume was shown to yield high fluorescent signal for both the blue and green channels with peak heights decreasing as input sample volumes were reduced. Higher input volumes were considered, but we wanted to balance using the least volume of sample while obtaining peak heights that are high, but do not saturate the detector. Therefore, we selected to use a sample cocktail comprised of 3 µL sample, 4 µL ILS, and 6 µL water as this yields the most robust detection of both ILS peaks and sample amplicons peaks.

The optimal channel temperature was assessed by heating the stage under the separation chip to 37 °C throughout electrophoresis or omitting heating on the *µ*EDisc. Since the capillaries on conventional systems are heated by an oven during separation, it was hypothesized that heating of the COC channel on the *µ*EDisc would be advantageous. It was important to balance the peak height of the targets in the blue and green channels with high peaks in the red channel. Results showed that heating during a separation caused the peak heights to decrease (**Figure 53B**). It was theorized that there was a heat gradient vertically through the channel that could impede the separation due to a change in viscosity of the polymer. Alternatively, the heat produced from the voltage through the capillary combined with extra heating from the metal plate could cause joule heating affecting the resolution of the peaks, leading to smaller peak heights. Due to these possibilities and the experimental data, the metal plate was not heated during electrophoresis.

Finally, optimization of sample injection time was seminal in balancing maximum peak height with minimal peak broadening. The electrokinetic injection was performed by applying 600 V to the S and SW electrodes, since this voltage was previously shown to give successful separations

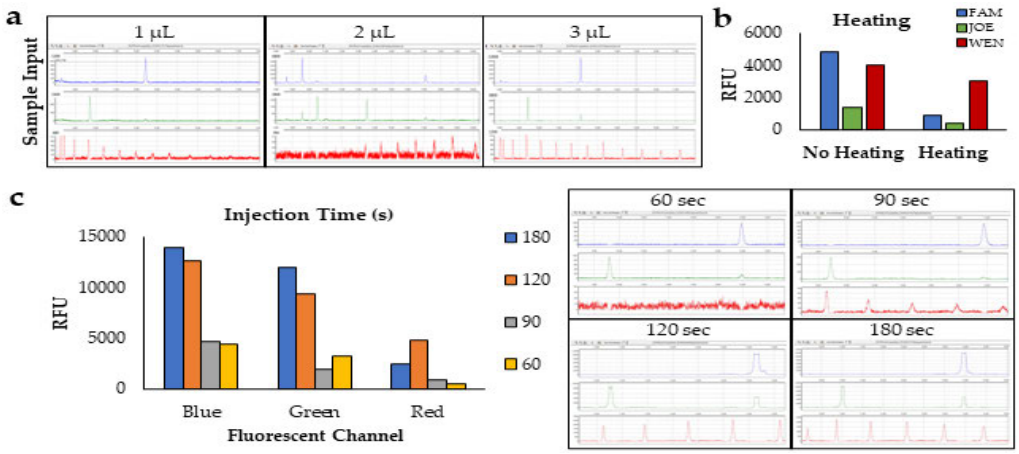

Figure 53. Optimization of separation parameters through comparison of electrophoresis peaks. (a) Resulting electropherograms from reagents containing 1, 2, or 3 µL of sample in a 13 µL sample volume. (b) Electrophoresis peak heights for each fluorescent channel in terms of relative fluorescence units (RFU) comparing results when the separation channel is heated to 37 °C or not heated. (**c**) Electropherograms showing the difference in peaks when injecting for 60, 90, 120, or 180 seconds, and a bar graph comparing the peak heights in term of relative fluorescent units.

on a similar system[32]. If the injection time is not long enough, the sample will not reach the cross-t for sufficient fluorescent detection; on the other hand, if the injection time is too long, the bulk of the sample may bypass the cross-t leading to decreased fluorescent signal. **Figure 53C** shows a representative resulting electropherogram from various injection times, including 60, 90, 120, and 180 seconds. With a 60-second injection, the amplicon peaks associated with mRNA targets and ILS peaks were not present. However, using a 90-second injection the peaks associated with amplicons of mRNA targets were present and ILS peaks were detected with lower peak heights over time. Detection of the ILS peaks, especially in the 80 – 200 base pair range, is critical for accurate sizing of the amplicon peaks since all of the mRNA targets in the panel range from 100 to 200 bp in size. Of all the injection times, the 120- and 180-second injections were the only two that detected the ILS peaks well after the 200-base pair peak and all of the sample peaks associated with mRNA targets; the corresponding electropherograms show peaks in the FAM and HEX channels saturating the detector (as indicated by the flat, cut-off peak). While either injection time could be used to detect all the necessary ILS peaks with the on-chip electrophoresis, we selected 120-second injection, ultimately decreasing overall separation time by one minute, making the overall separation time 10 mins (i.e., a 2 minute injection facilitated by 600 V applied to the S and SW reservoirs followed by an 8 minute separation via application of 1500 V across the 5 cm electrophoresis channel).

3.4 Single Source Fluid Comparison on μEDisc

Once the on-chip electrophoresis was optimized for amplicon separation, separation of all body fluids was examined and the microfluidic data was compared to a commercial ABI 3130xL. Due to the differences in instrument sensitivity, the resultant peak heights, in terms of relative fluorescent units (RFU), were minimum-maximum normalized for each detection system to more accurately compare between the separation platforms[33].

Using this normalization, the normalized peak heights for each body fluid mRNA target were compared for commercial and microfluidic instruments (**Figure 54**). It is worth noting that samples separated on the commercial instrument were only analyzed replicates of 1 as this is often standard practice in forensic laboratories due to limited starting sample volumes, but multiple replicates for microfluidic data were run. The 11 peaks associated with mRNA targets produced following amplification via the three panels (Duplex, Quadruplex, and Pentaplex) were consistently detected in the samples separated on the μEDisc, showing comparable results with respect to peak height with the commercial instrument; variability in RFUs for each allele are expected as samples were collected from different donors. These results are significant because not only did the μEDisc

detect all of the gene peaks associated with amplicons of the mRNA targets, but in some of the body fluids the μEDisc detected the peaks as well or better than the commercial systems. For example, peaks associated with amplicons of both mRNA targets specific to venous blood (HBD and SLC4A1) were detected with the microfluidic system in all samples with comparable intensity

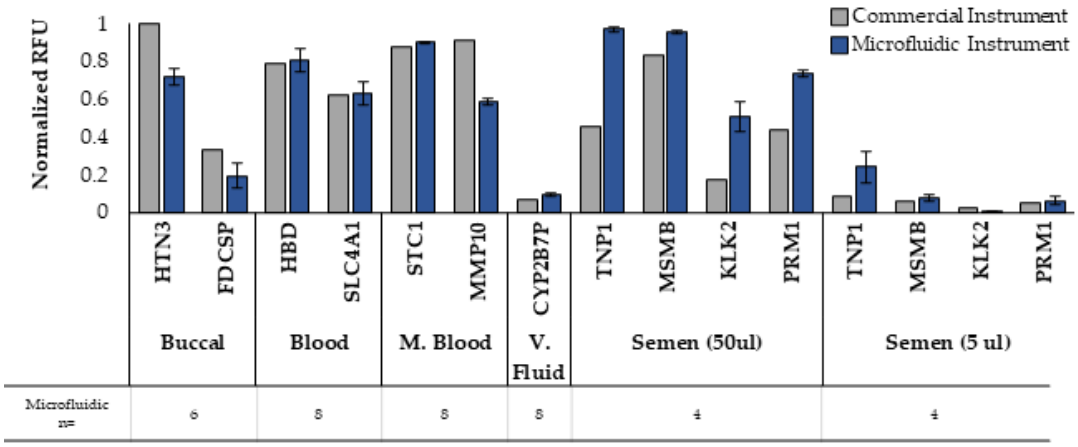

Figure 54. **Single source fluid comparison of normalized peak heights from a commercial CE instrument and the chip microfluidic system.**

relative to the commercial instrument. These samples consistently showed peak heights from the μEDisc that were higher than or similar to the commercial instrument. Similar trends were observed when considering the two peaks associated with menstrual blood targets (STC1, MMP10). As expected, the two peaks associated with venous blood targets (HBD, SLC4A1) were also detected in both menstrual blood samples, but in much lower peak heights using the μEDisc. This demonstrates that the μEDisc can allow for detection of multiple amplicons with high and low fluorescent signal.

The duplex peaks associated with amplicons of mRNA targets specific to buccal (HTN3, FDCSP) were consistently detected in both systems in multiple amplified samples from buccal swabs. **Figure 54** shows the HTN3 peak to be consistently higher than the FDCSP peak using the μEDisc system, which was also found in the commercial system.

Finally, the Pentaplex panel containing the vaginal fluid and semen mRNA targets was detected on both separation platforms using two vaginal fluid donors and two semen donors (50 µL and 5 µL). While the vaginal fluid marker (CYP2B7P) was one of the lowest normalized peak heights detected across both platforms, the peak height was consistently detected using the μEDisc system**.** Higher peak heights were observed for CYP2B7P on the μEDisc system than the commercial system, showing the μEDisc platform compares well with the gold standard instrument. Similarly, all four peaks associated with amplicons of semen mRNA targets (TNP1, MSMB, KLK2, PRM1) were detected using the μEDisc system at higher or comparable peak heights than the commercial instrument with the 50 µL semen sample, again showing a strong comparison between the μEDisc system and the gold standard instrument. This trend continued with the 5 µL semen sample, with the exception of the KLK2 gene, which was manually called with a peak height of 845 RFU using the μEDisc system. This data shows that even though the

sample was small in volume, the μEDisc system was still able to detect all of the semen genes in the Pentaplex panel in 10 mins. Additionally, the data shows that all of the vaginal fluid and semen samples were detected in the μEDisc platform.

3.5 Multiple Source Fluid Comparison on µEDisc

While detection of single-source fluids is important, many forensic samples are not single source; they can contain anywhere from one fluid to all five fluids, plus others not tested here. To further test the size separation of the panels on the μEDisc, the amplified products from two mixed samples were separated on both platforms for comparison. To simulate types of samples that would be present at a crime scene, swabs containing vaginal fluid were spiked with semen or saliva and

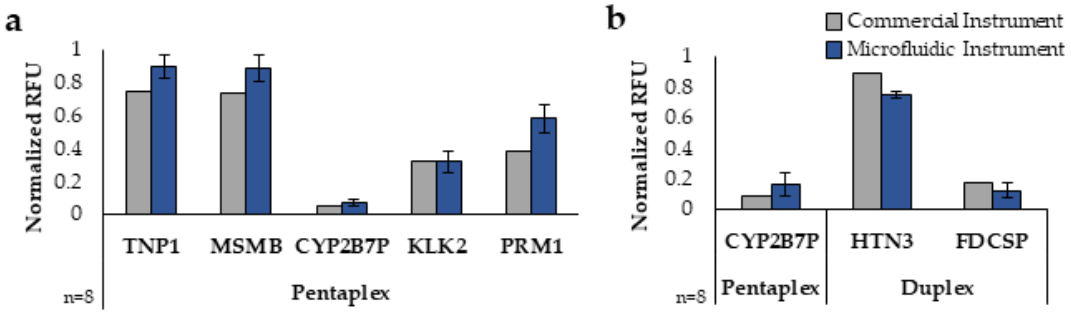

Figure 55. Multi-source fluid comparison of peak heights from gold-standard CE systems and the chip microfluidic system. (a) Electrophoresis of contrived mixed sample containing vaginal fluid and semen amplified with the Pentaplex panel of primers. (b) Normalized peak heights from a mixed sample containing vaginal fluid and saliva amplified with the Pentaplex and Duplex primers.

amplified using the Pentaplex or Duplex panel of primers (**Figure 55**). **Figure 55A** shows simultaneous detection of all 5 Pentaplex targets from a swab containing vaginal fluid and semen using the commercial instrument and the microfluidic system. The semen target (TNP1) and seminal fluid target (MSMB) amplicons were detected using the μEDisc system at peak heights higher than the commercial system after normalization, while the other three genes in the panel for vaginal fluid (CYP2B7P), seminal fluid (KLK2) and semen (PRM1) had comparable peak heights between instruments. The second mixture sample was comprised of vaginal fluid and buccal fluid and was amplified with the Duplex and Pentaplex panels (**Figure 55B**). The buccal amplicon (HTN3) was detected on the μEDisc with lower peak heights compared to the commercial instrument, while the vaginal fluid (CYP2B7P) and buccal (FDCSP) genes exhibited similar peak height between platforms. While there is variation in peak heights between the two platforms (which is expected as samples were collected from different donors at different times), the key takeaway is that there was successful separation, detection, and identification of all body fluids present in the contrived samples. This data shows the μEDisc system can perform just as well as or better than the gold standard systems with single- and multiple-body fluid samples. It also shows replicate consistency in the μEDisc system among both types of samples.

3.6 On-chip Detection Sensitivity

We sought to interrogate the sensitivity of our μEDisc system by empirically determining an analytical limit of detection for each body fluid panel. Any analytical system has thresholds that differentiates an actual peak from background noise. For the μEDisc system, we determined the analytical threshold by taking 10% of the gene with the lowest peak height from a run. Each PCR product was serially diluted from the neat sample to a 1:32 factor and electrophoresed on the microfluidic system to simulate low-concentration samples frequently encountered in forensic casework (**Figure 56**). Unsurprisingly, after a 1:2 dilution, the fluorescence signal considerably decreased for all amplicons in the three panels. Even with the decrease in signal, 10 of the 11 genes were automatically detected by the GeneMarker software at the 1:32 dilution. The KLK2 gene was the only one that completely dropped below the analytical threshold of the microfluidic platform (100 RFU) after a 1:4 dilution of the 5 μL semen sample (**Figure 56 inset**). Further, the vaginal fluid gene (CYP2B7P) was detected at the lowest dilution of 1:32 using the μEDisc system. Using both our guidelines (threshold and detection of all body fluid amplicons), the sensitivity of the μEDisc system for semen is a 1:2 dilution of a 5 μL sample and for vaginal fluid, a 1:16 dilution of a whole swab sample. Similarly, the sensitivity of targets associated with the quadruplex panel showed that after a 1:2 dilution there was a sharp decline in fluorescent signal, but even at the 1:32 dilution both genes for venous blood and menstrual blood were detected above the analytical threshold using the μEDisc system. Using the same standards, the μEDisc system for venous blood and menstrual blood is a 1:32 dilution of liquid or whole swab sample, respectively. Finally, the two buccal targets in the Duplex panel (HTN3, FDCSP) were detected with the μEDisc system. The peak associated with the amplicon of mRNA target HTN3 was detected well above the threshold, but peaks associated with the FDCSP amplicon were only detected above the threshold up to the 1:8 dilution. For the Duplex panel, the sensitivity of the μEDisc system for buccal fluid is a 1:8 dilution of a whole swab sample.

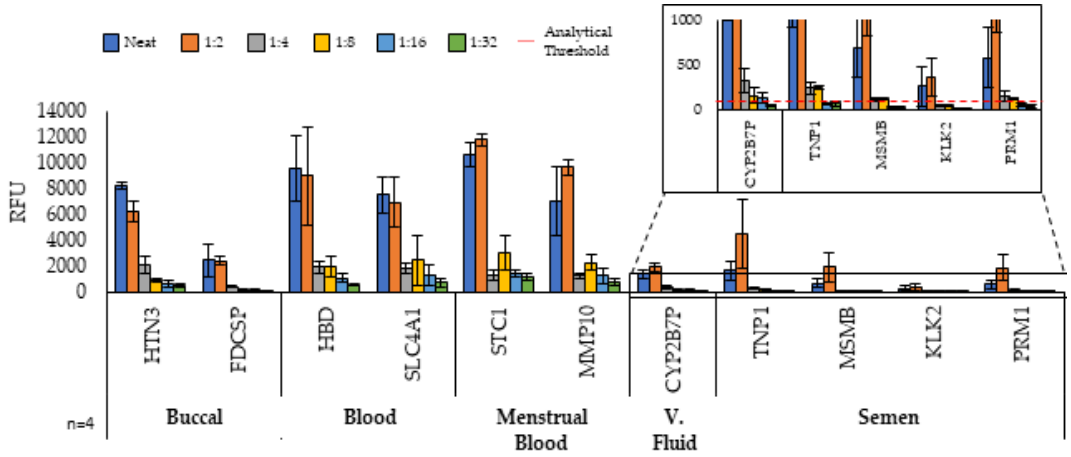

Figure 56. Separation of all single-source body fluids to determine the sensitivity of on-chip fluorescent detection. Amplified neat samples were serially diluted down to a 1:32 dilution to examine the sensitivity of the microfluidic platform. The inset shows a closeup of the Pentaplex panel of targets and the analytical threshold (100 RFU) of the μEdisc.

This resource was prepared by the author(s) using Federal funds provided by the U.S. Department of Justice. Opinions or points of view expressed are those of the author(s) and do not necessarily reflect the official position or policies of the U.S. Department of Justice.

4. System Engineering

4.1 Engineering for On-Disc Amplification

While the in-tube assay and microfluidic architecture were being optimized, the faSTR system was being modified for rapid, multiplexed RT-PCR. This instrument was previously built to integrate DNA extraction, multiplexed PCR, ME, and LIF detection for rapid DNA analysis, specifically STR typing.[25] **Figure 57** shows the fully-enclosed faSTR system and corresponding microdisc, and the schematic of internal hardware labels components relevant to on-disc operations. In brief, the disc is mounted on a spin motor that generates centrifugal force through controlled rotation, while the photo-interrupter switch enables accurate angular positioning of the disc, and the red laser can open valves. The optics stack, excitation source input (i.e., 488 nm sapphire laser), objective, and heater connected to a metal stage ('Heater') are relevant for electrophoresis and LIF detection on the microdisc. Similarly, hardware necessary for amplification on-disc includes the clamping motor that vertically moves the upper and lower clamping stages, which each house Peltiers and fans for active contact heating and cooling. The dual clamps can be programmed to clamp around the disc more tightly or loosely depending on what function is required. The red laser, excitation source input, and objective are all mounted to linear actuators (not visible in schematic) to facilitate movement in one direction. For example, the red laser moves in the x-direction for radial positioning relative to the microdisc while the objective moves in the z-direction to focus the fluorescence excitation light in the separation channel.

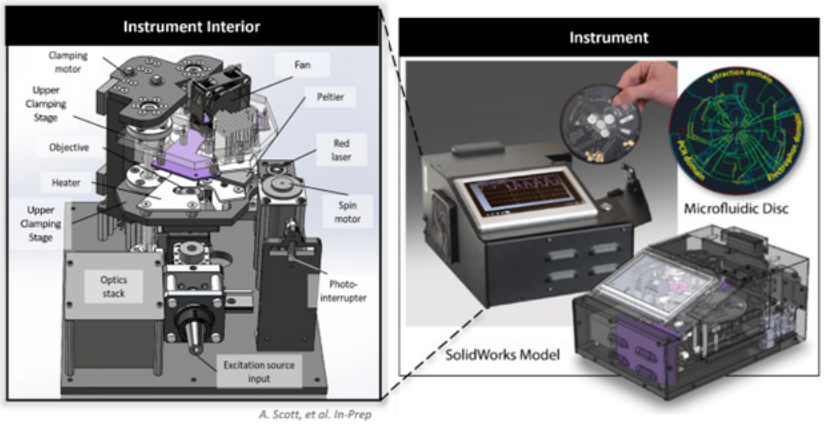

Figure 57. The integrated faSTR system for automated, rapid STR typing on a microfluidic disc. The exploded view depicts a schematic of the interior of the instrument with relevant hardware components labeled. This instrument is being leveraged, and the microfluidic disc redesigned, for rapid bodyfluid detection and identification at the point of need. *Adapted from Scott, A. et al.*[25]

For the purposes of BFID, the system needed to be able to perform RT-PCR concurrently in three amplification chambers, which required replacement of hardware and reprogramming software. Old hardware, including set screws controlling the clamping motor, linear actuators,

motors, fans, Peltiers, and thermal couples connected to the Peltiers for real-time temperature feedback were replaced with new components. This was to ensure functionality and minimize the chance of something breaking during future experiments that would require deconstructing and reprogramming the system from the beginning. Additionally, screws and other small parts were replaced on account of being brittle, stripped, or broken from use over time. Upon replacing multiple hardware components, modifications to the software were made to enable rapid, reproducible thermal cycling for RT-PCR amplification. Specifically, software modifications, detailed below, included (1) recoding the instrument and graphical user interface (GUI) for RT-PCR, not just PCR, (2) adjusting the clamping settings to ensure efficient contact heating and heat transfer, (3) programming proportional, integral, and derivative (PID) values for accurate and fast thermal cycling, and (4) determining input temperatures that achieve the desired on-disc temperatures.

4.2 Recoding for RT-PCR

The original faSTR system required a 'two-stage' PCR amplification, which included an initial polymerase activation step followed by thermal cycling between two stages – denaturation and annealing. **Figure 58A** shows a truncated temperature profile, taken inside the microamplification chamber, in which the annealing and denaturation steps are cycling out of order once the initial polymerase activation step is conducted. Not only is cycling out of order an issue that needed remedied, but ESR's validated two-step RT-PCR chemistry and the newly selected TaqPath chemistry both required additional stages. Since initial software modifications coincided with optimization of ESR's two-step amplification protocol, the system was reprogrammed to perform a polymerase activation, cycling between three stages – denaturation, annealing, and extension – followed by a final extension step (**Figure 58B**); note, this protocol did not need a built-in RT step because RT was conducted separately prior to PCR. Once the TaqPath chemistry was selected, an RT stage prior to the polymerase activation was added, and even though this chemistry did not require a cycling extension or final extension stage, these stages remained to increase the applicability of the instrument to amplification protocols. All changes to the software were reflected in the GUI for simplicity of user input. To adjust the thermal cycling protocol, the user only needs to type in the target temperatures and incubation times for each stage (**Figure 58C**). After successfully recoding the instrument to perform multi-stage amplification, with cycling stages in the correct order, we needed to ensure heat could be efficiently transferred from the instrument (via Peltiers) to the microdisc.

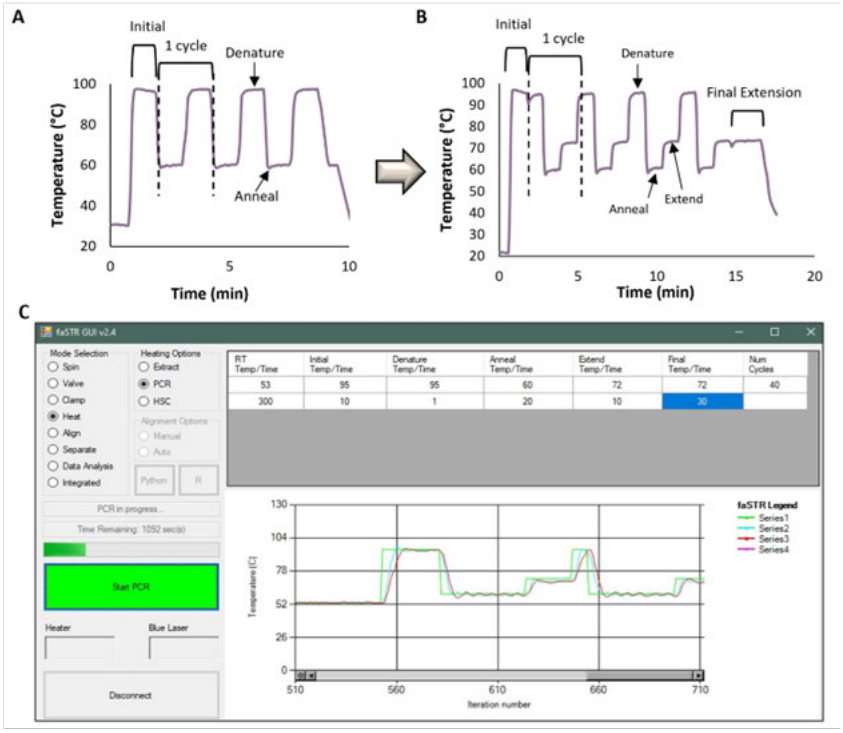

Figure 58. Temperature profiles collected on-disc when reprogramming the faSTR system to be amenable to 3-stage thermal cycling. (**A**) The original two-stage thermal cycling program for STR typing. (**B**) Modified three-stage thermal cycling compatible with ESR's two-step RT-PCR chemistry. (**C**) Screenshot from the faSTR operating computer showing the GUI programmed for RT-PCR and the feedback loop monitoring the temperature on the surface of the Peltiers.

4.3 Clamping Optimization

Rapid heat transfer and efficient amplification on-disc is dependent on sufficient contact between the Peltiers and the microamplification chamber. As discussed, the clamping motor moves the upper and lower clamping stages, containing Peltiers and fans for thermal cycling, in the vertical direction, and these dual clamps can be programmed to move set distances to control clamping around the microdisc. The distance the clamp travels along the set screw is based on the stepper motor that turns the set screw. Since set screws and motors were replaced, and the clamping distances are based on arbitrary units inherent to the stepper motor, the default clamping distances needed to be adjusted in the instrument code.

Figure 59 illustrates different clamping distances. This is a 'Goldilocks' situation: if the clamps, and therefore Peltiers, are not clamping the disc tight enough, heat transfer is inefficient, causing overall PCR efficiency to diminish due to a lack of contact between the Peltiers and amplification chamber (**Figure 59A**). Conversely, if the clamps are too tight around the microchamber the disc will be deformed, causing fluid to be physically pushed out of the chamber, and possibly the disc, or delaminating the disc. **Figure 59C** shows clamps sitting around the disc too tightly, resulting in indentations from the clamp – specifically, from the thermal couple attached to the surface of the Peltier – on the disc after thermal cycling. Thus, a Goldilocks distance must be found to ensure the clamps sit tight enough to thermal cycle in the microchamber, yet not so tight as to deform the disc (**Figure 59B**). Adjusting the clamping distances requires a guess-and-check methodology, but based on the criteria discussed here, clamping values of 58,000 and 11,000 A.U. were selected for the top and bottom clamps, respectively. Every time the clamping platforms are removed from the set screw, this optimization must be performed to ensure the clamps sit on the microdisc. Since the clamping distances impact heat transfer from the Peltiers to the microchamber, thermal cycling parameters, (e.g., PID values and input temperatures) must be adjusted accordingly each time the clamping distances are modified.

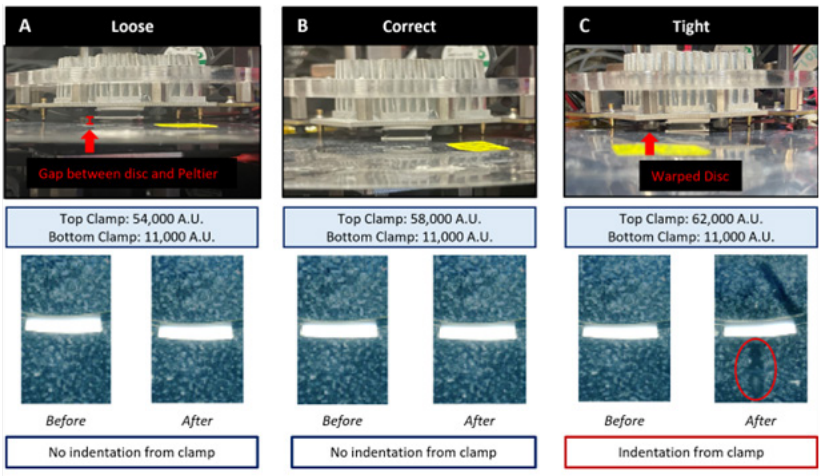

Figure 59. Various clamping distances relative to the microamplification chamber. Clamping distances measured in arbitrary units (A.U.) inherent to the stepper motor, show Peltiers situated (A) loosely (B) correctly, and (C) tightly around the micro disc. Each condition shows an image of the clamps and the disc, the clamping values input into the system, and the images of the amplification chamber before and after thermal cycling to illustrate whether the disc was deformed from the clamp settings.

4.4 PID Value Adjustment

In addition to sufficient contact between the Peltiers and microamplification chamber, efficient thermal cycling relies on rapid ramping between temperatures as well as fast thermal stabilization at desired temperatures. These processes are dictated by the Peltiers and their corresponding programming. Similar to the clamping settings, anytime Peltiers are replaced, the

This resource was prepared by the author(s) using Federal funds provided by the U.S. Department of Justice. Opinions or points of view expressed are those of the author(s) and do not necessarily reflect the official position or policies of the U.S. Department of Justice.

corresponding control settings of a PID circuit must be reprogrammed to ensure the Peltiers work precisely and accurately. PID values are responsible for creating a control mechanism for real-time feedback and automatic correction. An everyday example of this is the cruise control on a car, where going downhill would normally cause the car to accelerate if it were not for a PID algorithm maintaining desired speed by measuring the error between the target speed and the real-time speed and adjusting the engine power accordingly.[34–37] In this application, PID values control how quickly Peltiers change and adjust to the programmed input temperature.

For the software to work correctly to carry out experimental procedures, PID response math[38] was implemented as it dictates operation and efficiency of the heaters (Peltiers). Ideally, we want the Peltiers to rapidly heat and cool (with assistance from fans) while allowing the temperatures inside of the microfluidic disc to reach the ideal set temperature in the shortest amount of time. **Table 8** illustrates how changing PID variables affects thermal cycling. The proportional response controls the ramp rate, or how fast the Peltiers reach the set temperature. For rapid PCR on-disc, the goal is to have a steep or rapid temperature change. The integral response is responsible for the overshoot and subsequent correction. A slight overshoot is intentional and serves to allow the internal temperature in the microamplification chamber to reach the desired temperature faster.[39] However, constant overshooting and overcorrecting of the temperature can cause an oscillating thermal profile during what should be a stabilized temperature hold. The derivative variable is responsible for stabilizing the Peltier response by reducing the overshoot to smooth out the temperature response. Each Peltier has a corresponding set of PID values, and separate PID values

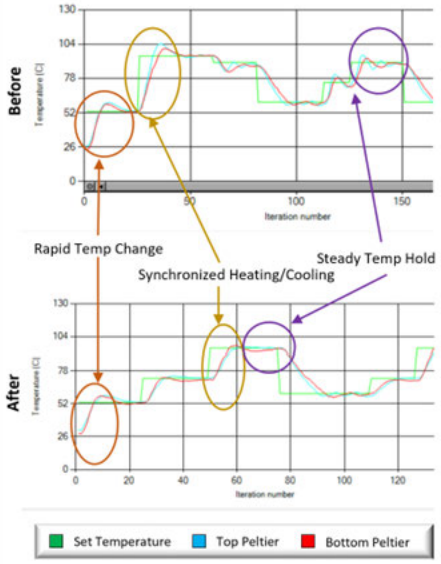

Figure 60. Temperature profiles collected from the faSTR GUI showing changes in thermal cycling before and after PID value adjustments. Noticeable changes to thermal profiles are notated

Changed Variable	Baseline				Proportional				Integral				Derivative				Ideal			
PID Values		P	I	D		P	I	D		P	I	D		P	I	D		P	I	D
	Top	4	.5	0	Top	15	.5	0	Top	4	1	0	Top	4	.5	.5	Top	9	.3	1
	Bottom	6	.3	0	Bottom	15	.3	0	Bottom	.6	1	0	Bottom	6	.3	.5	Bottom	5	.2	1
Example of Partial Cycling Profile	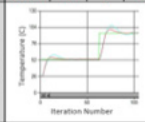				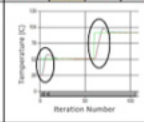				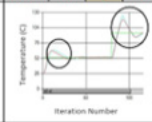				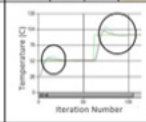				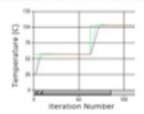			
Notes	Initial PID Values				Rapid Temperature Change				Large Overshoot & Slow/Large Overcorrection				Smoother Correction & Stable Temperature Hold				Rapid Temperature Change, Small Overshoot, Rapid Correction, Smooth Temp Hold			
Key	Set Temperature Top Peltier Bottom Peltier																			

Table 8. Examples of how modifying the PID values associated with the first two stages of amplification changes the thermal cycling obtained from the faSTR GUI. Yellow highlighted boxes correspond to the variable that was changed under each condition. Black circles highlight the resulting changes in the temperature profile.

are needed for different stages of thermal cycling (e.g., heating versus cooling).

This resource was prepared by the author(s) using Federal funds provided by the U.S. Department of Justice. Opinions or points of view expressed are those of the author(s) and do not necessarily reflect the official position or policies of the U.S. Department of Justice.

Based on the data illustrated in **Table 8**, a trial-and-error method was implemented to determine ideal PID values that result in a desired thermal cycling profile (**Figure 60**); for simplicity, only a portion of the thermal cycling program is shown. The blue and red lines correspond to thermal couples connected to the top and bottom Peltiers, respectively, and the green line is the target, or set, temperature programmed into the system. The colored circles indicate the transitions between setpoints where PID response math becomes valuable. The orange circles show how temperature changes from one set temp to another, also referred to as the ramp rate. The time between the target temperature being set and the Peltier reaching said temperature averages approximately 2 sec, which will correspond to ramp rates ~8-9 °C/s on-disc, roughly 2-4 times those seen in conventional instrumentation. The yellow circles highlight where PID values were modified to allow the top and bottom Peltiers to change temperatures simultaneously, avoiding potential temperature gradients in the microdisc that would diminish amplification efficiency. Finally, the purple circles designate temperature correction and steady temperature incubations after PID adjustments.

Adjusting PID values for both Peltiers for each stage of amplification was successful and resulted in a beautiful temperature profile that was consistent across multiple cycles of PCR (**Figure 61**). At this point, the temperature program was being set for the TaqPath chemistry, which is why the cycling extension step is reduced to a 1 second incubation at the annealing temperature.

A

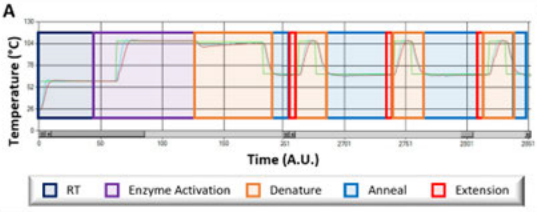

B

Variable	Peltier	P	I	D
RT & Enzyme Activation	Top	9	.3	1
	Bottom	5	.2	1
Cycling Stages	Top	10	.3	1
	Bottom	8	.2	.2
Final Extension	Top	10	0	1
	Bottom	10	0	1

Figure 61. RT-PCR temperature profile achieved once PID values were optimized. (A) Thermal cycling program from the faSTR system showing color-coded stages of amplification. (B) Final PID values programed into the code for both the top and bottom Peltiers during various stages of amplification.

Each stage of amplification has a rapid temperature change from the previous temperature, a slight overshoot that is quickly corrected, and a steady temperature hold. Once the code was set for rapid, reproducible temperature cycling, the next step of the engineering process was to adjust input temperatures to achieve the desired on-disc temperature.

4.5 Input Temperature Optimization & Evaluation of Thermal Cycling

Programming PID values ensured the thermal cycling protocol could be achieved efficiently with rapid transitions between temperatures, but we still needed to verify that temperatures inside the microamplification chamber matched the desired temperature. While thermal couples were attached to the surface of the Peltiers for real-time temperature feedback into the faSTR system,

This resource was prepared by the author(s) using Federal funds provided by the U.S. Department of Justice. Opinions or points of view expressed are those of the author(s) and do not necessarily reflect the official position or policies of the U.S. Department of Justice.

the temperature inside the microamplification chamber will differ from that on the Peltier surface based on heat transfer efficiency of the disc materials and the pressure applied by the clamps. Therefore, we needed to monitor the temperature inside the amplification chamber during thermal cycling and adjust the input temperatures accordingly. By this point, it was established that TaqPath chemistry would be used for on-disc amplification, so temperatures for RT-PCR were input based on the TaqPath protocol. **Figure 62** shows results from this set of experiments, wherein one set of temperatures was input, and the on-disc temperature was measured. For these experiments, a trial-and-error method was implemented until the target temperatures were achieved on-disc. **Figure 62A** indicates the input temperatures necessary to achieve the desired target temperature, and **Figure 62B** shows those input temperatures adjusted by ±1 °C, illustrating the accuracy of the selected input temperatures. Specifically, temperatures of 59, 106, 107, and 68 °C were needed to achieve on-disc temperatures of 53, 95, 95, and 60 °C, respectively. The successive 95 °C steps required slightly different input temperatures to account for the slight overshoot created by the PID values when transitioning from the initial 95 °C enzyme activation step to the first cycling denature step at 95 °C.

A

Stage	Target Temp (°C)	Input Temp (°C)
Reverse Transcription (RT)	53	59
Enzyme Activation (EA)	95	106
Cycling Denature	95	107
Cycling Annealing	60	68

B

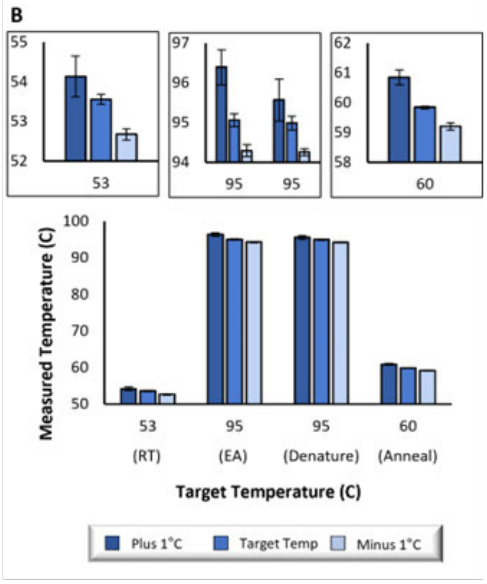

Figure 62. Optimization of input temperatures on the faSTR system. (A) Input temperatures required to achieve the desired on-disc temperatures based on the TaqPath thermal cycling protocol. (B) Graphs illustrating the accuracy with which the determined input temperatures achieve the target temperature, and showing how the measured temperature changes when the input temperature is varied by 1°C

Optimizing all engineering variables up to this point, including recoding for three-stage PCR thermal cycling, adjusting clamping distances, modifying PID values, and determining the input temperatures, culminated in the final stage of engineering for amplification on-disc: the evaluation of full RT-PCR temperature profiles. This was necessary to ensure consistency across 40 cycles in a single run and reproducibility across multiple runs. Additionally, an experimental calculation of ramp rates was performed based on this data. All experiments for this portion of the project were performed by measuring the in-chamber temperature for the most accurate assessment of what the amplification chemistry would undergo on-disc.

Figure 63A shows five overlayed RT-PCR temperature profiles with dashed lines representing the target denature and annealing temperatures (95 °C and 60 °C, respectively). A complete amplification consumed 32 minutes, as expected. It is evident that across all 40 cycles in individual runs, each cycle is consistently achieving the target temperatures and the small, expected overshoot at each temperature is present. This is consistent across all five runs, as well.

This resource was prepared by the author(s) using Federal funds provided by the U.S. Department of Justice. Opinions or points of view expressed are those of the author(s) and do not necessarily reflect the official position or policies of the U.S. Department of Justice.

A

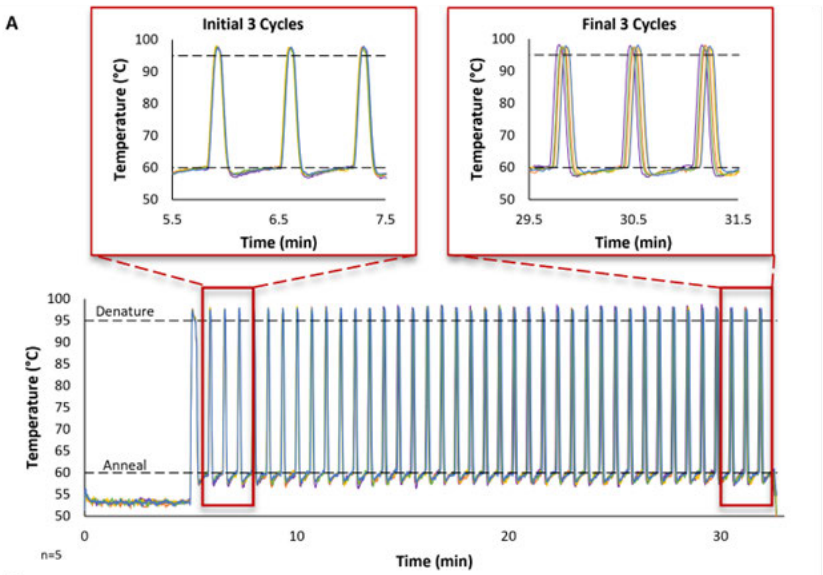

B

Stage	Target Temp. (°C)	Statistic	Run 1	Run 2	Run 3	Run 4	Run 5	Grand Mean	Grand Standard Deviation
RT	53	Average (°C)	53.41	53.05	53.32	53.29	53.25	53.27 °C	0.13 °C
		Standard Deviation (°C)	0.41	0.48	0.37	0.44	0.47		
Enzyme Activation	95	Average (°C)	96.43	96.47	96.05	96.26	95.78	96.20 °C	0.28 °C
		Standard Deviation (°C)	0.81	0.59	0.73	0.71	0.79		
Denature	95	Average (°C)	97.59	96.98	96.97	97.01	97.36	97.18 °C	0.28 °C
		Standard Deviation (°C)	0.56	0.50	0.49	0.51	0.58		
Anneal	60	Average (°C)	58.88	58.91	59.06	59.02	59.25	59.02 °C	0.15 °C
		Standard Deviation (°C)	0.98	0.81	0.80	0.77	0.72		
Ramp Rates (°C/s)		Heating Average (°C/s)	9.95	9.70	9.71	9.82	9.78	9.78 °C/s	0.090 °C/s
		Cooling Average (°C/s)	9.58	9.46	9.46	9.41	9.37	9.46 °C/s	0.071 °C/s

Figure 63. Evaluation of full RT-PCR temperature profiles obtained from monitoring temperature in the microamplification chamber. (A) Five overlayed thermal cycling profiles with exploded views of the first and last three runs of PCR. (B) Table with calculated in-chamber temperature averaged for individual runs and across all five runs (grand mean and standard deviation). The final rows show calculated heating and cooling ramp rates for individual runs as well as the averaged rates across five runs.

The exploded graphs highlight the first and last three cycles for each temperature profile; here, the consistent overshoot and rapid correction are more evident. It is noteworthy that there is a <2.5 second phase shift in cycles seen when looking at the final three cycles, indicating excellent run-to-run reproducibility. **Figure 63B** shows the average measured temperature and calculated standard deviation for each RT-PCR stage through individual runs, with the grand mean and standard deviations calculated across all five runs. Here, target temperatures were accurately and precisely achieved with a deviation of ±0.28 °C or less. Furthermore, average heating and cooling ramp rates were calculated for individual runs and averaged across all runs, resulting in a grand averaged ramp rates of 9.78 °C/s (±0.090 °C/s) and 9.46 °C/s (±0.071 °C/s) for heating and cooling, respectively. These ramp rates are significantly faster than rates on conventional instrumentation that range from ~1-4 °C/s.

Overall, this data demonstrates successful reprogramming of the instrument to perform three-stage PCR thermal cycling. After optimizing clamping distances and determining ideal PID values for the upper and lower Peltiers, the in-chamber temperature was measured throughout full RT-PCR runs on the modified faSTR system. Overlayed temperature profiles show thermal cycling consistency within individual runs and reproducibility across multiple runs. Calculated averages and standard deviations indicated the accurate and precise achievement of target temperatures. Finally, heating and cooling ramp rates were determined to be 2-4 times faster than those exhibited on thermal cycling conventional instruments. Collectively, this optimization resulted in a modified faSTR system that is capable of performing RT-PCR with incredibly robust thermal cycling on the developed microfluidic disc.

4.6 Laser Valving Parameter Optimization

In order to see consistent valve opening on the microfluidic device and translate to an autonomous system the laser valving parameters must be optimized. In order to perform valve optimization a few parameters of the optics system must be address. These components include setting of laser power, time, z-height, as well as, determining the radial and angular positions of the valves so that the system can automatically go to these positions. The radial and angular positions of the valves on the final versions of microfluidic devices are determined by measuring the radial distance from the center notch of the disc and the angular distancing from a homing position along the radial edge of the disc that is denoted as 0°. Example values shown in **Table 9.**

Domain 1	Radial Distance (mm)	Angular Measurement
Valve 1	37.5	9°
Valve 2	42.7	12°
Valve 3	47.6	12°
Domain 2	Radial Distance (mm)	Angular Measurement
Valve 1	37.5	100°
Valve 2	42.7	103°
Valve 3	47.7	103°
Domain 3	Radial Distance (mm)	Angular Measurement
Valve 1	37.0	190°
Valve 2	42.3	193°
Valve 3	47.7	192°
Domain 4	Radial Distance (mm)	Angular Measurement
Valve 1	37.5	279°
Valve 2	42.9	283°
Valve 3	47.6	283°

Table 9. Laser Valving Positions. Angular and radial distance values calculated from AutoCAD designs.

Once the positional components of the valves are determined the other parameters of laser power, time, and z-height were then assessed for optimal settings. By raising and lowering the laser height the laser beam can fan out as the height is increased and come to a pinhole as it is lowered. In order to assess the laser height setting the z-height of the diode was varied starting at its lowest position and flashing the laser until a height was reached that resulted in a uniform circle within the valve. For the power and time setting the desired setting would provide a uniform pinhole within the valve without ablating the capping PET materials as too much power would result in an excess in thermal energy absorbed by the black PET and melt through the other layers of the disc. To assess this the power and time setting the laser was programmed to its lowest parameters and fired along valves in increasing increments until the valves on the microfluidic device were able to be uniformly opened with enough area for fluid to pass through the valving component to downstream architecture with final settings being 600mW and 2500mS.

4.7 Temperature Gradient Evaluation

During input temperature evaluation, a temperature gradient was observed from chamber to chamber with the amplification chamber closest to the center of the disc running ~4 degrees or greater hotter than the chamber closest to the disc edge (**Figure 64**). This temperature testing was completed by placing a thermal couple within each of the three PCR thermal cycling chambers

and then running full PCR runs on the system to assess how each chamber was heating individually as opposed to just examining the middle chamber that was measured within previous temperature testing. From this testing it was realized that a heating gradient could be observed within the thermocycling chamber especially within the top and bottom PCR chambers and this would affect amplification efficiencies. Previous testing was done within the middle chambers of the PCR discs sue to assumption that with the rapid heat transfer associated on the microfluidic disc and the little distance seen between the three chambers on the heaters that a heating gradient would not be observed. Once this testing was completed it was realized that the peltiers used on the system do not have even heat transfer across the entire heater having patches of heating going towards the peripheral. It was observed that directly in the middle of the heater temperatures are consistently hit to target but the top and bottom chambers which reach towards the edges have approximately a +/- 2-4 degree difference in heating. Testing to address the heating gradient by adding gold plating to the heaters to help aid a more even heat transfer was attempted but with the addition of the metal, the input temperatures required to have enough energy to get all chambers to the highest target temperature was higher than the system software would allow without burning out the peltiers. To greater quantify this effect the PCR incubation temperatures were assessed in-depth to determine at what temperature ranges amplification would not be seen, as the heating gradient could not be addressed within the system without completely replacing the heaters with a different manufacturer and redoing all system optimization.

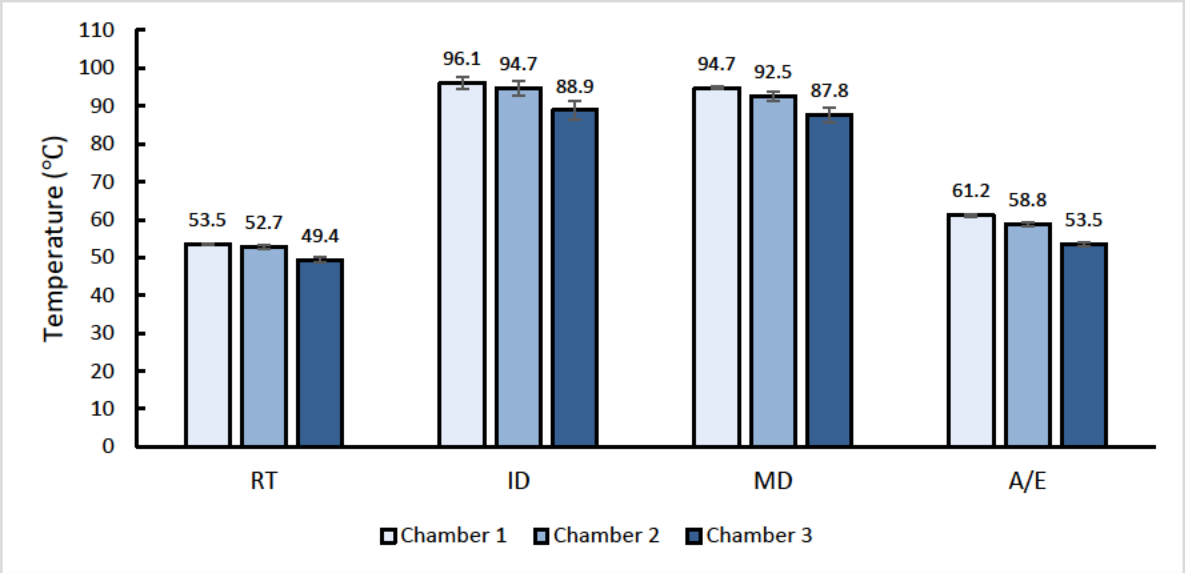

Figure 64. Full PCR runs assessing temperature gradients between the three thermocycling chambers. Average temperatures hit in each amplification chamber during thermocycling within the top, middle, and bottom chamber during each heating step of the PCR reaction. (Reverse transcription, Initial Denature, Middle Denature, and Anneal/ Exend (n=3).

4.8 Varying PCR Incubation Conditions

Based on the temperature gradient observed during initial faSTR input testing, incubation conditions for each step of the PCR cycle and their respective effect on amplification were evaluated in-tube. Qiagen-extracted saliva RNA was amplified on the Veriti thermocycler under five separate conditions shown in **Table 10** varying in the RT activation and denaturation step temperatures by plus or minus 2 degrees. Conditions 4 and 5 resulted in the greatest amplification signal, demonstrating that 2 degrees cooler in the initial enzyme activation step and 2 degrees hotter during the first couple of denaturation cycles is more efficient (**Fig. 65**). From this testing it was seen that a range of target temperatures can be observed with amplification still successful at microfluidic volumes. This is most likely due to the rapid heat transfer that is able to be reached within the microfluidic regime. Ultimately, the manufacturer conditions (**Condition 2**) were used but this testing demonstrated that a small variation in degree within these target temperatures on the heating system will still result in amplification of the desired markers.

Table 10. Thermocycling conditions tested with in-tube amplification of saliva RNA.

Condition	Reverse Transcription	Initial Denature	Middle Denature	Anneal/Extend
Condition 1	**53**	**93**	**93**	**56**
	5 min	10s	7s	30s
	x1		X40	
Condition 2	**53**	**95**	**95**	**60**
	5 min	10s	7s	30s
	x1		X40	
Condition 3	**55**	**97**	**97**	**62**
	5 min	10s	7s	30s
	x1		x40	
Condition 4	**53**	**95**	**97/95**	**60**
	5 min	10s	7s	30s
	x1		x3/37	x40
Condition 5	**51**	**95**	**95**	**60**
	5 min	10s	7s	30s
	x1		x40	

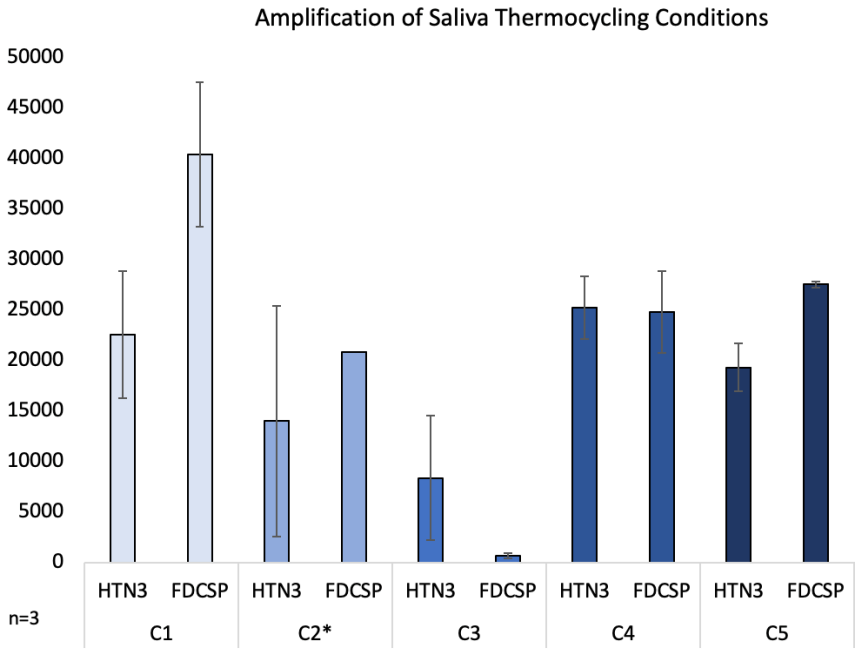

Figure 65. Assessing varied thermal cycling conditions for RT-PCR. For each condition particular parts of the RT-PCR amplification reaction were increased or decreased by 2 degrees to assess the extend of temperature gradient that could be observed and still result in successful amplification

III. Conclusions

In summary, the project resulted in the optimization of chemistry for microfluidic enzymatic extraction for saliva and seminal fluid, RT-PCR amplification, and electrophoresis. Work was completed on the development of cost-effective microfluidic discs for an integrated sample preparation disc consisting of the architecture from the enzymatic extraction disc and the RT-PCR microdisc, as well as, microchip electrophoresis. For the enzymatic extraction, an initial optimization was tested in order to convert the three different buffers required for each body fluid (red for blood, blue for saliva, and orange for vaginal fluid and seminal fluid) into a singular universal buffer for the implementation on-disc. This testing resulted in varied results for which body fluids were amenable with the extraction chemistry. Saliva and seminal fluid have consistently shown better results for the enzymatic extraction but fluids such as venous blood, menstrual blood, and vaginal fluid have required additional work. These experiments were then followed by various DNase testing, incubation studies, enzymatic volume titrations, inhibition studies, buffer titrations, cotton and FLOQ swab testing, and column purifications that did not result in a universal extraction method for all body fluids. Specifically, the bloods and vaginal fluid proved to be incompatible with the prepGEM enzyme, even in combination with the gold standard Qiagen RNA extraction methods with prepGEM used over the conventional Pro K. However, these

results are not entirely surprising as many researchers who conduct forensic body fluid research often have trouble with blood and vaginal fluid.[40–43] The enzymatic extraction was able to be used with saliva and seminal fluid resulting in successful extraction of these body fluids on the microfluidic device developed within ten minutes. This work was done alongside the ESR, as they tested their standard CellTyper II method alongside the prepGEM protocol for concordance testings along with mock samples.

Copious work was attributed to the in-tube optimization of the RT-PCR reaction time from a three hour amplification to a total of 37 minutes for all body fluids. This work began with the optimization of the reverse transcription chemistry onto the μAMP disc. This disc was validated via dye studies and image analysis to successfully show a device with architectures for reverse transcription, and overflow cDNA chamber, and downstream PCR with approximately 6μL of cDNA centrifugally driven inot the PCR chambers. This chemistry was also optimized to show successful reverse transcription on disc within 11 minutes. While work was started on the optimization of the PCR portion on the microfluidic device, a thorough literature evaluation was completed on ESR's amplification chemistry and alternative chemistries that could be used. While prior work in the lab successfully reduced their 135 minute RT assay to 10 minutes, their 3.5 hour amplification protocol could not be shortened below 2.5 hours, and the long incubation times at high temperatures caused deformation of the microfluidic disc. It was determined that after reducing ESR's PCR thermal cycling parameters to values that could be implemented on disc, the hit in sensitivity was too great, requiring alternative chemistry to be examined along with the ESR. This study tested numerous kit chemistries until the One-Step Multiplex Taq Mastermix was selected as a one-step RT-PCR chemistry as apposed to ESR's two-step assay. These RT-PCR parameters were optimized in-tube by dwell time reductions, primer titrations, and salt/enzyme titrations that resulted in 30 minute amplification – a significant improvement over ESR's 3 hour PCR. This chemistry was then translated on-to the newly redesigned microfluidic disc for a one-step amplification. While the in-tube assay optimization was underway, development of the microfluidic architecture, via the PCL fabrication method, was performed concurrently, beginning with the amplification architecture. Initial development of the microdisc began while ESR's amplification chemistry was being evaluated; therefore, architecture for a two-step RT-PCR protocol was developed. Modifications to the architecture included reducing the PCR chamber size and adding a closable channel to mitigate fluidic mixing from thermal expansion. However, initial dye studies using this architecture quickly showed that the long incubations associated with ESR's chemistry were not compatible with our microfluidic discs as delamination and a total loss of fluid were observed after just 10 cycles of PCR. A new disc was designed for amplification of the three separate body fluid panels using the TaqPath chemistry. Incorporation of a hydrophobic membrane and a closable valve enabled fluid retention throughout the entire amplification process, making this architecture promising in terms of applying the assay to the disc. In parallel, an initial disc was designed for co-extraction via enzymatic chemistry. Here, preliminary dye studies indicated that fluid was successfully retained during the extraction thermal program. A further evaluation of this architecture is underway, including optimizing the volumes of fluid metered to the PCR reagent

chambers and evaluating different swab types in-tube to see which is compatible with the chemistry and the microfluidic architecture.

After countless experiments, we were not successful in applying the new RT-PCR assay to the microdevice; however, a lengthy call to the manufacturer of the heat-sensitive adhesive (HSA) used to bond layers of our disc clarified that there was a proprietary change to the HSA coating, which was inhibiting our amplification reaction. This issue resulted in the redesign and development of a new fabrication method using an alternative pressure sensitive adhesive (PSA) that had not been previously used. This fabrication change regressed progress as the microfluidic devices had to be completely re-optimized, but resulted in a fabrication method that was now compatible with on-disc PCR amplification. This microdevice was validated via dye studies and image analysis was completed to ensure that after amplification enough amplicon was retained to perform microchip electrophoresis. This testing confirmed that average amplicon recovered varied between 8-10µL, more than enough fluid for the 1µL required for ME.

In collaboration with ESR, work was also done towards the development of a multiplex primer panel for the implementation of these amplification assays on-to the microfluidic device, as previously each body fluid was amplified with their individual primer panel (duplex for saliva, quadraplex for venous blood and menstrual blood, and pentaplex for seminal fluid, semen, and vaginal fluid). This is not representative of what testing would be completed in the field as these body fluids would not be known. This testing began with ESR as they narrowed down which primers would be used within the panel for each body fluid, ultimately deciding on HTN3 for saliva, CYP2B7P for vaginal fluid, MMP10 for menstrual blood, HBD for venous blood, and KLK2 and TNP1 for seminal fluid and semen. Work was then completed to optimize the concentrations of the primers to result in a primer panel without non-specific amplification and peak overlap for each body fluid. Once this optimization was finalized the primer panel was then sent to UVA for concordance testing. UVA's experimentation resulted also required a primer re-optimization as the difference in CE instrument senstivity (ABI 3500 vs 3100) between the establishments often required a 10x primer concentration increase. This was tested but when mixtures were assessed it was shown that salvia and blood were unable to be amplified when in combination. This resulted in the doubling of those primers in-tube which appeared to address the problem, but as the assay was tested on the microfluidic device amplification of the desired markers were much lower than the desired 5000 RFU threshold set. This required another 10x concentration increase which showed exemplary amplification of all markers as well as mixtures without nonspecific amplification. Current testing is being done towards the amplification of body fluids with the multiplex on the microfluidic device, as well as mixtures.

In addition to the enzymatic extraction and RT-PCR microfluidic devices, an integrated sample preparation device with the architecture for extraction and amplification is presented. This device was validated via dye studies and showed successful metering of approximately 2 µL of extraction eluate into the PCR Sample Chambers. Here, the One-Step Taq Mastermix would eventually be lyophilized and rehydrated, and the combined eluate and PCR chemistries centrifugally driven into the thermal cycling chambers. This microdevice went through 14 versions

of the microfluidic architecture as problems such as backpressure and fluid wicking was observed when the individual architectures were combined onto one domain. Copious time was spent to present a microfluidic design that was able to complete the extraction and amplification requirements within 60, which was achieved as extraction required 10 minutes and amplification 45 leaving additional time for on-disc work. While this microdevice was able to be validated using these dye studies, with the fabrication issue presented within the RT-PCR section the translation of this device from the HSA material to the PSA material resulted in issues with valve closure that could not be addressed by laser optics resulting in issues with fluid being driven out of the thermal cycling chambers, resulting in no amplification seen when saliva and seminal fluid were tested on disc. Because of this, an alternative valving strategy had to be assessed and a magnetically actuated pinch valve was determined to be the best option going forward. Due to these setbacks and valve issues, successful extraction and amplification were not able to be realized on the sample prep disc, but a microfluidic device capable of these parameters is presented with a novel valving strategy that is being further assessed to achieve consistent amplification on disc.

Work was completed towards the optimization of a microdevice capable of complete electrophoretic separation within 10 minutes. This includes the initial design and testing of the μEDisc and the optimization of the system parameters for separation to be achieved on system. The device achieved microchip electrophoresis using a cyclic olefin copolymer (COC) chip that contained a cross sectional where polymer could be spun down to fill the separation channel. Gold leaf electrodes were fabricated alone the separation channel and two wells were offset around the COC chip, one for buffer and one for waste in which sample can be centrifugally driven to the opening of the separation channel and as a voltage is applied buffer and sample will be pulled through to the detection window where the optics system will excite and transmit the resulting fluorescence signal. The separation parameters had to be fully optimized for the bespoke system as they would be completely different than any used on a benchtop capillary system. These parameters included the initial sample volume, heating, and injection time to achieve electrophoretic separation within 10 minutes. The fluorescence channels were also optimized for color channels and peak heights resulting in three color lanes used, blue and green for sample and red for the internal lane standard. With these parameters addressed, single source fluid was evaluated on chip, as well as, multiple source for sixteen mock samples. Finally, a sensitivity study was also tested to determine the limit of detection for the input sample with ratios as low as 1:32 sample volume successfully seen on-disc.

Lastly, system engineering was also explored with the instrument development requiring software and hardware optimization. The system first had to be recoded to allow for on-disc amplification and the development of a graphical user interface (GUI) in order for amplification parameters to be input within the system. Clamping values of the peltiers were then assessed for optimal heating along the microfluidic device. With these initial software and hardware adjustments, the heating could then be reprogrammed starting with the proportional, integral, and derivative (PIDs) for the systems control loop in order achieve fast and consistent ramp up/ramp down rates that cannot be achieved on standard systems. Conventional thermal cyclers consider

4°C/sec a fast ramp rate while the system was able to be optimized to achieve ramp rates of 9°C/sec. This temperature optimization resulted in the ability to achieve incredibly precise and fast thermal cycling. Once the PID values were optimized, an input temperature testing was then addressed to determine exactly what inputs within the system would be required to achieve the exact temperature required within the thermocycling chamber for amplification on-disc.

The in-tube optimizations were then applied to the microfluidic devices for assay integration showing successful extraction and amplification within the individual devices that all together results in a complete workflow under 90 minutes. Work with ESR resulted in a single primer panel for all body fluids for the downstream integration of the extraction and amplification of body fluids on the sample preparation disc. System optimization was also completed using PID value optimization for precise ramp up and ramp down heating profiles for fast and consistent heating on the microfluidic devices, as well as, laser optimization for valving on the microfluidic devices.

Ultimately, work presented by UVA and the ESR under this project resulted in a one-step enzymatic extraction for saliva and seminal fluid on a microfluidic device in under 10 minutes. The optimization of a two-step RT-PCR amplification to a one-step amplification that can be realized in under 45 minutes as opposed to the initial 3 hour amplification. A microfluidic device for RT-PCR with successful amplification of all body fluids addressed. The development of a multiplex primer panel for forensically relevant body fluids capable of single source and multiple source amplification. A sample preparation microfluidic disc with a novel magnetically actuated valve. The development of a μEDisc that demonstrated successful ME of all body fluids and 16 mock samples within 10 minutes, and finally the development and optimization of a system capable of precise and consistent heating profiles, clamping, electrophoretic separation, a three channel optics system, and laser valving. This work was able to approach each aim of the grant and, while it was realized that some aims would need to be addressed in a different manner, all work has contributed to the overarching goal of the development of a rapid, automated body fluid identification system. Despite the numerous hurdles that were experienced throughout the life of the project, each challenge resulted in new information and the development of alternative approaches that were not realized within the beginning of this project. It is UVA and ESR's hope that the copious work presented within this report aids in the goal of bringing the benchtop chemistries of BFID to the crime scene in an accessible manner to achieve faster and definitive results to forensic investigators, victims, and families.

Bibliography

(1) John Butler. *Advanced Topics in Forensic DNA Typing: Methodology*; Elsevier/Academic Press: Walthan, MA, 2012.

(2) Albani, P. P.; Fleming, R. Developmental Validation of an Enhanced mRNA-Based Multiplex System for Body Fluid and Cell Type Identification. *Sci. Justice* **2019**, *59* (3), 217–227. https://doi.org/10.1016/j.scijus.2019.01.001.

(3) Lonsdale, J.; Thomas, J.; Salvatore, M.; Phillips, R.; Lo, E.; Shad, S.; Hasz, R.; Walters, G.; Garcia, F.; Young, N.; Foster, B.; Moser, M.; Karasik, E.; Gillard, B.; Ramsey, K.; Sullivan, S.; Bridge, J.; Magazine, H.; Syron, J.; Fleming, J.; Siminoff, L.; Traino, H.; Mosavel, M.; Barker, L.; Jewell, S.; Rohrer, D.; Maxim, D.; Filkins, D.; Harbach, P.; Cortadillo, E.; Berghuis, B.; Turner, L.; Hudson, E.; Feenstra, K.; Sobin, L.; Robb, J.; Branton, P.; Korzeniewski, G.; Shive, C.; Tabor, D.; Qi, L.; Groch, K.; Nampally, S.; Buia, S.; Zimmerman, A.; Smith, A.; Burges, R.; Robinson, K.; Valentino, K.; Bradbury, D.; Cosentino, M.; Diaz-Mayoral, N.; Kennedy, M.; Engel, T.; Williams, P.; Erickson, K.; Ardlie, K.; Winckler, W.; Getz, G.; DeLuca, D.; MacArthur, D.; Kellis, M.; Thomson, A.; Young, T.; Gelfand, E.; Donovan, M.; Meng, Y.; Grant, G.; Mash, D.; Marcus, Y.; Basile, M.; Liu, J.; Zhu, J.; Tu, Z.; Cox, N. J.; Nicolae, D. L.; Gamazon, E. R.; Im, H. K.; Konkashbaev, A.; Pritchard, J.; Stevens, M.; Flutre, T.; Wen, X.; Dermitzakis, E. T.; Lappalainen, T.; Guigo, R.; Monlong, J.; Sammeth, M.; Koller, D.; Battle, A.; Mostafavi, S.; McCarthy, M.; Rivas, M.; Maller, J.; Rusyn, I.; Nobel, A.; Wright, F.; Shabalin, A.; Feolo, M.; Sharopova, N.; Sturcke, A.; Paschal, J.; Anderson, J. M.; Wilder, E. L.; Derr, L. K.; Green, E. D.; Struewing, J. P.; Temple, G.; Volpi, S.; Boyer, J. T.; Thomson, E. J.; Guyer, M. S.; Ng, C.; Abdallah, A.; Colantuoni, D.; Insel, T. R.; Koester, S. E.; Little, A. R.; Bender, P. K.; Lehner, T.; Yao, Y.; Compton, C. C.; Vaught, J. B.; Sawyer, S.; Lockhart, N. C.; Demchok, J.; Moore, H. F. The Genotype-Tissue Expression (GTEx) Project. *Nat. Genet.* **2013**, *45* (6), 580–585. https://doi.org/10.1038/ng.2653.

(4) Wu, C.; Orozco, C.; Boyer, J.; Leglise, M.; Goodale, J.; Batalov, S.; Hodge, C. L.; Haase, J.; Janes, J.; Huss, J. W.; Su, A. I. BioGPS: An Extensible and Customizable Portal for Querying and Organizing Gene Annotation Resources. *Genome Biol.* **2009**, *10* (11), R130. https://doi.org/10.1186/gb-2009-10-11-r130.

(5) Teoh, S. L.; Das, S. MicroRNAs in Various Body Fluids and Their Importance in Forensic Medicine. *Mini-Rev. Med. Chem.* **2022**, *22* (18), 2332–2343. https://doi.org/10.2174/1389557522666220303141558.

(6) Lee, H. Y.; Park, M. J.; Choi, A.; An, J. H.; Yang, W. I.; Shin, K.-J. Potential Forensic Application of DNA Methylation Profiling to Body Fluid Identification. *Int. J. Legal Med.* **2012**, *126* (1), 55–62. https://doi.org/10.1007/s00414-011-0569-2.

(7) Frumkin, D.; Wasserstrom, A.; Budowle, B.; Davidson, A. DNA Methylation-Based Forensic Tissue Identification. *Forensic Sci. Int. Genet.* **2011**, *5* (5), 517–524. https://doi.org/10.1016/j.fsigen.2010.12.001.

(8) Dobay, A.; Haas, C.; Fucile, G.; Downey, N.; Morrison, H. G.; Kratzer, A.; Arora, N. Microbiome-Based Body Fluid Identification of Samples Exposed to Indoor Conditions. *Forensic Sci. Int. Genet.* **2019**, *40*, 105–113. https://doi.org/10.1016/j.fsigen.2019.02.010.

(9) Gorkin, R.; Park, J.; Siegrist, J.; Amasia, M.; Lee, B. S.; Park, J.-M.; Kim, J.; Kim, H.; Madou, M.; Cho, Y.-K. Centrifugal Microfluidics for Biomedical Applications. *Lab. Chip* **2010**, *10* (14), 1758. https://doi.org/10.1039/b924109d.

(10) Mark, D.; Haeberle, S.; Roth, G.; Stetten, F. von; Zengerle, R. Microfluidic Lab-on-a-Chip Platforms: Requirements, Characteristics and Applications. *Chem. Soc. Rev.* **2010**, *39* (3), 1153–1182. https://doi.org/10.1039/B820557B.
(11) Kovarik, M. L.; Ornoff, D. M.; Melvin, A. T.; Dobes, N. C.; Wang, Y.; Dickinson, A. J.; Gach, P. C.; Shah, P. K.; Allbritton, N. L. Micro Total Analysis Systems: Fundamental Advances and Applications in the Laboratory, Clinic, and Field. *Anal. Chem.* **2013**, *85* (2), 451–472. https://doi.org/10.1021/ac3031543.
(12) Reyes, D. R.; Iossifidis, D.; Auroux, P.-A.; Manz, A. Micro Total Analysis Systems. 1. Introduction, Theory, and Technology. *Anal. Chem.* **2002**, *74* (12), 2623–2636. https://doi.org/10.1021/ac0202435.
(13) Turiello, R.; Nouwairi, R. L.; Landers, J. P. Taking the Microfluidic Approach to Nucleic Acid Analysis in Forensics: Review and Perspectives. *Forensic Sci. Int. Genet.* **2023**, *63*, 102824. https://doi.org/10.1016/j.fsigen.2022.102824.
(14) Thompson, B. L.; Ouyang, Y.; Duarte, G. R. M.; Carrilho, E.; Krauss, S. T.; Landers, J. P. Inexpensive, Rapid Prototyping of Microfluidic Devices Using Overhead Transparencies and a Laser Print, Cut and Laminate Fabrication Method. *Nat. Protoc.* **2015**, *10* (6), 875–886. https://doi.org/10.1038/nprot.2015.051.
(15) Dignan, L. M.; Woolf, M. S.; Tomley, C. J.; Nauman, A. Q.; Landers, J. P. Multiplexed Centrifugal Microfluidic System for Dynamic Solid-Phase Purification of Polynucleic Acids Direct from Buccal Swabs. *Anal. Chem.* **2021**, *93* (19), 7300–7309. https://doi.org/10.1021/acs.analchem.1c00842.
(16) Thompson, B. L.; Birch, C.; Li, J.; DuVall, J. A.; Roux, D. L.; Nelson, D. A.; Tsuei, A.-C.; Mills, D. L.; Krauss, S. T.; Root, B. E.; Landers, J. P. Microfluidic Enzymatic DNA Extraction on a Hybrid Polyester-Toner-PMMA Device. *Analyst* **2016**, *141* (15), 4667–4675. https://doi.org/10.1039/C6AN00209A.
(17) Turiello, R.; Dignan, L. M.; Thompson, B.; Poulter, M.; Hickey, J.; Chapman, J.; Landers, J. P. Centrifugal Microfluidic Method for Enrichment and Enzymatic Extraction of Severe Acute Respiratory Syndrome Coronavirus 2 RNA. *Anal. Chem.* **2022**, *94* (7), 3287–3295. https://doi.org/10.1021/acs.analchem.1c05215.
(18) A. Hagan, K.; R. Reedy, C.; M. Bienvenue, J.; H. Dewald, A.; P. Landers, J. A Valveless Microfluidic Device for Integrated Solid Phase Extraction and Polymerase Chain Reaction for Short Tandem Repeat (STR) Analysis. *Analyst* **2011**, *136* (9), 1928–1937. https://doi.org/10.1039/C0AN00922A.
(19) Le Roux, D.; Root, B. E.; Reedy, C. R.; Hickey, J. A.; Scott, O. N.; Bienvenue, J. M.; Landers, J. P.; Chassagne, L.; de Mazancourt, P. DNA Analysis Using an Integrated Microchip for Multiplex PCR Amplification and Electrophoresis for Reference Samples. *Anal. Chem.* **2014**, *86* (16), 8192–8199. https://doi.org/10.1021/ac501666b.
(20) Lounsbury, J. A.; Karlsson, A.; Miranian, D. C.; Cronk, S. M.; Nelson, D. A.; Li, J.; Haverstick, D. M.; Kinnon, P.; Saul, D. J.; Landers, J. P. From Sample to PCR Product in under 45 Minutes: A Polymeric Integrated Microdevice for Clinical and Forensic DNA Analysis. *Lab. Chip* **2013**, *13* (7), 1384–1393. https://doi.org/10.1039/C3LC41326H.
(21) Ouyang, Y.; Duarte, G. R. M.; Poe, B. L.; Riehl, P. S.; dos Santos, F. M.; Martin-Didonet, C. C. G.; Carrilho, E.; Landers, J. P. A Disposable Laser Print-Cut-Laminate Polyester Microchip for Multiplexed PCR via Infra-Red-Mediated Thermal Control. *Anal. Chim. Acta* **2015**, *901*, 59–67. https://doi.org/10.1016/j.aca.2015.09.042.

(22) Layne, T. R.; Nouwairi, R. L.; Fleming, R.; Blair, H.; Landers, J. P. Rapid Microchip Electrophoretic Separation of Novel Transcriptomic Body Fluid Markers for Forensic Fluid Profiling. *Micromachines* **2022**, *13* (10), 1657. https://doi.org/10.3390/mi13101657.
(23) Thompson, B. L.; Birch, C.; Nelson, D. A.; Li, J.; DuVall, J. A.; Roux, D. L.; Tsuei, A.-C.; Mills, D. L.; Root, B. E.; Landers, J. P. A Centrifugal Microfluidic Device with Integrated Gold Leaf Electrodes for the Electrophoretic Separation of DNA. *Lab. Chip* **2016**, *16* (23), 4569–4580. https://doi.org/10.1039/C6LC00953K.
(24) *Rapid DNA*. Law Enforcement. https://le.fbi.gov/science-and-lab/biometrics-and-fingerprints/codis/rapid-dna (accessed 2024-11-14).
(25) A. Scott, C. Birch, D. Mills, R. L. Nouwairi, R. Turiello, S. Panesar, J. Li, D. Le Roux, D. Nelson, B. Thompson, M. Startseva, T. Layne, A. Khim, C. Clark, D. Cook, J. DuVall, C. Sprecher, D. Storts, K. Kroupa, J. Bienvenue, B. Root and J. P. Landers. In-Prep.
(26) Woolf, M. S.; Dignan, L. M.; Lewis, H. M.; Tomley, C. J.; Nauman, A. Q.; Landers, J. P. Optically-Controlled Closable Microvalves for Polymeric Centrifugal Microfluidic Devices. *Lab. Chip* **2020**, *20* (8), 1426–1440. https://doi.org/10.1039/C9LC01187K.
(27) Turiello, R.; Nouwairi, R. L.; Keller, J.; Cunha, L. L.; Dignan, L. M.; Landers, J. P. A Rotationally-Driven Dynamic Solid Phase Sodium Bisulfite Conversion Disc for Forensic Epigenetic Sample Preparation. *Lab. Chip* **2023**, *24* (1), 97–112. https://doi.org/10.1039/D3LC00867C.
(28) Layne, T. Microscale mRNA Amplification, Separation and Detection for Forensic and Clinical Point-of-Care Applications, University of Virginia, 2021. https://doi.org/10.18130/QV5V-WX49.
(29) Roux, D. L.; Root, B. E.; Hickey, J. A.; Scott, O. N.; Tsuei, A.; Li, J.; Saul, D. J.; Chassagne, L.; Landers, J. P.; Mazancourt, P. de. An Integrated Sample-in-Answer-out Microfluidic Chip for Rapid Human Identification by STR Analysis. *Lab. Chip* **2014**, *14* (22), 4415–4425. https://doi.org/10.1039/C4LC00685B.
(30) Roeder, A. D.; Haas, C. mRNA Profiling Using a Minimum of Five mRNA Markers per Body Fluid and a Novel Scoring Method for Body Fluid Identification. *Int. J. Legal Med.* **2013**, *127* (4), 707–721. https://doi.org/10.1007/s00414-012-0794-3.
(31) Haas, C.; Hanson, E.; Ballantyne, J. Capillary Electrophoresis of a Multiplex Reverse Transcription-Polymerase Chain Reaction to Target Messenger RNA Markers for Body Fluid Identification. *Methods Mol. Biol. Clifton NJ* **2012**, *830*, 169–183. https://doi.org/10.1007/978-1-61779-461-2_12.
(32) Scott, A. C. Novel Analytical Systems for Rapid Forensic Nucleic Acid Detection, University of Virginia, 2020. https://doi.org/10.18130/V3-6VFN-W188.
(33) Cao, X. H.; Stojkovic, I.; Obradovic, Z. A Robust Data Scaling Algorithm to Improve Classification Accuracies in Biomedical Data. *BMC Bioinformatics* **2016**, *17* (1), 359. https://doi.org/10.1186/s12859-016-1236-x.
(34) Dos-Reis-Delgado, A. A.; Carmona-Dominguez, A.; Sosa-Avalos, G.; Jimenez-Saaib, I. H.; Villegas-Cantu, K. E.; Gallo-Villanueva, R. C.; Perez-Gonzalez, V. H. Recent Advances and Challenges in Temperature Monitoring and Control in Microfluidic Devices. *Electrophoresis* **2023**, *44* (1–2), 268–297. https://doi.org/10.1002/elps.202200162.
(35) Ferrari, S.; Schuck, C.; Pernice, W. Waveguide-Integrated Superconducting Nanowire Single-Photon Detectors. *Nanophotonics* **2018**, *7* (11), 1725–1758. https://doi.org/10.1515/nanoph-2018-0059.

(36) Miralles, V.; Huerre, A.; Malloggi, F.; Jullien, M.-C. A Review of Heating and Temperature Control in Microfluidic Systems: Techniques and Applications. *Diagnostics* **2013**, *3* (1), 33–67. https://doi.org/10.3390/diagnostics3010033.
(37) Ji, J.; Hu, C.; Pang, X.; Liang, J.; Huang, Q.; Hu, S.; Mei, Q.; Ma, H. Open Thermal Control System for Stable Polymerase Chain Reaction on a Digital Microfluidic Chip. *ACS Omega* **2024**, *9* (9), 10937–10944. https://doi.org/10.1021/acsomega.3c10312.
(38) J. A. Shaw. *Process Control Solutions*; 2003; Vol. 2.
(39) Nouwairi, R. L.; Cunha, L. L.; Turiello, R.; Scott, O.; Hickey, J.; Thomson, S.; Knowles, S.; Chapman, J. D.; Landers, J. P. Ultra-Rapid Real-Time Microfluidic RT-PCR Instrument for Nucleic Acid Analysis. *Lab. Chip* **2022**, *22* (18), 3424–3435. https://doi.org/10.1039/D2LC00495J.
(40) Dobay, A.; Haas, C.; Fucile, G.; Downey, N.; Morrison, H. G.; Kratzer, A.; Arora, N. Microbiome-Based Body Fluid Identification of Samples Exposed to Indoor Conditions. *Forensic Sci. Int. Genet.* **2019**, *40*, 105–113. https://doi.org/10.1016/j.fsigen.2019.02.010.
(41) Zubakov, D.; Boersma, A. W. M.; Choi, Y.; Van Kuijk, P. F.; Wiemer, E. A. C.; Kayser, M. MicroRNA Markers for Forensic Body Fluid Identification Obtained from Microarray Screening and Quantitative RT-PCR Confirmation. *Int. J. Legal Med.* **2010**, *124* (3), 217–226. https://doi.org/10.1007/s00414-009-0402-3.
(42) Virkler, K.; Lednev, I. K. Analysis of Body Fluids for Forensic Purposes: From Laboratory Testing to Non-Destructive Rapid Confirmatory Identification at a Crime Scene. *Forensic Sci. Int.* **2009**, *188* (1–3), 1–17. https://doi.org/10.1016/j.forsciint.2009.02.013.
(43) Richard, M. L. L.; Harper, K. A.; Craig, R. L.; Onorato, A. J.; Robertson, J. M.; Donfack, J. Evaluation of mRNA Marker Specificity for the Identification of Five Human Body Fluids by Capillary Electrophoresis. *Forensic Sci. Int. Genet.* **2012**, *6* (4), 452–460. https://doi.org/10.1016/j.fsigen.2011.09.007.

Individuals who have worked on the project (for entire project)

Name: James Landers
Project Role: Principal Investigator
Nearest person month worked: 1.0
Collaborated with individual in foreign country: Yes
Travelled to foreign country: Yes

Name: Ashleigh Williamson
Project Role: Graduate Student
Nearest person month worked: 3
Collaborated with individual in foreign country: No
Travelled to foreign country: No

Name: Carter Jones
Project Role: Graduate Student
Nearest person month worked: 3
Collaborated with individual in foreign country: No
Travelled to foreign country: No

Name: Jamila Marshall
Project Role: Graduate Student
Nearest person month worked: 2
Collaborated with individual in foreign country: No
Travelled to foreign country: No

Name: Junyi Yao
Project Role: Graduate Student
Nearest person month worked: 4
Collaborated with individual in foreign country: No
Travelled to foreign country: No

Name: Killian O'Connell
Project Role: Graduate Student
Nearest person month worked: 3
Collaborated with individual in foreign country: No
Travelled to foreign country: No

Name: Larissa Cunha
Project Role: Graduate Student
Nearest person month worked: 1
Collaborated with individual in foreign country: No
Travelled to foreign country: No

Name: Miracle Enwere
Project Role: Graduate Student
Nearest person month worked: 1
Collaborated with individual in foreign country: No
Travelled to foreign country: No

Name: Rachelle Turiello
Project Role: Graduate Student
Nearest person month worked: 3
Collaborated with individual in foreign country: No
Travelled to foreign country: No

Name: Renna Nouwairi
Project Role: Graduate Student
Nearest person month worked: 2
Collaborated with individual in foreign country: No
Travelled to foreign country: No

Name: Sadie Kiendzior
Project Role: Graduate Student
Nearest person month worked: 2
Collaborated with individual in foreign country: No
Travelled to foreign country: No

Name: Taylor Chambers
Project Role: Graduate Student
Nearest person month worked: 15
Collaborated with individual in foreign country: Yes
Travelled to foreign country: No

Name: Samuel McCollam
Project Role: Undergraduate student
Nearest person month worked: 2
Collaborated with individual in foreign country: No
Travelled to foreign country: No

Name: Zoey Golabeck
Project Role: Undergraduate student
Nearest person month worked: 2
Collaborated with individual in foreign country: No
Travelled to foreign country: No

Name: Hannah Aiken

Project Role: Undergraduate student
Nearest person month worked: 1
Collaborated with individual in foreign country: No
Travelled to foreign country: No

Name: Allison Burton
Project Role: Undergraduate student
Nearest person month worked: 1
Collaborated with individual in foreign country: No
Travelled to foreign country: No

Name: Emmanuel Kenscoff
Project Role: Undergraduate student
Nearest person month worked: 1
Collaborated with individual in foreign country: No
Travelled to foreign country: No

Name: Liam Tolburt
Project Role: Undergraduate student
Nearest person month worked: 1
Collaborated with individual in foreign country: No
Travelled to foreign country: No

Name: Rachel Fleming (ESR, New Zealand)
Project Role: Co-Investigator
Nearest person month worked: 0.6
Collaborated with individual in foreign country: ESR is in New Zealand
Travelled to foreign country: ESR is in New Zealand

Name: Liam Barry (ESR, New Zealand)
Project Role: Technician
Nearest person month worked: 2
Collaborated with individual in foreign country: ESR is in New Zealand
Travelled to foreign country: ESR is in New Zealand

Other organization involved as partners

A subaward has been issued to ESR (New Zealand)

Other special reporting requirements specified in the award terms and conditions not covered by questions above

None.

Products

(1) Nouwairi, R. Microfluidic Systems for Rapid Nucleic Acid Analysis, University of Virginia, 2024. https://doi.org/10.18130/S971-3E69.
(2) Layne, T. Microscale mRNA Amplification, Separation and Detection for Forensic and Clinical Point-of-Care Applications, University of Virginia, 2021. https://doi.org/10.18130/QV5V-WX49.
(3) Layne, T. R.; Nouwairi, R. L.; Fleming, R.; Blair, H.; Landers, J. P. Rapid Microchip Electrophoretic Separation of Novel Transcriptomic Body Fluid Markers for Forensic Fluid Profiling. *Micromachines* **2022**, *13* (10), 1657. https://doi.org/10.3390/mi13101657.
(4) Nouwairi, R.; Chambers, T.; Cunha, L.; Burton, A.; Gollabek, Z.; McCollam, S.; Williamson, A. Microfluidic Amplification of Nucleic Acids for Transcriptomic Body Fluid Identification. *-Prep*.

Dissemination: (presentations at conferences)

Integrated Microfluidic System for Rapid Identification of Forensically-Relevant Body Fluids. Taylor G. Chambers, Renna Nouwairi, Larissa Cunha, Zoey Gollabek, Sam McCollam, James P. Landers. **Oral Presentation. 2024** 76th American Academy of Forensic Sciences (AAFS) Annual Scientific Meeting. Denver, CO, USA.

This resource was prepared by the author(s) using Federal funds provided by the U.S. Department of Justice. Opinions or points of view expressed are those of the author(s) and do not necessarily reflect the official position or policies of the U.S. Department of Justice.